Politecnico di Torino

Master's Degree in Biomedical Engineering

Short and Long term Investigation of Brainwave Entrainment induced by Binaural Beats: A Multivariate EEG Analysis and In-Depth Characterization of Alpha Rhythm Modulation

Supervisors:
Prof. Luca Mesin
Ing. Matteo Raggi

Candidates:
Giacomo Battù
Ludovico Lupo

A.Y. 2024–2025

Abstract

The brainwave entrainment (BWE) hypothesis suggests that it is possible to induce neuro modulation through non-invasive auditory or visual stimulation, enhancing the power of cortical activity around the stimulation frequency. Numerous studies in the literature have explored the BWE effect of binaural beats (BB), applying stimulation within the main EEG frequency bands with the aim of modulating cognitive functions or inducing specific mental states. However, experimental evidence regarding the efficacy of BB in altering brain activity remains controversial and inconsistent.

One limitation of many existing studies is that they rely on a single acquisition session, using a fixed stimulation protocol applied uniformly across subjects. To address this, the present study introduces a protocol design to assess both short and long term effects of BB stimulation. The primary goal is to determine whether it is possible to differentiate cortical activity during and after BB exposure compared to resting conditions, and to explore changes within the frequency band targeted by the stimulation.

The study was conducted on a group of 11 university students (7 males and 4 females), with a mean age of $24,8 \pm 1,6$ years. The experimental protocol spanned two weeks and included three acquisition checkpoints, each lasting 20 minutes. Each session was divided into three phases (Baseline, Stimulation, Post Stimulation) during which EEG and ECG signals were recorded for each participant. During the first checkpoint, a personalized audio track was created for each subject, and their initial response to the stimulation was recorded. Over the following 10 days, participants were asked to listen to the audio track daily for 10 minutes. At the end of this training period, the second acquisition session was conducted. Between the second and third checkpoints, home stimulation was discontinued. The audio track containing the BB was designed using a carrier tone (f_0) of 250 Hz, while the stimulation frequency (δf) was personalized for each subject, adapting it to their Individual Alpha Frequency (IAF).

The EEG signals recorded during the various phases of the experimental protocol were analyzed in both the time and frequency domains using linear and complexity based measures. A multivariate approach based on Principal Component Analysis (PCA) and k-means clustering was applied. Additionally, a specific analysis focused on the alpha rhythm was conducted, based on the morphological characterization of the alpha spindles and Detrended Fluctuation Analysis (DFA) of the signal envelope.

The outcome of the K-means clustering on the PCA transformed data showed a mean accuracy of over 81,68% in distinguishing stimulation from baseline observations, and over 89,90% in the comparison between baseline and post stimulation, across all acquisition sessions. Excellent results were also obtained by conducting the analysis on an extended dataset aggregating data from all three checkpoints, yielding accuracy values of 74,40% and 85,09% for the stimulation and post stimulation phases, respectively. The statistical significance of the K-means results was assessed at both levels of analysis using a non parametric permutation test. The alpha rhythm analysis revealed statistically significant changes (at least $p < 0.05$) in the frontal region, particularly F3 and F4. These included an increased incidence rate and a decreased average duration of alpha spindles, accompanied by a reduction in alpha band power. Moreover, the α exponent obtained via DFA decreased significantly in almost all channels, both during and after stimulation.

The results suggest that BB are capable of modulating brain activity, enabling a clear distinction between the stimulation and post stimulation phases compared to rest. The greater separation observed after stimulation suggests that during listening, the effects of stimulation confirm the ability of BB to modulate brain rhythms at the stimulation frequency, especially in the frontal region. Furthermore, the lack of statistical significant differences between stimulation and post stimulation phases suggests a prolonged entrainment effect.

Contents

List of Figures

1 Nervous System

The nervous system is primarily categorized into two main divisions: the Central Nervous System (CNS) and the Peripheral Nervous System (PNS).

The CNS is composed of the brain and spinal cord, while the PNS includes all the neural pathways that extend from the brain, called cranial nerves, and spinal cord, called spinal nerves. Within the PNS, there are three key subdivisions: the Somatic Nervous System (SNS), the Autonomic Nervous System (ANS), and the Enteric Nervous System (ENS).

The ANS is further split into sympathetic and parasympathetic nervous systems, which are distinguished by the origin of their neurotransmitters and the varying length of their preganglionic and postganglionic fibers.

The main focus of this section will be the brain which serves as the center for mental activities such as learning, thought processing, memory, as well as for carrying out essential regulatory and communication functions in the body.

1.1 Brain's Anatomy

The human brain is anatomically organized into four principal regions: the cerebrum, diencephalon, cerebellum and brainstem. each of these regions serves distinct functional purposes within the nervous system. Beyond this classification, the brain is often further divided into forebrain, midbrain and hindbrain. Additionally, the brain is split into two hemispheres, left and right, each contributing differently to cognition and behavior. Developmental abnormalities in these regions may result in serious neurological conditions and impairments in brain function [1].

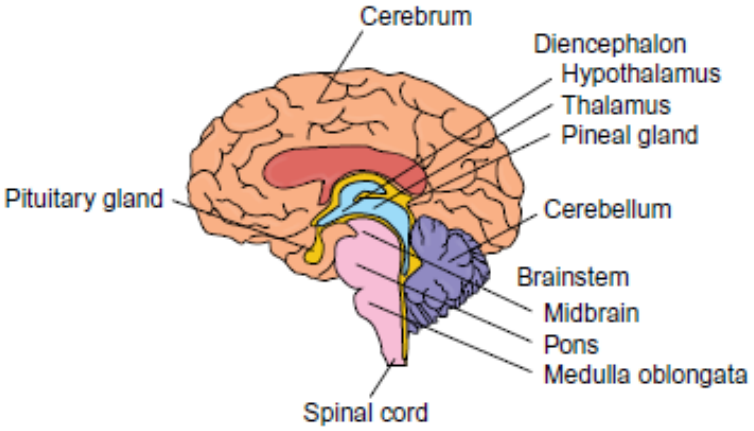

Figure 1: Brain's general structure.

1.1.1 General Structure

Among the brain's regions, the cerebrum is the largest and most functionally diverse. It manages critical processes such as voluntary movement, sensory integration, olfaction, language, memory formation and learning. Divided into left and right hemispheres, the cerebrum supports functional lateralization, often associated with logical tasks on the left and creative processes on the right. Its outermost layer, the cerebral cortex, is composed predominantly of grey matter and is segmented into four major lobes: frontal, parietal, temporal and occipital. These will be addressed in more detail later. Deeper within the cerebrum lie structures including the hippocampus, basal ganglia and olfactory bulb, each contributing uniquely to brain operations. The hippocampus, named for its resemblance to a seahorse, is integral to the formation of long-term memories and includes both the hippocampus proper and the dentate gyrus, the latter being a notable site of adult neurogenesis. The basal ganglia, positioned lateral to the thalamus in the diencephalon, work in tandem with this structure to regulate motor control, primarily via glutamatergic transmission. As the brain's main information messengers,

neurons enable complex communication systems throughout the body. Dysfunction in the basal ganglia is associated with various neurological disorders, such as Parkinson's disease, ADHD, the olfactory bulb contains the neural receptors necessary for processing smells and relays this sensory data to other areas of the brain [1].

Located at the back of the forebrain, the diencephalon comprises two primary components. the thalamus and the hypothalamus. The thalamus functions as a critical relay station, receiving sensory information across the nervous system and directing it to cerebral cortex. It also contributes to maintaining awareness and alertness. The hypothalamus plays a regulatory role in autonomic and endocrine systems, governing physiological processes such as temperature regulation, hunger and hormone secretion. Impairments in this region are linked to conditions including obesity diabetes and neurodegenerative diseases such as Alzheimer's [1].

The brainstem, which includes elements of the midbrain and hindbrain, serves as a conduit between the brain and spinal cord. It plays a fundamental role in autonomic regulation and the transmission of motor and sensory information. Core physiological functions such as breathing and heart rate are controlled by brainstem structures. It also influences consciousness and sleep cycles. Because of its responsibility for involuntary vital functions, damage to the brainstem can be fatal. Additionally, many cranial nerves that control facial movement and sensation originate from this area. The medulla oblangata, the brainstem's lower section, continues as the spinal cord and oversees critical involuntary functions like respiration and cardiac regulation. Injuries in this region often result in life threatening outcomes. Another structure, the pons, though small, plays an essential role in relaying messages between the cerebrum and cerebellum and is also central to regulating REM sleep, the phase associated with dreaming [1].

Positioned in the posterior region of the brain and connected to the brainstem, the cerebellum primarily supports motor coordination and balance. It ensures that voluntary movements are accurate and fluid. Damage to this region can result in ataxias, neurological disorders characterized by difficulties in movement precision and postural stability [1].

1.1.2 Major Brain Regions

As previously discussed, the brain is divided in four main lobes, as shown in Figure 2:

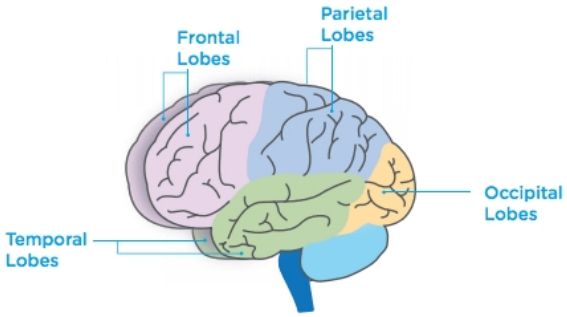

Figure 2: Brain's four main lobes.

- **Frontal lobes**
  Positioned at the anterior portion of the brain, the frontal lobes are considered the executive control due to their involvement in complex cognitive and behavioral regulation. These lobes integrate sensory data and association signals to plan and execute purposeful actions. They are key in decision making, reasoning, organizing sequential behavior and executing goal directed tasks. Their contribution also extends to language and speech regulation, facilitated through connections with motor planning networks. The orbitofrontal cortex, located in the lower front part of this region, plays a major role in processing emotions and in adapting behavior based on past outcomes. When damaged, the

frontal lobes can cause profound deficits in emotional regulation, personality stability and cognitive judgment, reflecting their importance in psychological functioning and executive behavior [2].

- **Parietal lobes**
  Located posterior to the primary somatosensory cortex, the parietal lobes are integral to integrating sensory input with cognitive processes, supporting perception, spatial orientation and memory. These lobes help individuals formulate action strategies and interact with their surroundings through spatial awareness and motor planning. The posterior part, in particular, is involved in constructional and spatial abilities such as replicating shapes, assembling parts or coordinating tasks that require visual-spatial reasoning. The right hemisphere of the parietal is especially involved in body awareness and spatial cognition, helping map the position of the body parts in space. Lesions in this region may lead to deficits in spatial relationships and tactile processing, impacting motor coordination and perception [2].

- **Temporal lobes**
  Situated on the sides of the brain, the temporal lobes are responsible for processing auditory stimuli and facilitating language understanding. They allow the brain to interpret environmental sounds and spatial properties such as distance and depth. At the core of this region is the auditory cortex, which is vital for sound perception and closely tied to memory formation. These lobes also support the connection between auditory experiences and mental visualization, enabling internal reconstruction of head information. This auditory imagery link is crucial in learning, as the temporal lobes play a significant role in creating and retaining long term auditory memories. Damage in this region can impair auditory memory, resulting in conditions like amnesia or disruptions in speech comprehension [2].

- **Occipital lobes**
  Found in the posterior-inferior part of the brain, the occipital lobes serve as the primary visual processing center. These lobes decode incoming visual information, transforming raw stimuli into coherent images that the brain can understand and store. Containing the brain's primary and secondary visual cortices, the occipital region supports recognition, movement detection, spatial orientation and also contributes to language comprehension through visual input. The visual memories formed here connect past experiences to present observations, helping to interpret and react to new stimuli. Damage to this area can significantly affect visual recognition, making it difficult to recognize faces, identify objects or associate images meaning and language, resulting in various forms of visual agnosia [2].

1.1.3 Neurons

Neurons are the primary operational units of the nervous system, structured with specialized regions that support their functional role. These cells are inherently asymmetrical, possessing distinct parts dedicated to receiving incoming signals and sending information onward. Communication between neurons occurs through the release of chemical messengers called neurotransmitters, which are discharged into the synaptic cleft, the small space separating two neurons.

Neurotransmitters, which can be proteins, peptides or small molecules, carry messages across this gap to the adjacent neuron, where they are received through endocytosis. The neuron dispatching the signal is called the presynaptic neuron, while the one receiving it it is called postsynaptic neuron. Inside each neuron, messages are conveyed via action potentials, brief and rapid electrical events triggered by shifts in the cell's membrane potential. These electrical signals allow for fast and efficient transmission throughout the nervous system.

The neuron's ability to transmit these signals relies on its key components: dendrites, a cell body (soma) and an axon, as shown in Figure 3. Dendrites, which are short, branching extensions, collect information from other neurons. The extent and complexity of these branches influence how signals are received and processed[1].

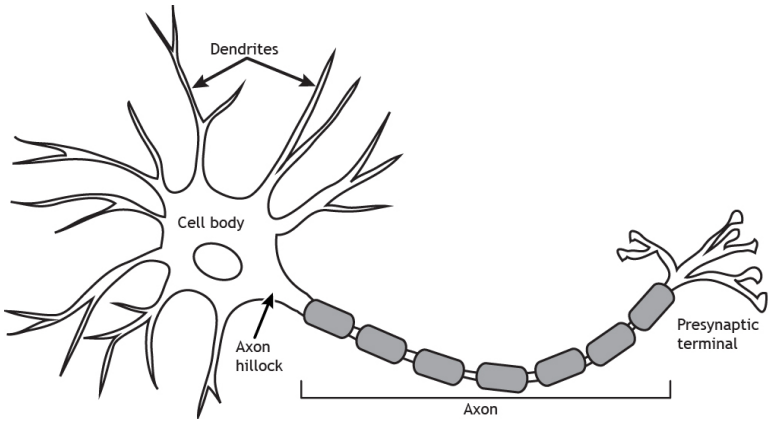

Figure 3: Neuron's components.

These dendritic structures emerge from the soma, which contain the nucleus and is responsible for producing proteins like neurotransmitters. These substances must be transported to precise locations within the neuron, especially to sites where they are secreted into synapses to influence neighboring neurons. The axon, a long and narrow projection, carries these signals away from the cell body. It originates at the axon hillock, a region crucial for both protein synthesis and the initiation of action potentials once sufficient stimulation has been received. The axon hillock also controls which proteins enter the axon, maintaining tight regulation of signal transmission. Neurotransmitters are ultimately released from the presynaptic terminals at the end of the axon.

Neurons can be categorized in several ways based on their form and function. The three main types are sensory neurons, motor neurons and interneurons.

Sensory neurons, typically unipolar in structure, have two short extensions, a dendrite and an axon, that facilitate the relay of sensory input. Motor neurons are multipolar, featuring numerous extensions that allow them to transmit motor commands. Interneurons, which connect sensory and motor neurons and also contribute to memory and decision making, generally display a bipolar form. While sensory and motor neurons operate both the central and peripheral nervous systems, interneurons are found exclusively within the central nervous system. Additionally, neurons may be classified based on whether they stimulate, excitatory, or inhibit, inhibitory, signal transmission, or by the specific neurotransmitters they release [1].

1.2 Electroencephalogram

Electroencephalography (EEG) is a non-invasive method used to record the brain's electrical activity by measuring potential fluctuations on the scalp. This technique offers a dynamic representation of brain function and is widely used in both clinical and research settings. It is particularly valuable for diagnosing neurological conditions as epilepsy, brain tumors, head trauma, sleep disorders, dementia and for monitoring anesthesia depth during surgical procedures. EEG can also assists in assessing behavioral and developmental conditions like autism, attention deficits, learning challenges and speech delays.

The history of EEG dates back to 1929, when Hans Berger first introduced a device capable of recording the brain's electrical signals. Berger, a neuro psychiatrist, coined the term 'Elektrenkephalogram' to describe these recording and proposed that brain activity varies depending on the brain's functional state, including sleep, anesthesia and pathological conditions.

EEG recordings are obtained by placing multiple electrodes on the scalp, typically using conductive paste or temporary adhesives. These electrodes detect the tiny voltage changes generated by neurons, which are then am-

plified and visualized as waveforms on a computer screen. Depending on the setup, an EEG may involve from just a few electrodes to over 250, in what are called multichannel recordings. Each recording channel reflects the voltage difference between two points on the scalp [3].

There are two main EEG recording types: scalp EEG, where electrodes are placed externally on the scalp, and intracranial EEG, which involves the insertion of electrodes directly into the brain tissue. A variant of intracranial EEG called electrocorticography (ECoG) involves placing electrodes on the cortical surface during surgery. The typical amplitude of EEG signals recorded from the scalp ranges from 1 to 100 μV, whereas subdural recordings can reach amplitudes of 10-20 mV.

The positioning of the scalp electrodes is crucial, as the brain's anatomical regions are functionally specialized. The internationally accepted 10-20 system standardizes electrode placement using proportional distances (10% or 20%) between specific cranial landmarks, namely the nasion (bridge of the nose) and the inion (lower back of the skull). Electrode labels indicate both their cortical location (F for frontal, T for temporal, C for central, P for parietal, O for occipital) and hemisphere (even numbers for the right, odd for the left and 'z' for the midline).

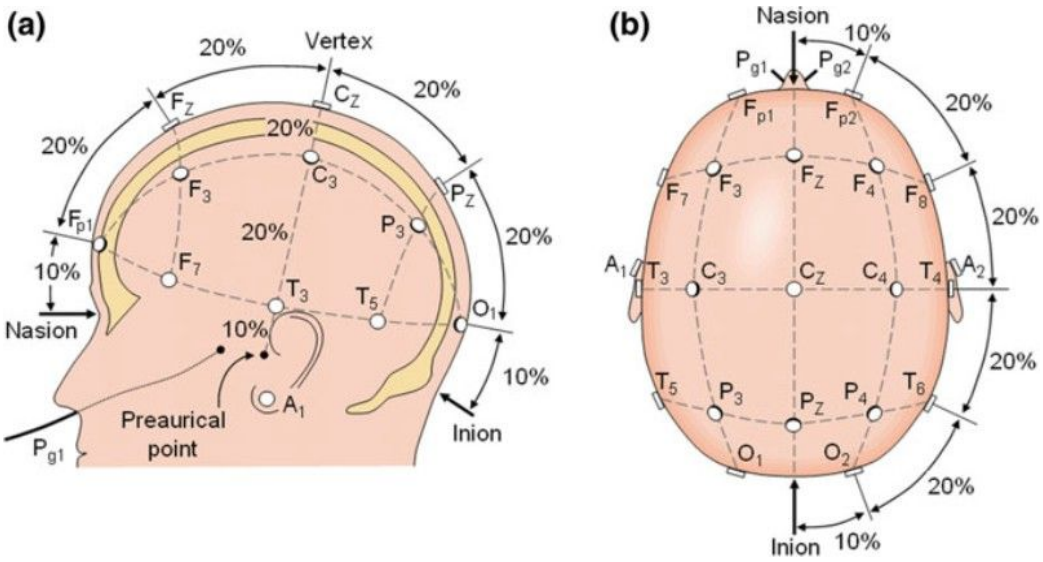

Figure 4: 10-20 % international system used to place electrodes on the scalp.

Various electrode configurations are used to display EEG signals. In a bipolar montage, each channel represents the voltage difference between two adjacent electrodes. A referential montage uses a single reference electrode for comparison against all other electrodes. The average reference montage calculates the mean signal across all electrodes as the baseline, while the Laplacian montage subtracts a weighted average of surrounding electrodes from each electrode's signal to improve spatial resolution [3].

The underlying signals captured in EEG recordings are generated by synchronized activity in large groups of neurons, primarily in the cerebral cortex. The cortex is the most significant contributor due to its proximity to the scalp and its role in higher cognitive processes such as decision making, language, movement and complex visual processing. The primary electrical events relevant to EEG are postsynaptic potentials (PSPs), which result from ion flows in dendrites and soma of pyramidal neurons. These low-frequency PSPs can summate and generate dipolar fields strong enough to be detected on the scalp. Conversely, action potentials, although fundamental to neuronal com-

munication, do not substantially influence EEG recordings because they are too localized and short lived.

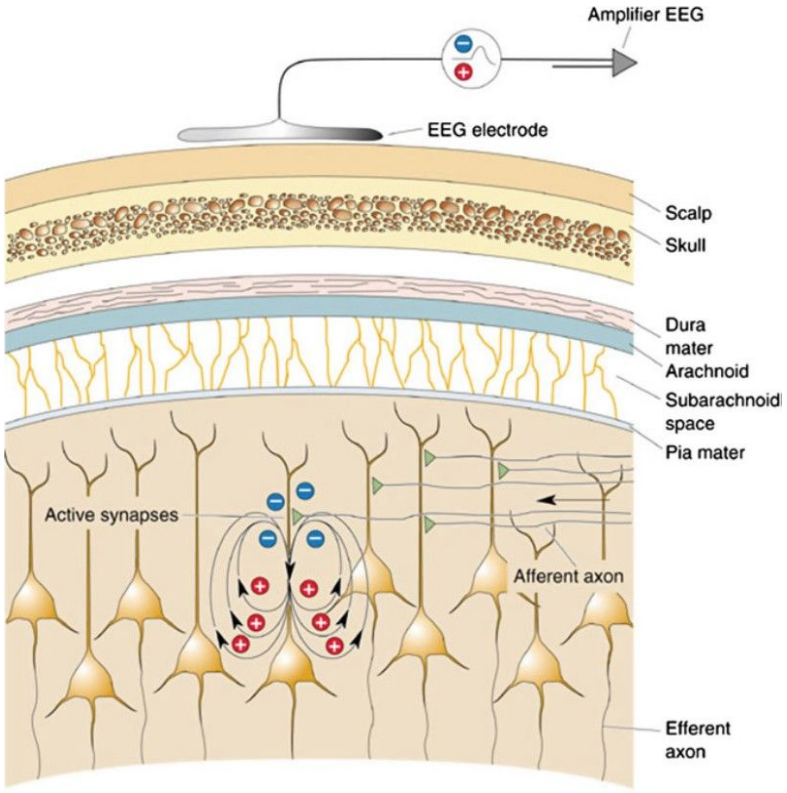

Figure 5: Generation of small electrical fields by synaptic currents in pyramidal cells.

Neural activity is governed by action potentials, where ion channels alter membrane potentials to create fast electrical impulses along axons. Neurotransmitters released at synapses allow neurons to communicate. If a postsynaptic potential is strong enough to reach a threshold, it may initiate a new action potential in the receiving neuron, continuing the cycle of neural signaling [3].

EEG signals are typically analyzed in terms of frequency, which helps characterized different mental and physiological states. Human brain rhythms are

divided into five major frequency bands: delta (0,5-4 Hz), theta (4-8 Hz), alpha (8-13 Hz), beta (13-30 Hz) and gamma (>30 Hz). Each band is associated with specific brain states: delta with deep sleep and certain pathologies, theta with drowsiness and emotional processing, alpha with relaxed wakefulness, beta with active thinking and focus and gamma with higher level cognitive functions. In healthy adults, EEG frequencies and amplitudes vary based on the mental state.

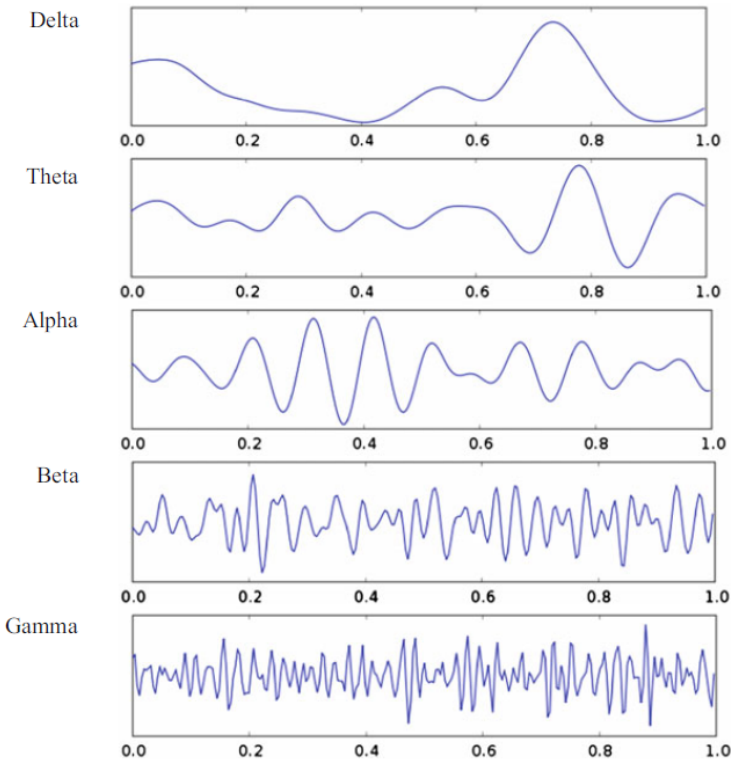

Figure 6: EEG frequencies band.

Delta waves are the slowest and highest in amplitude, commonly seen during deep sleep or in some abnormal brain states. Theta waves are associated with creativity, emotional responses and meditation. Alpha activity is typically observed when the eyes are closed and the subject is relaxed, especially in the

occipital regions. Beta activity is linked to alertness and active cognition, especially in the frontal lobes. Gamma oscillations, which may reach 80-100 Hz, are thought to reflect processes related to perception, memory and consciousness [3].

Despite its utility, EEG recordings are susceptible to various artifacts that can obscure true brain signals. Artifacts may arise from eye movements, poor electrode contact, swallowing or issues with the reference electrode. These often manifest as large-amplitude, slow waves or broad disruptions across channels and must be carefully managed during data pre-processing to ensure pathological interpretation.

In summary, EEG is a powerful tool for exploring brain function and diagnosis neurological and psychiatric conditions. By capturing the brain's rhythmic electrical activity across multiple channels and frequencies, EEG enables researchers and clinicians to gain insights into both normal brain function and pathological states.

2 Cardiac System

The heart is a vital organ for the human body, understanding its anatomy is essential for comprehending how electrical impulses are generated and propagated, which is reflected in the electrocardiogram (ECG) signal. The ECG serves as an important tool in monitoring the heart's electrical activity, offering insights into both normal and cardiac function and various pathological conditions.

2.1 Heart Anatomy

The heart is a muscular organ located within the thoracic cavity, specifically in the middle region of the mediastinum, just above the diaphragm. It sits at a slightly tilted angle, with the apex directed forward, downward and to the left. The heart is enclosed in a protective double layered sac known as the pericardium. This sac includes an outer fibrous layer and an inner serous layers. The serous pericardium is further divided into two parts: the visceral layer (epicardium), which adheres to the heart surface, and the parietal layer, which lines the inner surface of the fibrous pericardium. Between these layers lies a thin film of pericardial fluid that acts as a lubricant, reducing friction during heart contractions [4].

The heart wall is composed of three primary layers. The outermost layer, the epicardium, is followed by the myocardium, thick muscular layer responsible for contraction, and the innermost endocardium, a thin lining of endothelial tissue. The myocardium varies in thickness across different chambers, being particularly robust in the left ventricle and the inter-ventricular septum, where is organized into sub-epicardial, middle and sub-endocardial muscle layers. This muscular tissue also houses specialized conductive fibers and nodal tissue vital for initiating and transmitting electrical impulses.

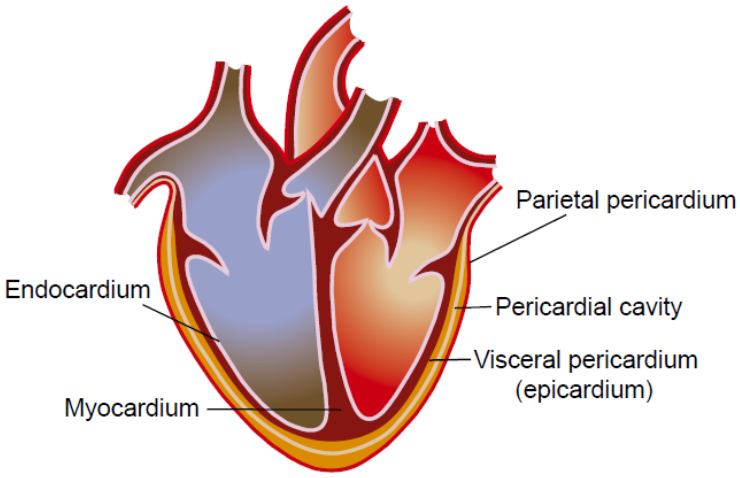

Figure 7: Heart's layers.

Structurally, the heart is divided into four chambers: two upper atria and two lower ventricles. The atria have thinner walls and function primarily to collect blood returning from the body and lungs, passing it into the ventricles. These ventricles are muscular chambers tasked with pumping blood either to the lungs (right ventricle) or to the systemic circulation (left ventricle). Four valves, tricuspid, pulmonary, mitral and aortic, ensure unidirectional blood flow through these chambers.

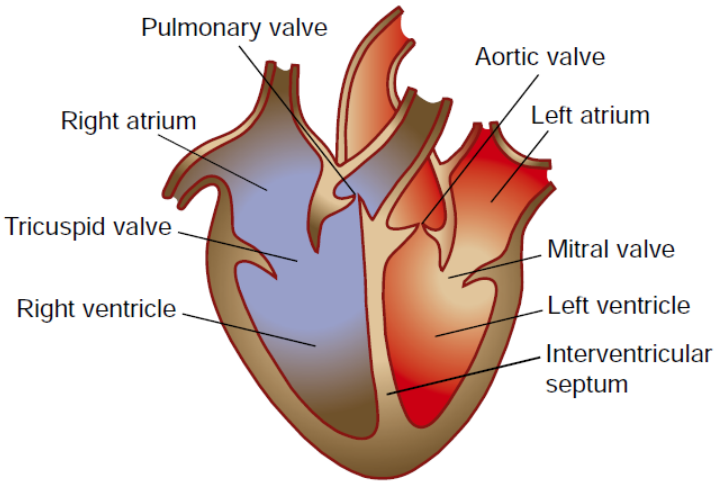

Figure 8: Heart's chambers and valves.

Embedded within the heart is a fibrous skeleton that provides structural support and electrically isolates the atria from the ventricles. This skeleton also serve as an anchoring framework for the cardiac valves. Within this fibrous structure is the central fibrous body, which includes the right and left trigones and the membranous part of the inter-ventricular septum. It plays a vital role in housing and protection the conduction system as it penetrates the septum [4].

Cardiac muscle fibers contain specialized contractile units called sarcomeres, composed of action and myosin filaments. These fibers are striated and mono-nucleated and are connected via intercalated discs, which facilitate synchronized contraction. The contraction mechanism relies heavily on calcium ion dynamics. T-tubules transmit action potential deep into the muscle fibers, triggering calcium release from the sarcoplasmic reticulum and initiating contraction.

The electrical activity of the heart is coordinated by the cardiac conduction system, which includes the sinoatrial (SA) node, atrioventricular (AV) node,

bundle of His, bundle of branches and Purkinje fibers. The SA node, located in the right atrium, acts as the heart's natural pacemaker, initiating electrical impulses that spread through the bundle of His and into the ventricles via the Purkinje network, ensuring synchronized contraction.

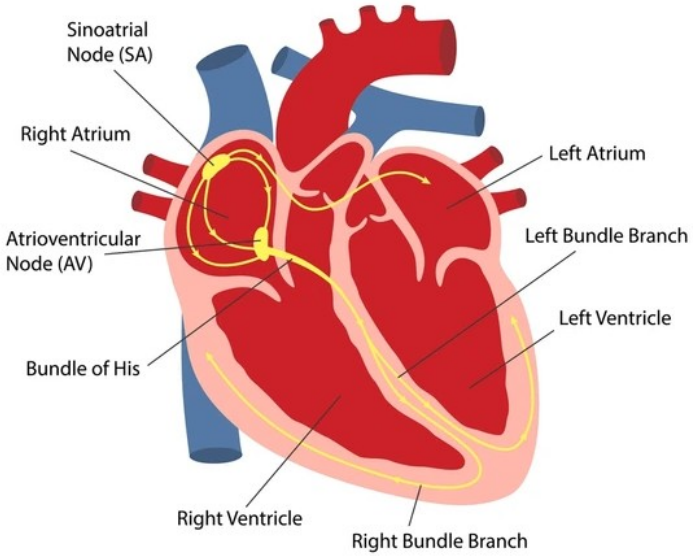

Figure 9: Heart's electrical conduction system.

Autonomic regulation of the heart is managed by the cardiac plexus, which contains sympathetic and parasympathetic fibers. Sympathetic stimulation increases heart rate and contractility, while parasympathetic input, primarily via the vagus nerve, exerts an inhibitory effect. This balance is modulated by central nervous system structures such as the medulla and hypothalamus, responding to feedback from baroceptors and chemoceptors throughout the body [4].

Functionally, the heart operates in a cycle of contraction (systole) and re-

laxation (diastole). The cycle begins with atrial contraction, followed by ventricular contraction and subsequent ejection of blood. Electrical impulses precede these mechanical actions, observable on an electrocardiogram as the P wave, QRS complex and T wave . Heart sounds generated during this cycle are indicators of normal or abnormal cardiac function.

Finally, the heart's performance is tightly linked to its structural and electrical integrity. Disruption in any anatomical or physiological component can result in impaired cardiac output, arrhythmia, or systemic complications. The comprehensive understanding of heart anatomy is therefore essential in diagnosing and treating cardiovascular conditions effectively.

2.2 Electrocardiogram (ECG)

The electrocardiogram (ECG) is a fundamental diagnostic tool in cardiac electrophysiology, used to monitor the electrical activity of the heart in both clinical and critical care settings. It provides a non invasive way to observe and evaluate the rhythmic and conduction properties of cardiac function over time. This electrical activity is primarily generated by specialized pacemaker cells, which possess the intrinsic ability to depolarize and repolarize spontaneously, functioning similarly to a relaxation oscillator. These impulses, once generated, propagate through the cardiac tissue, ensuring coordinated contraction.

The SA node, serving as the heart's primary pacemaker, under normal physiological conditions sets the rhythm of the heartbeats. The AV node acts as a secondary pacemaker, possessing slower intrinsic rhythm that only initiates impulses when the SA node fails or is delayed. Once an impulse originates in the SA node, it travels across the atrial muscle. The atria and ventricles are connected through the AV node, a region that conducts impulses slowly to allow a delay between atrial and ventricular activation. From there, the signal proceeds into the bundle of His , which divides into left and right

bundle branches. These branches further distribute through Purkinje fibers, facilitating efficient excitation of the ventricular myocardium [5].

The ECG represents the voltage differences detected by electrodes placed on the body surface in specific configurations called leads. These electrodes capture the electrical signals resulting from cardiac depolarization and repolarization. Classical limb leads (leads I, II, III) record potential difference between pairs of electrodes on the limbs, following Einthoven's triangle and satisfying Einthoven's law :

$$LeadII = LeadI + LeadIII \tag{1}$$

In addition to the standard limbs, augmented leads (aVR, aVL, aVF) are derived by comparing each limb electrode to a calculated average potential known as the Wilson Central Terminal (WCT), created by connecting equal resistors to the three limb electrodes. Precordal or chest leads (V1,. . . ,V6) further complement the recording by providing spatial information from the anterior chest wall overlying the heart [5].

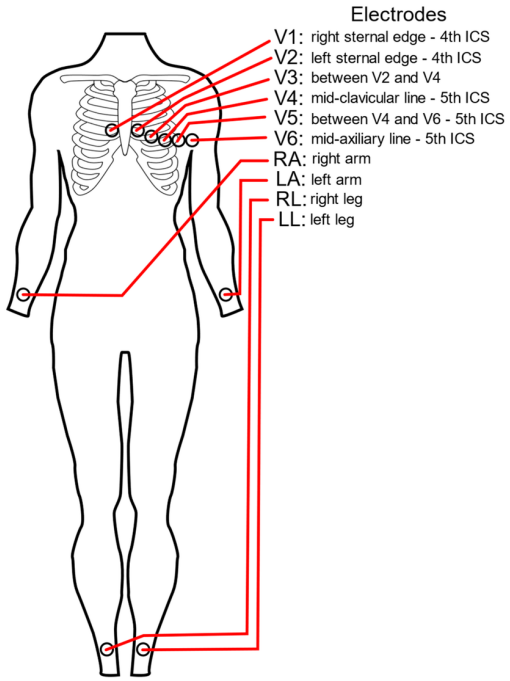

Figure 10: Leads electrodes placement.

A typical ECG trace consists of several characteristics waveforms corresponding to different phases of the cardiac cycle. The P wave reflects atrial depolarization. The QRS complex represents rapid ventricular depolarization and is usually the most prominent feature. The T-wave follows, indicating ventricular repolarization. In some cases, a U wave appears after the T wave, though its origin remains debated; it is thought to be linked to after-depolarizations or late phases of repolarization. The atrial repolarization is usually masked by the QRS complex due to its smaller amplitude.

The components of the QRS complex include the Q wave (initial negative deflection), the R wave (first positive peak) and the S wave (subsequent negative deflection). Not every component appears in all leads and additional notches or deflections may also be observed depending on the individual cardiac morphology [5].

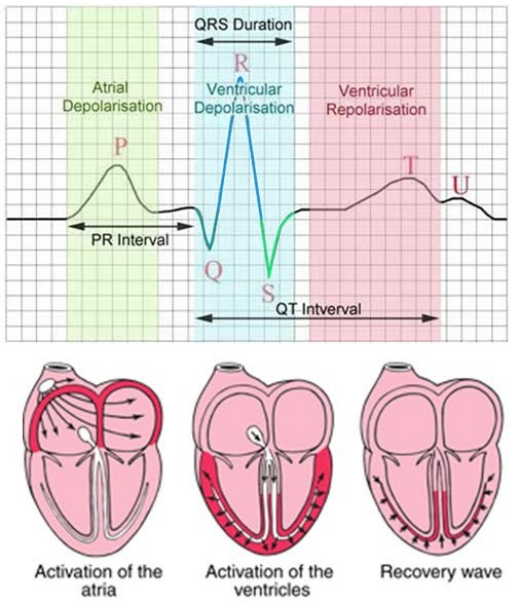

Figure 11: ECG waves.

ECG analysis involves evaluating both the morphology of the waveforms and their temporal relationships. Variations across multiple cardiac cycles can reveal valuable insights into rhythm abnormalities, conduction disturbances, or myorcardial damage. Moreover, factors influencing the signals may be intrinsic (changes in action potential, propagation) or extrinsic (changes in tissue conductivity). In some clinical cases, internal electrodes (placed in the esophagus or directly on the heart) are used for higher resolution recordings, particularly to diagnose arrhythmia or conduction defects.

Ultimately, the ECG remains an indispensable tool in cardiovascular medicine, offering critical diagnostic information with broad applicability across health care and research settings.

3 Binaural Beats

This section is dedicated to the discussion of the *Binaural Beats* (BB), with the aim of providing a clear definition and a deeper understanding of how they work. Initially, research on BB focused on understanding the functioning of the binaural auditory system. However, over the past couple of decades, the focus has shifted toward investigating their effects on cortical activity. These aspects will be discussed in a more detailed way in the following sections.

What has sparked growing interest in this field is the fact that BB are an illusory perception that manifests when two sine waves, played separately to each ear, differ by an amount between 2-30 Hz, allowing to stimulate the cerebral activity within a range of frequencies that covers most of its spectral content [6].

Specifically, this research was motivated by the Brainwave Entrainment Hypothesis associated with BB, which refers to the possibility of modulating brain's electro cortical activity thanks to the application of a visual or auditory stimulus, making it oscillate at or around the frequency of stimulation [7]. Based on this theoretical framework, BB were employed in this study as a non invasive brain stimulation technique.

3.1 Description

The BB phenomenon was described for the first time in 1839 from a german experimenter H.W. Dove, and he referred to slow modulation that were perceived after a neural elaboration of particular mechanisms of the auditory binaural system, when two pure tones (sine waves) with slightly different frequencies were presented simultaneously, separately to each ear. [8].

To clarify the concept, let's consider what is shown in Figure 12. If the right ear is presented with a pure tone at a frequency of 400 Hz, and the left ear simultaneously receives a pure tone at 410 Hz, a third one (known

as a beating tone) will be perceived. This tone will have amplitude that fluctuates cyclically with a frequency of 10 Hz.

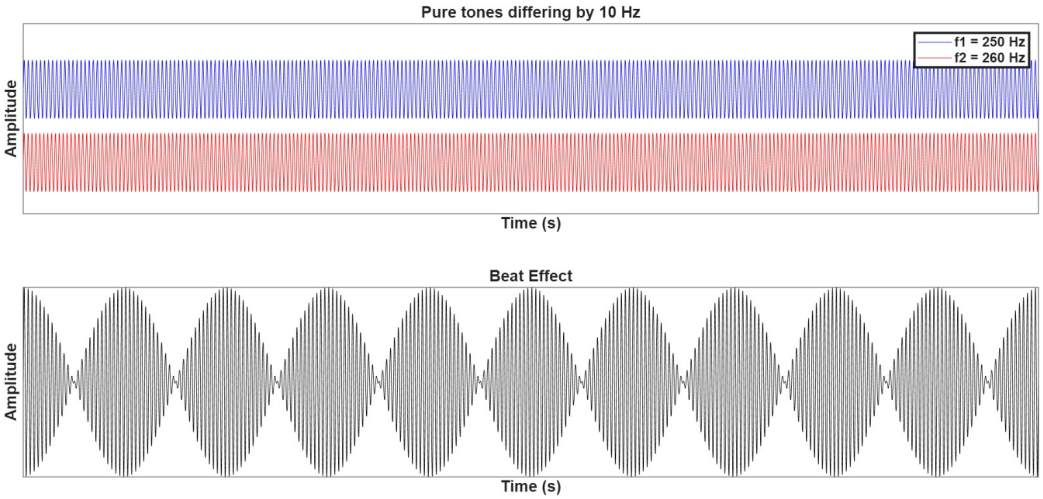

Figure 12: Visual description of the beat effect.

3.2 State of the Art

A large portion of literature on BB has developed during the second half of the 20th century. Authors such as Oster, Licklider, Perrott and Nelson have significantly contributed to the field through systematic studies aimed at better understanding the relationship between stimulation parameters and auditory perception [9].

The perception of BB depends on several factors, primarily related to the design parameters of the auditory stimulus. These include the carrier frequency, the frequency difference between two sine waves (also referred to as stimulation frequency, beat frequency, or interaural frequency), the intensity of the tones, and the duration of the signal.

One of the most investigated aspects concerns the identification of the frequency range of the carrier tone within which binaural beats are perceptible.

Some studies suggest that below 90 Hz, participants tend to confuse the beat with the tones used to generate it, making the phenomenon difficult to detect as a distinct percept [8]. However, Licklider et al. reported a lower perceptual threshold of approximately 63 Hz for BB [10].

As for the upper limit, there is general agreement in the scientific community that the ability to perceive BB, gradually decreases as the carrier frequency exceeds 1000 Hz [10][8]. In this context, the study by Perrott and Nelson is particularly noteworthy: they assessed beat perception as the carrier frequency (f_0) increased, and found that at frequencies of 1000 Hz, 1200 Hz, 1500 Hz and 1800 Hz, the percentage of recognized beats was below 35% [11]. Nevertheless, the literature presents a high degree of heterogeneity regarding the absolute upper limit of BB perception. Above a certain carrier frequency, the beats may no longer be perceived, and this threshold can vary depending on several factors, including the specific stimulation parameters used in different experimental protocols and individual differences in auditory processing. Licklider also highlighted that one of the key factors influencing BB perception is the frequency difference (δf) between two tones. Another important finding from his research was the identification of the maximum frequency difference at which binaural beats remain clearly perceptible. Specifically, it was shown that BB could be correctly identified with frequency differences up to 35 Hz, particularly when the carrier frequency was around 400 Hz [10].

The difference between the two tones not only influences the upper frequency limit for the perception of BB, but also affects the way the sound is perceived.

If the frequency difference between the two sine waves is too small, the listener perceives a singles auditory image that appears to move from one ear to the other at a rate equal to the interaural frequency difference. This phenomenon is known as a rotating tone. As the frequency differences increases, the listener begins to perceive periodic fluctuations in sound intensity. Within the range of approximately 2 to 10 Hz, a single tone is perceived that seems

to pulse, modulating in amplitude. This response is generally associated with the perception of BB.

If the frequency separation continues to increase, the intensity fluctuations become progressively less distinct. When the interaural frequency difference exceeds 20 Hz, the perceived tone acquires a rough quality, and the beat becomes too rapid to be interpreted as an amplitude modulation in the way BB are typically understood.

Finally, when the frequency difference between the two tones surpasses a certain threshold, the tones are no longer fused centrally, and the listener perceives the mas two distinct sounds, each localized separately in one ear [10][12].

The relationship between δf and f_0 in the perception of binaural beats has been further explored by David R. Perrott and Michael A. Nelson [11]. In their study, the authors produced a series of curves illustrating the efficiency of BB identification as a function of both the carrier frequency and the interaural frequency range for BB perception is between 250 and 500 Hz [11].

Other factors that actively influence the perception of BB include the intensity difference between the two tones and the duration of the stimulus. It has been shown that, when the signal is presented continuously, the two tones must have equal amplitude in order for BB to be perceived. This requirement, however, doesn't apply when the stimulus is presented alternately with a reference tone [13].

Regarding the influence of signal duration, it has been observed that binaural fusion typically occurs for durations exceeding 320 ms [14].

Since each brain wave frequency band can be directly correlated to specific psychological and physiological states, the idea has been to specifically select the oscillation frequency of BB in order to guide the subject towards a particular mental state [15].

This has recently led research efforts to investigate the psychological effects induced by the stimulation through BB [16]. Specifically, studies examined the effects of listening to BB on information processing and elaboration [17] [18] [19], mood [20] [21], pain perception [22] [23], increased concentration [24], meditation [25] and relaxation [26].

Although it is easy to understand how the brain's cortical activity can adapt and synchronize with an external stimulus, if its frequency falls within one of the EEG bands, leading to constructive interference increasing the power within the specific band, the evidence and the results presented in the literature appear to be controversial and contradictory [27], making it difficult to confidently assert that BB can interfere with cortical activity, modulating actively brain waves.

In the cited studies, BB were applied using a fixed stimulation frequency without personalization to individual characteristics, and were administered in a single session, thereby excluding the possibility that their effects might require a training period.

3.3 Experimental Question

The study conducted within this thesis aims to answer the following experimental questions:

- *"Can EEG signals show real changes in brain activity or physiological state during or after listening to BB?"*
- *"Is the BB effect on the cerebral rhythm immediate or does it require a training period in which the subject can synchronize more efficiently with the rhythm of the beats?"*
- *"Does BB stimulation modulate the cerebral rhythm in the target frequency band?"*

Therefore, the goal of the study is to understand if BB can interact with cerebral rhythm and to examine their long term-effects. To answer all of it a experimental protocol has been created, which will be discussed in the next section.

4 Materials and Methods

This chapter will provide a detailed overview of the protocol design phase and of the techniques and instrumentation used for the acquisition and processing of EEG and ECG signals recorded during the various acquisition sessions.

4.1 Instrumentation and Software

4.1.1 Enobio

The Enobio 8 is the main instrument used in this study, enabling the acquisition of EEG data through its channels. Specifically, this experimental protocol employs the Enobio 8 version, which consists of the Enobio Necbox (Neuroelectronics Control Box) the central unit that contains all the electronics components and communicates with the computer via Bluethooth connection, eight Ag/AgCl electrodes known as NG Geltrodes shown in Figure 14, which are placed inside a neoprene cap, and a 10 channel connector, of which 8 are used for the active signal acquisition and 2 channels serve as references (CMS and DRL). The neoprene cap features 64 slots, corresponding to the positions defined by the international 10-10 system, allowing for custom electrode placement based on experimental needs. The Enobio 8 system records the EEG signals at a sampling frequency of 500 samples per second (SPS) and operates within a frequency bandwidth ranging from 0 to 125 Hz. The configuration of the system is shown in Figure 13 [28]. EEG data acquisition is managed through the NIC2 software, which allows real time signal analysis.

Figure 14: NG Geltrode.

Figure 13: Enobio 8 setup.

4.1.2 NIC2

The NIC2 software is essential for operating the Enobio 8 system. It communicates with the Necbox via a Bluetooth connection, allowing the real-time streaming of recorded EEG data.

The software enables users to configure the recording protocol by customizing several parameters such as the duration of the acquisition, the insertion of event triggers, the assignment of specific channels to defined scalp positions, the reference configuration and the use of notch filters to reject power line interference at 50 Hz or 60 Hz, depending on the recording environment. Regarding the electrodes assignment caution is required: as previously mentioned, the neoprene cap follows the international 10-10 system, whereas the software interface is based on the international 10-20 system, as shown in Figure 15. Therefore, when selecting electrode positions within the software, it is essential to choose slots that are common to both systems, in order to ensure correct correspondence between physical and virtual placement.

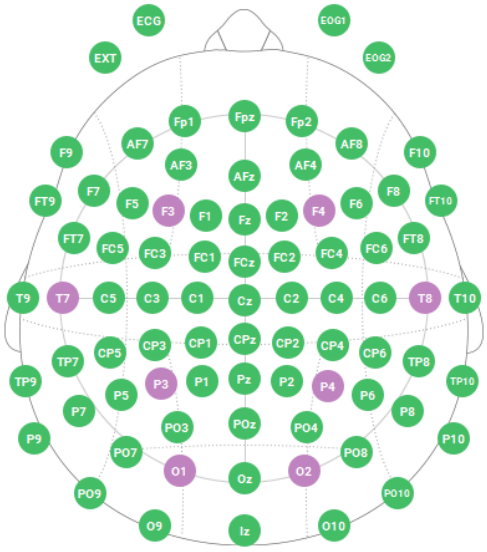

Figure 15: Taken from the NIC2 software, this interface shows the electrodes positions of the 10-10 system: selected electrodes are highlighted in purple, while unused ones in green.

Specifically during the acquisition, it is possible to visualize the live EEG signals, selecting specific channels of interest, adjusting the preferred amplitude scale, choosing the referencing method and inserting event triggers to mark specific occurrences, which facilitates offline data analysis. Real time signal evaluation is further supported by the presence of a indicator called Quality Index (QI), which informs the user whether the acquisition is proceeding correctly, as shown in Figure 16.

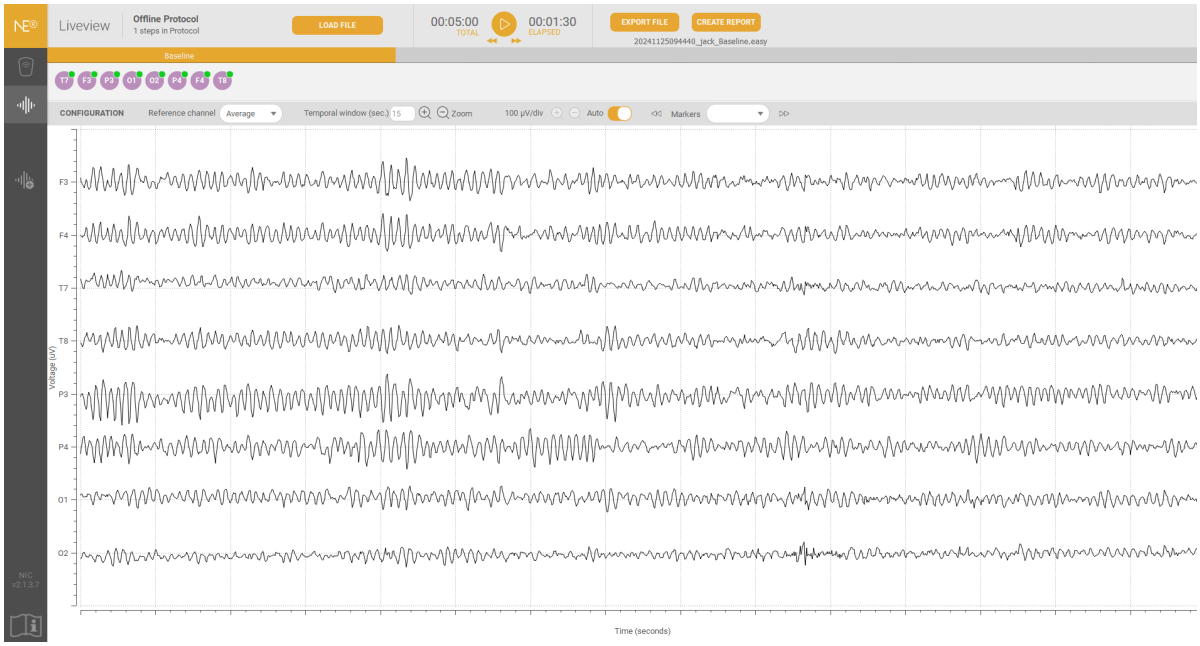

Figure 16: Live stream of the EEG recording.

The software allows EEG data to be saved the in various formats, including *.easy*, *.edf*, *.nedf* and *.sdeeg*. In this study, the *.easy* format was used, and an additional *.info* file is generated containing the metadata related to the acquisition parameters.

The *.easy* file is organized into 13 columns. The first 8 contain the temporal samples expressed in ηV of the EEG signal recorded from each channel selected during the protocol design phase. Columns 9 to 11 report the acceleration values along the three axes of the reference system by the acquisition device, located inside the Necbox. Lastly, columns 12 and 13 respectively contain the event trigger, if any, and the Timestamp expressed in ms.

4.1.3 Matlab

This software is fundamental for the offline analysis of the signals recorded with the Enobio 8. It provides a virtual environment where custom algo-

rithms can be programmed using the software's proprietary language. In this study, it was used as the main platform to implement the entire signal analysis pipeline, starting from pre-processing to feature extraction, clustering using a k-means algorithm and statistical analysis. This is made possible by built-in functions and toolboxes that support specific algorithms tailored to particular data. Specifically, the EEGLAB toolbox was used, which is dedicated to EEG signal analysis and offers advanced tools for managing, visualizing and processing electroencephalographic data.

4.1.4 Polar H10

The Polar H10, shown in Figure 17, is a high precision heart rate equipped with the *Polar Pro* chest strap. It is considered by numerous sources to be one of the most accurate heart rate monitors available, capable of delivering high quality readings with minimal interference.

The sensor allows for data connection and transfer via *Bluetooth®* e *ANT+™* connected, offering a wide range of connectivity options with compatible sportwatches, smartwatches and training apps [29].

Figure 17: Polar H10.

4.1.5 Visual Studio Code

Visual Studio Code (VS Code) is a source code editor developed by Microsoft, compatible with most operating systems currently available on the market, including *Windows*, *macOS* and *Linux*.

This editor is widely used among developers thanks to its appealing features: it is free to use, supports various programming languages such as *Python*, *C++*, *JavaScript* and *HTML*, and offers an integrated debugger, built-in syntax checking, and intelligent code completion based on IntelliSense.

In addition, it allows developers to work on remote environments, all through a versatile and user friendly graphical interface.

4.2 Data Analysis Techniques

4.2.1 ICA

Independent Component Analysis (ICA), originally proposed by Pierre Comon in 1992 [30], is a widely adopted signal processing approach used to recover hidden source signals that have been linearly combined and recorded across multiple sensors. This methods belongs to the category of blind source separation techniques, as it functions without requiring prior knowledge about the mixing mechanism or the nature of the original signals. ICA aims to isolate latent components by minimizing statistical dependencies among them, relying solely on the temporal dynamics of the input data to apply a linear transformation that maximizes independence [31] [32].

The ICA model assumes that, at any given time point k, the observed signal vector $x(k) = [x_1(k), ..., x_n(k)]^T$, is generated by a linear mixture of m unknown source signals $s_i(k)$such that :

$$\mathbf{x}(k) = \sum_{i=1}^{m} a_i s_i(k) = \mathbf{A}\mathbf{s}(k) \tag{2}$$

Where $s(k) = [s_1(k), \ldots, s_n(k)]$ represents the statistically independent sources and $A = [a_1, \ldots, a_m]$ represents the unknown mixing matrix. ICA seeks to estimate these sources $\hat{s}(k)$ through an un-mixing matrix $B = A^{-1}$ allowing source reconstruction:

$$\hat{\mathbf{s}}(k) = \mathbf{B}\mathbf{x}(k) \tag{3}$$

To function correctly, ICA relies on several assumptions. First, the source signals must be mutually statistically independent. Additionally, it is typically required that both the mixing process and the distributions of the source signals remain stationary during the analysis window. A further constraint is that the number of sources doesn't exceed the number of sensors, ensuring the mathematical tractability of the model and the invertibility of the mixing matrix [33].

In electroencephalography (EEG) studies, ICA has proven especially valuable. Scalp EEG signals are thought to reflect linear mixtures of underlying cortical activity, where each neural source contributes with varying strength across different electrodes. These projections are influenced by factors like the electrode-source distance, dipole orientation and conductive properties of the brain and surrounding tissues.

Due to the predominance of short range cortical connections and limited long range connectivity,a biologically plausible assumption is that cortical regions tend to act as relatively independent sources over time. This supports the application of ICA to EEG data under the assumption of spatial and temporal independence between such patches [32].

Key applications of ICA in EEG include the removal of non neural artifacts, such as eye blinks or muscle activity, and the decomposition of EEG data for the analysis of brain responses to stimuli. Multiple ICA algorithms exist for this purpose, including JADE [34], Infomax [35] and FastICA [36]. In this

study, the algorithm used is the extended Infomax ICA variant developed by Lee et al. 1999 [31].

Extended Infomax ICA

The extended version of the Infomax algorithm builds upon the original framework introduced by Bell and Sejnowski, maintaining its foundational architecture. The core principle behind the Infomax approach is grounded in the observation that independent sources in real-world signals, such as EEG, tend to exhibit non Gaussian distributions. However, when multiple sources are combined linearly, their resulting mixture approximates a Gaussian distribution, as predicted by the central limit theorem [35].

The algorithm's objective is to reverse this mixing process by identifying a transformation that separates the recorded signals into statistically independent components that are as non Gaussian as possible. To achieve this, the observed signal vector x is linearly transformed into a new vector u, using weight matrix W and a bias term W_o:

$$u = W * x + W_o \tag{4}$$

A non linear activation function $g()$ is then applied to u produce the system's output y:

$$y = g(u) \tag{5}$$

The use of a non linear function is crucial, as it enables access to higher order statistical features of the data, which are essential for assessing and enhancing the non Gaussianity of the recovered sources [35].

The process of making the sources independent in Infomax revolves around maximizing the mutual information between the system's input x and output y, defined as:

$$I(Y, X) = H(Y) - H(Y|X) \tag{6}$$

Where $H(Y)$ is the entropy of the output and $H(Y|X)$ is the conditional entropy of the output given the input. When the transformation from x to y is deterministic, the conditional entropy term vanishes, and maximizing the mutual information becomes equivalent to maximizing the output entropy.

In practice, the algorithm also seeks to reduce redundancy aiming outputs by minimizing mutual information between them. For two outputs, y_1 and y_2, the joint entropy is expressed as:

$$H(y_1, y_2) = H(y_1) + H(y_2) - I(y_1, y_2) \tag{7}$$

Hence, by maximizing the joint entropy through reducing mutual information $I(y_1, y_2)$ the algorithm ensures that the outputs are statistically independent. The ultimate goal is to determine a weight matrix W that produces an output vector y whose components are both maximally informative and mutually independent.

The extended Infomax algorithm, developed by Lee, Girolami and Sejnowski [31], introduces an adaptive learning mechanism that extends the original model's capabilities. Unlike the standard Infomax, which uses a fixed non linearity, this version dynamically adjusts the activation function based on the statistical properties of the sources. This adaptability allows it to effectively separate both super Gaussian sources, characterized by sharply peaked distributions with heavy tails (positive kurtosis), and sub Gaussian sources, which typically exhibit flatter, sometimes bimodal distributions (negative kurtosis).

4.2.2 PCA

Principal Component Analysis (PCA) is a foundational tool in multivariate data analysis [37], commonly used for purposes such as reducing data dimensionality, visualizing underlying structures, filtering noise, selecting relevant features and constructing interpretable models. Moreover, PCA serve as a preliminary step in tasks such as clustering, classification, and outlier detection. While Pearson originally introduced PCA from a statistical standpoint [38], it was Hotelling who formalized the technique into its modern from in 1913 [39]. Although many variants have been proposed over time [40], this section focuses on the classical formulation of PCA.

At its core, PCA seeks to transform a set of correlated variables into a new set of uncorrelated variables known as Principal Components (PCs). Given a data matrix $X \in R^(np)$, where n is the number of observations and p the number of variables describing each observation, the goal is to find linear combinations of the original variables that capture the highest possible variance. These combinations are of the form:

$$\sum_{j=1}^{p} a_j x_j = Xa \tag{8}$$

where x_j is the observation vector for the j-th variable, and a is a vector of coefficients $[a_1, ..., a_j, \ldots, a_p]$. The variance of this linear combination is:

$$var(Xa) = a^T Sa \tag{9}$$

with $SR^{(pp)}$ being the covariance matrix of the dataset.

To determine the direction a that maximizes this variance, a constrain $a^T a = 1$ is imposed to ensure a unit norm. This leads to the optimization of the following Lagrangian:

$$a^T Sa - \lambda(a^T a - 1); \tag{10}$$

Where λ is a Lagrange multiplier. By differentiating with respect to a and setting the gradient to zero, we obtain the classic eigenvalue problem:

$$Sa = \lambda a \tag{11}$$

Thus, the principal components correspond to the eigenvectors of the covariance matrix S, and their associated variances are the eigenvalues λ. Each principal component Xa_k represents a new variable, where a_k contains the PC loadings, and the corresponding projections for all observations are called PC scores.

An equivalent approach to PCA involves applying Singular Value Decomposition (SVD) to the mean centered data matrix X^*. The decomposition takes the form:

$$X^* = ULA^T \tag{12}$$

Where:

- $A \in R^{(p \times r)}$ contains the right singular vectors (PC loadings),
- $U \in R^{(n \times r)}$ contains the left singular vectors (PC scores),
- $L \in R^{(r \times r)}$ is a diagonal matrix with the singular values of X^*.

The variance of each principal λ_i component can be derived from the singular values l_i of X^* as follows:

$$\lambda_i = \frac{l_i^2}{n-1} \tag{13}$$

To project the data onto a reduced q-dimensional space (where $q < r$), one may retain only the first q components of the SVD:

$$X_q^* = U_q L_q A_q^T \tag{14}$$

This projection provides the best rank-q approximation to the original data in terms of minimizing the mean squared reconstruction error. Among all such projections, this one preserves the greatest amount of variance, fulfilling Pearson's criterion for optimal linear approximation [38].

From this perspective, PCA is a specific case of SVD applied to the column centered data matrix. The PCs correspond to the right singular vectors, and projecting the data along these directions yields the optimal reduced dimensional representation in a linear subspace.

4.2.3 K-Means

Clustering is a fundamental task with widespread applications in areas such as pattern recognition, data mining, vector quantization, knowledge discovery and data compression. Among the various clustering techniques, k-means clustering stands out as one of the most widely used and well established approaches [41].

The core goal of the k-means algorithm is to partition a dataset $X \in R^d$, containing n elements, into k clusters such that the within cluster variance is minimized. This typically expressed through an objective function, often referred to as potential function Θ, which computes the sum of squared

distances between each data point and the nearest cluster centroid. The function is formally defined as:

$$\Theta = \sum_{x \in X} min_{c \in C} |x - c|^2 \tag{15}$$

Where $C = c_1, c_2, \ldots, c_k$ denotes the set of centroids.

The aim of k-means clustering is to identify the optimal configuration of centroids C hat minimizes Θ. Once the centroids are initialized, data points are assigned to the closest centroid, forming a partition of the dataset.

A commonly used algorithm to find such a solution is known as Lloyd's algorithm, which iteratively converges to a local minimum of the potential function [42] [41]. This algorithm proceeds in four primary steps:

1. Initialize k centroids $c_1, c_2, \ldots, c_k$.
2. Assign each data point to the nearest centroid, forming clusters $C_i \in X$ for $i = 1, \ldots, k$.
3. Update each centroid c_i to be the mean of the points in cluster C_i, using the formula:
$$c_i = \frac{1}{|C_i|} \sum_{x \in C_i} x \tag{16}$$
4. Steps 2 and 3 are repeated iteratively until the set of centroids C stabilized and no longer change.

The rationale behind the algorithm is that both the assignment step (Step 2) and the update step (Step 3) are guaranteed to decrease the potential function Θ, which measures the within cluster variance.

4.3 Protocol Design

The study has been conducted on a single group of 11 university students, with a mean age of $24,8 \pm 1,6$ years. Since there is evidence that, below a carrier frequency of 595 Hz there are no differences in terms of BB perception based on sex [43], both male and female participants were recruited, specifically the 4 females and 7 males.

To be included in the experimental study, participants were required to meet the following criteria:

- No hearing impairments or related auditory issues
- No history of neurological conditions, concussions, head trauma, or clinically diagnosed psychological disorders
- No prior experience with binaural beats

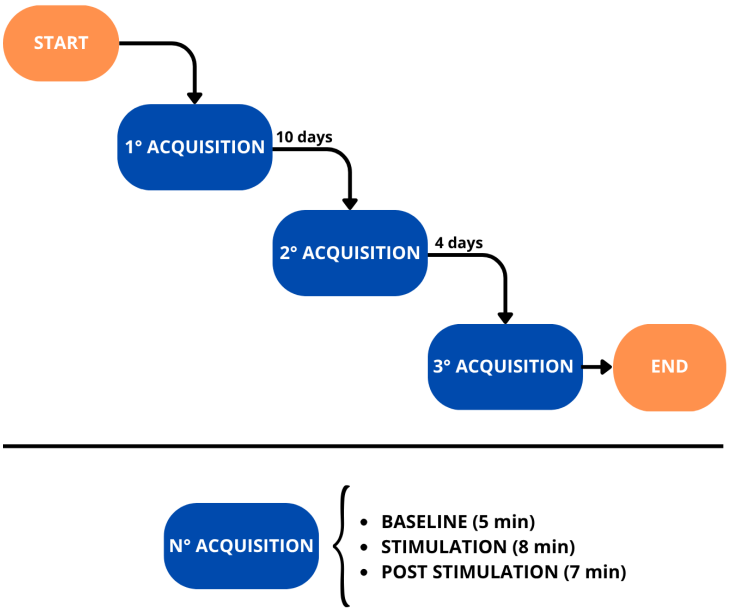

Figure 18: Experimental protocol flowchart.

The experimental protocol was organized into three sessions during a two week period. The first meeting was used to extract the 'Individual Alpha Frequency', necessary to create a personalized audio track for each subject. More details about the creation of the audio tracks will be provided in the 'Stimulus Track' section. Moreover, during the first session, EEG and ECG signals were recorded for the first time while the subjects were listening to their personalized audio stimuli.

During the ten days period between the first and the second acquisition session, each subject was asked to listen to their personalized audio track containing BB once per day for ten minutes, trying to reproduce the same listening conditions as during the first meeting. Home stimulation was monitored by reminding participants daily to complete the task and by having them log their completion in a diary.

During the second acquisition session, the same kind of physiological signals as in the previous meeting were recorded, with the difference that this time the participants had completed a ten day training period. For the following four days, the daily BB listening task was suspended, concluding the training period. On the fourteenth day, the last acquisition session was conducted.

The final phase of the experimental protocol aimed to verify if the training had induced a lasting adaptation to the stimulation or if the effect would result more similar to the initial condition once the training period was interrupted.

Each acquisition session lasted 20 minutes and was divided in three different steps:

- **Baseline:** in this phase, which lasted 5 minutes, no auditory stimuli was provided. Participants were asked to relax while keeping their eyes closed using a sleeping mask.
- **Stimulation:** during this step, the same audio track containing BB used for the daily listening task was administered to the subjects, shortened to a duration of 8 minutes while keeping their eyes closed.
- **Post-Stimulation:** after the end of the stimulation an additional 7 minutes of signals were recorded. Participants were instructed to remain in the same position and keep their eyes closed.

During each acquisition session the EEG signal was recorded using the Enobio 8 system, while the Polar H10 chest strap was used to collect both ECG data. On the headset of the instrumentation used to record the EEG data there is the possibility to position the electrodes inside dedicated slots, enabling a custom configuration that aligns with the international 10-10 system.

Since literature doesn't provide information regarding which cerebral area was most influenced by BB, the electrodes were placed to capture signals from all major cortical areas allowing to assess possible symmetries or asymmetries of the cortical activity. Specifically, the following positions were chosen: F3 and F4 for the frontal area, T7 and T8 for the temporal area, P3 and P4 for the parietal area, and O4 and O5 for the occipital area, as shown in Figure 19.

Before each session participants were asked to avoid consuming nicotine and alcohol because those substances could create excitatory or relaxing effects that could interfere with the final interpretation of the results.

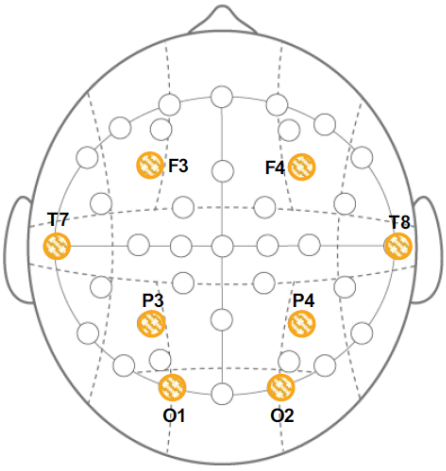

Figure 19: Illustration of all possible electrodes positions on the neoprene cap. The electrodes actually used during the experimental protocol are highlighted in yellow.

4.3.1 Acquisition Steps

For all three acquisition sessions, the participants underwent the same preparatory steps.

The first step of the experimental protocol involved positioning the Polar H10 band, following the instruction provided in the 'Polar H10 user manual'. After sanitizing the electrodes on the strap with a solution of water and 90% pure alcohol, the strap was placed around the subject's chest tightening the elastic so that the electrodes would adhere properly to the skin while remaining comfortable. Particular care was taken to ensure that the R peak of the ECG signal had a positive polarity.

Next, participants were seated in front of an empty desk. They were asked to prepare their personal smartphone and headphones, placing the device in front of them with the audio track ready to play and the volume already

set to ensure clear audibility without discomfort. However, the volume level varied among subjects because the stimulation track was played on different devices. Both the audio playback system and the volume of the audio track were kept the same for throughout the entire study.

The next step consisted of mounting the EEG signal recording instrumentation on the subject. Two patch electrodes were positioned behind each ear, at the level of the mastoid processes, for the connection of CMS and DRL electrodes. These respectively measure the common average potential and inject an inverse signal, with the aim of improving the signal to noise ratio (SNR) of the recorded EEG signal.

Subsequently, the subject was fitted with a neoprene cap with pre-inserted electrode holders, ensuring that electrode Cz was correctly positioned at the intersection of the sagittal plane and the line connecting the ears.

Each electrode was then prepared by gently moving the hair aside to expose the skin at the base of the NG Geltrodes. The area was cleaned with alcohol to ensure optimal contact with the scalp, reducing potential signal attenuation caused by the hair. Each electrode cup was then filled with conductive gel, making sure to avoid air bubbles, thus ensuring proper conductivity between the scalp and the electrode's conductive plate.

Once the subject was fully prepared, conductive cables were connected according to a specific mapping scheme, ensuring that during the analysis phase, the precise origin of the recorded signals could be accurately identified. Additionally, cable placement was carefully arranged to minimize clutter and prevent contact between different cables, reducing the risk of interference and noise. For last a sleeping mask was positioning on the subject's eye to help them to keep them closed.

4.3.2 Stimulus Tracks

To generate the audio track containing the binaural beats (BB) used to stimulate the subjects in the Stimulated Group, it was necessary to define the carrier frequency (f_0) and the frequency difference(δf), which represent the stimulation frequency.

Since in literature does not provide a clear consensus on the optimal configuration that maximize the effectiveness of BB, these parameters were selected following studies by David R. Perrot on BB perception [44].

In particular, the δf used in the study was personalized for each participant and corresponded to the *individual alpha frequency* (IAF) derived from their EEG recordings during the baseline phase of the first acquisition session. The δf value remained constant throughout the training period, as the IAF in healthy individuals tends to be stable, at least in the short term [45].

The most commonly used estimators to calculate IAF are the *Peak Alpha Frequency (PAF)* and the *Center of Gravity (CoG)*. Since PAF estimation can be limited by two main problems, the spectral resolution used to evaluate the power spectral density (PSD) and the possible absence of a dominant alpha peak [46]. For each channel the value of IAF has been calculated using the CoG estimation, which formula is reported in Equation (17):

$$\mathrm{IAF}_{\mathrm{ch}} = \frac{\sum_f f \cdot PSD(f)}{\sum_f PSD(f)} \tag{17}$$

Where f is a variable value within the frequency limits of the alpha band.

Given that a multichannel acquisition system was used, the global IAF value was calculated as the average of the IAFs across all EEG channels:

$$\mathrm{IAF}_{\mathrm{mean}} = \frac{1}{N} \sum_{ch=1}^{N} \mathrm{IAF}_{\mathrm{ch}}, N = 8 \tag{18}$$

Where N is the number of channels used.

Once the subject-specific Δf value was obtained, the carrier frequency f_0 was defined based on the BB perception curve shown in Fig. 2.

Although the literature suggests that a carrier frequency around 500 Hz maximizes BB perception near the center of the alpha band, a value of 250 Hz was chosen in this study. The choice was made because it still ensures a good BB perception while providing a more pleasant and less intrusive listening experience.

Once defined the parameters for the BB, the audio track was generated with a duration of 10 minutes using the software MATLAB. Specifically, two distinct sine waves were generated, one at 250 Hz and the other at $250 + \delta f$ Hz. The track was produced in stereo format, so that each sine wave could be played separately to the left (f_0) and right ($f_0 + \delta f$) ear using earphones, inducing, during the listening, the illusory perception of BB.

While in many previous studies BB are masked with white noise, colored noise or embedded with music tracks [47] [27] [48], in this study it was decided to keep them pure without any background noise or sound. This choice aimed to avoid potential acoustic interference that could compromise the perception of BB or alter its neural processing, as music is also an auditory stimulus.

4.4 Signal Analysis Pipeline

This section presents the core of the thesis work, that consists of the analysis method that allowed to extract the final results, which will be described in the following chapters.

The section begins presenting the analysis of the EEG signal, detailing the pipeline used to clean the raw data, the feature extraction process, and the implementation of a clustering algorithm used for handling multivariate data. The focus will be shifted to the analysis of the alpha rhythm and, finally, concludes with the ECG analysis.

All signal processing was performed offline using MATLAB software.

4.4.1 EEG signal pre-processing

Following the recording and the saving of the EEG signals, the raw data were imported on MATLAB to perform the pre-processing and cleaning phase, following the analysis steps in the works done by Subhra Chakraborty [49], Fazlul Karim Khondakar [50], Amer [51]. The complete EEG signal pre-processing pipeline is shown in Figure 20.

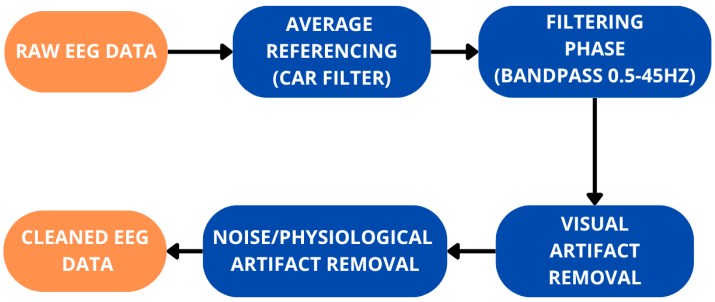

Figure 20: EEG signal pre-processing pipeline.

The first step of analysis consisted of converting the signal values to μV and creating a data structure compatible with MATLAB's toolbox EEGLAB.

This data structure included all the necessary information to characterize each acquisition, such as:

- The number of channels used and their positions on the scalp, consistent with the montage used during recording.
- The sample frequency, set at 500 Hz.
- The matrix containing the EEG signals from all the channels, along with duration expressed in number of samples.

The recorded signals were referenced to a single common reference, which can introduce a residual noise component shared across all channels, affecting the quality of the recordings.

To address the issue presented by the presence of one common reference, the average referencing technique (or common average reference, CAR) was applied to re-reference the EEG signals before proceeding to the filtering phase [52].

This method is based on the assumption that all the active channels are similarly affected by the noise component and are symmetrically distributed on a spherical surface, like the human scalp. Specifically, the technique involves calculating the average activity across all the active electrodes and subtracting it from each channel.

This approach is based on the theoretical principle that the integral of the potential distribution over a sphere, that includes the current dipoles, is zero. The use of an average reference allows for the removal of the DC component from the spatial frequency spectrum, thus producing potential maps centered around zero. This makes the average of the signals a good approximation of a neutral reference potential [53].

On the resulting signals, a band pass filter was applied: a fifth-order, zero-lag, anti-causal Butterworth filter, with a high-pass cut-off frequency of 0.5 Hz and a low-pass cut-off frequency of 45 Hz. This step ensures the preservation of the EEG signal's relevant frequency components. The filter's frequency response is shown in Figure 21, while Figure 22 shows the filtered signals with the CMS reference and Figure 23 shows the filtered signals with the average reference.

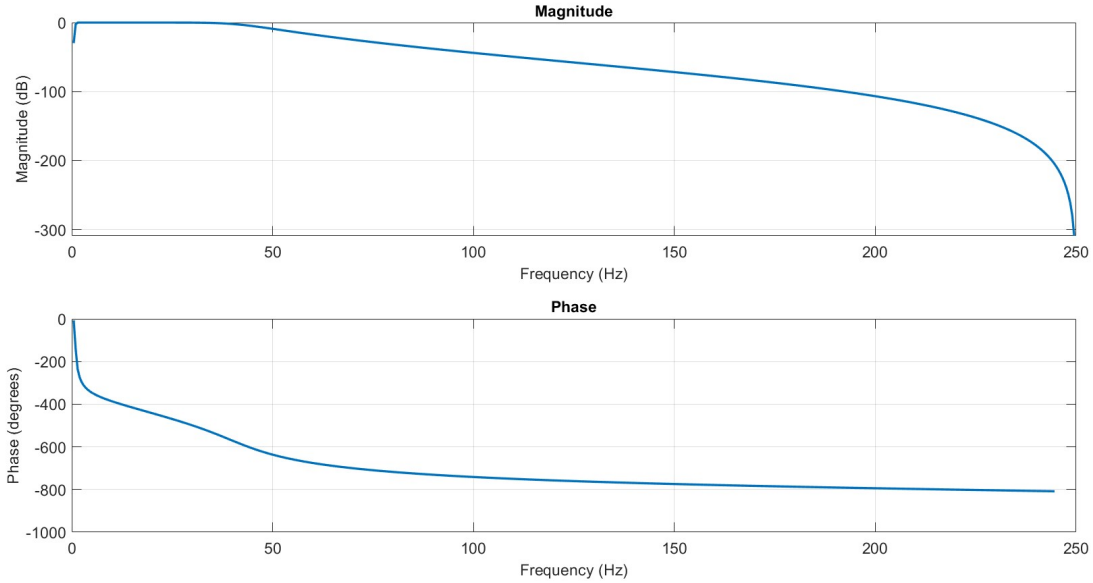

Figure 21: Frequency response of the bandpass filter applied to the EEG signal: the magnitude response is shown above and the phase response below.

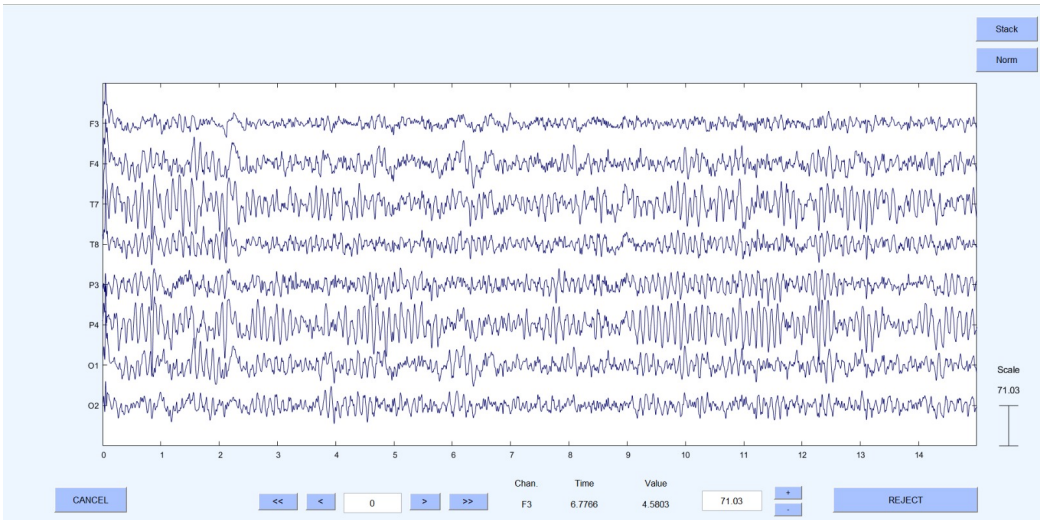

Figure 22: EEG signals based on CMS reference.

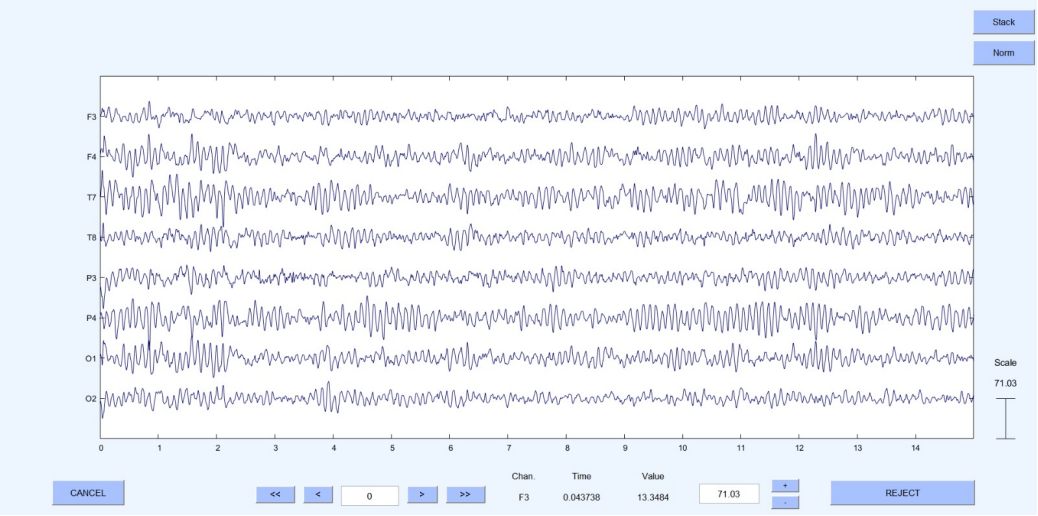

Figure 23: EEG signals based on average reference.

The last step of the pre-processing pipeline consists in detecting and removing artifacts and noisy components, both physiological and not physiological, overlapped with the EEG signal spectrum. The aim is to extract a signal that reflects, as closely as possible, only cortical activity.

The EEG traces from each channel were segmented into consecutive 1-second epochs by introducing artificial events to mark the start and the end of each signal block. This segmentation allows, through visual analysis, to evaluate and in case exclude signal fragments clearly affected by motion artifacts, that exhibit more chaotic activity and wider amplitude ranges than average, as shown in Figure 24.

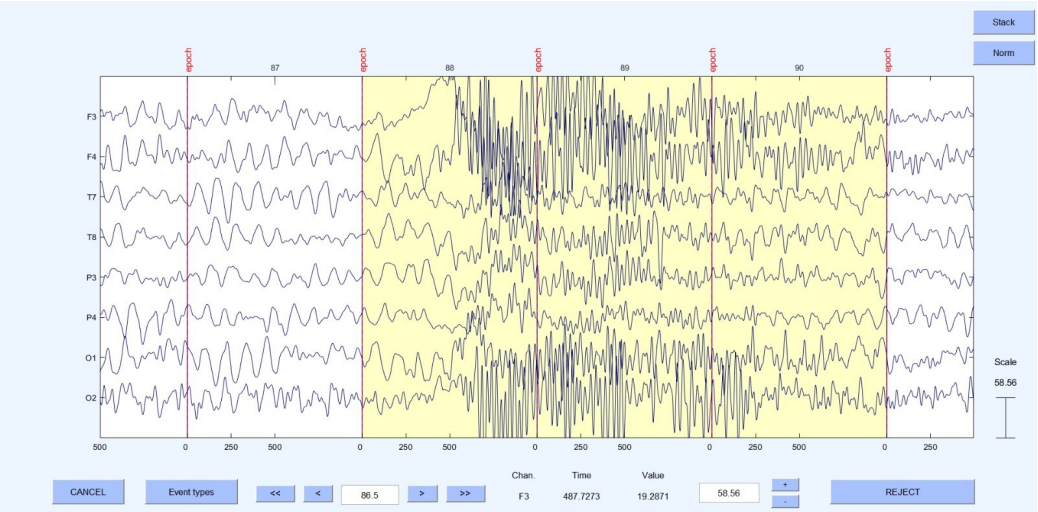

Figure 24: Visual artifact removal through selection of the specific epoch.

This was possible using the EEGLAB toolbox, which allows to select and remove portions from continuous data directly from the graphical interface.

At this stage an Independent Component Analysis (ICA) was performed using the algorithm 'Extended Informax', which is already implemented in EEGLAB. After decomposition, each Independent Component (IC) could be inspected based on several characteristics, including the time course of its amplitude, power spectral density, and spatial distribution, corresponding to the contribution of each component to each acquisition channel.

The set of independent activities from the decomposition algorithm was then analyzed by the plug-in ICLabel, included in EEGLAB, which classifies each

IC as either brain-related or as noise/physiological artifact, which some examples are shown in Figure 25.

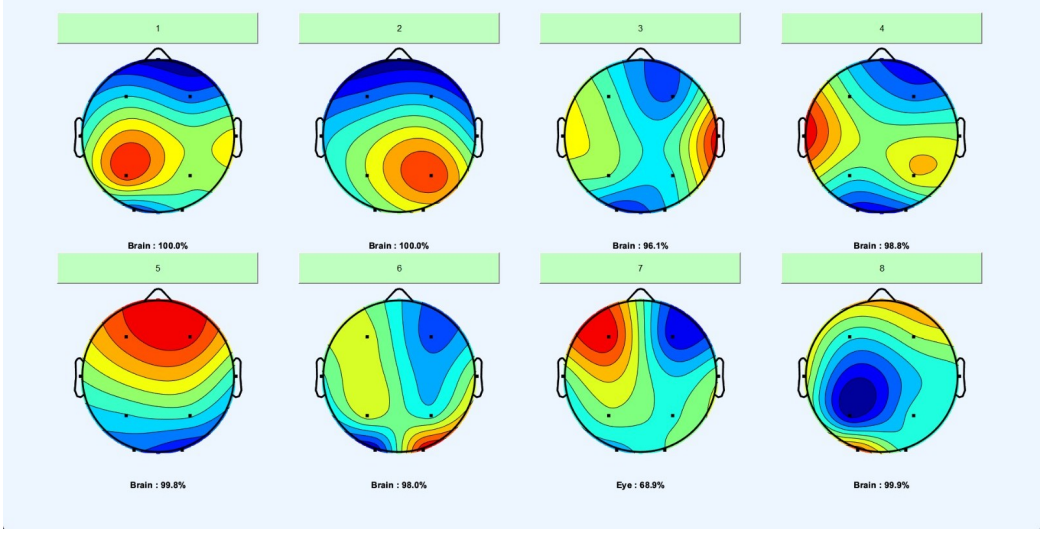

Figure 25: Classification of all the IC.

To obtain a broader understanding of the noise classification, ICA algorithm implemented in EEGLAB can be used to extract the features that characterize the behavior of specific components. Figure 26 presents the topographics, temporal and spectral characteristics of the IC classified as noise or artifact.

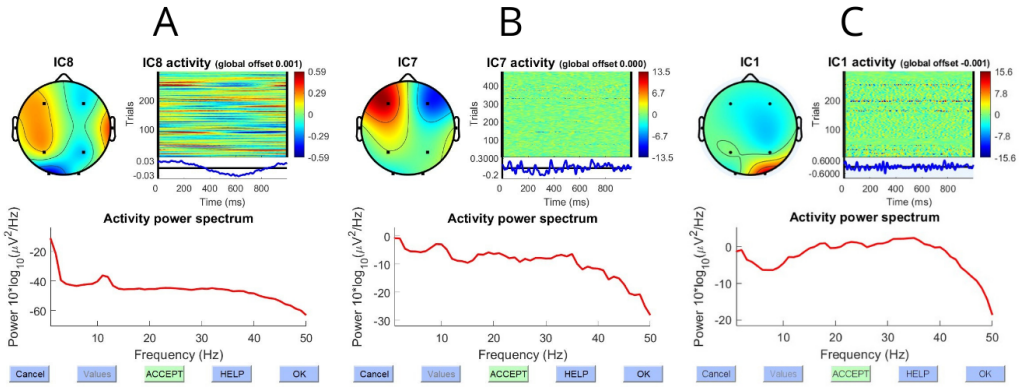

Figure 26: A: $1/f$ noise component, B: ocular artifact, C: muscular artifact.

The components labeled as non neuronal activity were selected and subtracted from the EEG signal, as pictured in Figure 27.

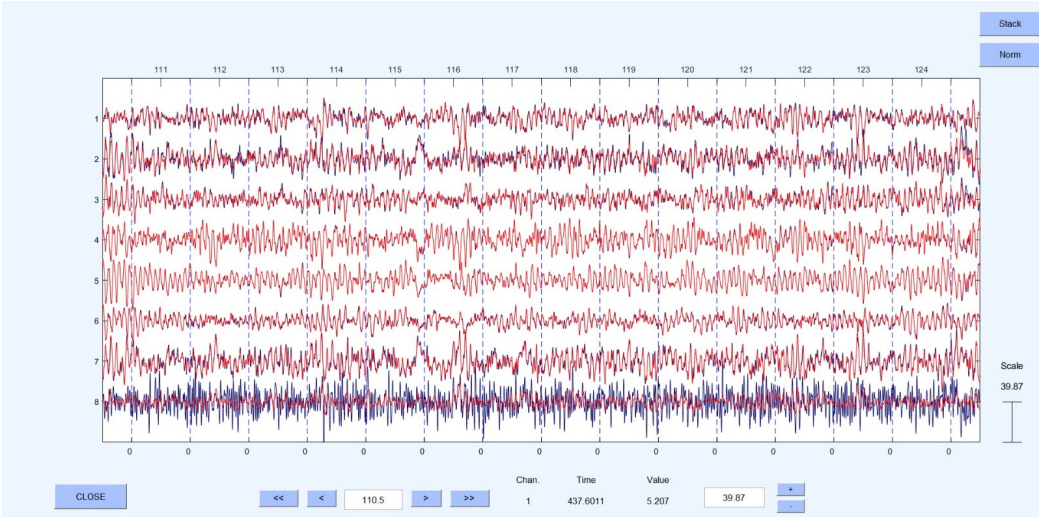

Figure 27: Noise/physiological artifact removal from EEG signals, in blue the original traces while in red the cleaned ones.

4.4.2 Features extraction

After the signal cleaning phase resulting in EEG traces that closely reflect the actual cortical neural activity the focus shifted to the extraction of descriptive parameters of brain activity. These parameters aim to translate complex and hard-to-interpret time series into measurable quantities that are representative of the subject's neuro physiological state.

To obtain a comprehensive and detailed representation of the EEG signal, the time series were analyzed using both linear techniques (in the time and frequency domains) and nonlinear techniques, which are capable of capturing the dynamic and more complex aspects of cortical activity.

The following section describes all the metrics used to quantify the EEG signal:

- **Frequency bands power**
  The power of the EEG signal in its various frequency bands was obtained from the estimation of its power spectral density (PSD). In particular, Welch's direct and non-parametric method was used, as implemented in MATLAB. The EEG time series was windowed using a 1-second Hamming window with a 50% overlap between consecutive epochs. The final PSD estimated was obtained with an apparent frequency resolution of 0.25 Hz.

The formula used to calculate the power content of the signal in a specific frequency band (P_{band}) is:

$$P_{\text{band}} = \int_{f_{\text{low}}}^{f_{\text{high}}} \text{PSD}(f)df \tag{19}$$

Where:

- f_{high} is the upper frequency limit of the specific band,
- f_{low} is the lower frequency limit of the specific band.

Using the same method, the power within a subrange of the alpha band was also evaluated, defined as a ± 1 Hz window centered on the Individual Alpha Frequency (IAF):

$$P_{\text{IAF}} = \int_{\text{IAF}-1}^{\text{IAF}+1} \text{PSD}(f)df \tag{20}$$

- **Power ratio**

  In addition to the absolute power values in each band, the relative percentual contribution of each band to the total signal power (P_{total}) was also computed:

$$\text{Power Ratio} = \frac{P_{\text{band}}}{P_{\text{total}}} \times 100 \tag{21}$$

In the case of the IAF power, however, the ratio was not calculated with respect to the total EEG power, but specifically with respect to the overall alpha band power (P_{alpha}):

$$\text{IAF Ratio} = \frac{P_{\text{IAF}}}{P_{\text{alpha}}} \times 100 \tag{22}$$

This decision was motivated by the nature of the auditory stimulation used. In fact, this metric allows to assess the extent to which the spectral power within the alpha band is concentrated around the stimulation frequency.

- **Alpha band centroid**
  To evaluate potential entrainment effects induced by listening to the audio track containing the BB, the temporal evolution of the alpha band centroid, was analyzed. This value represents the spectral "center of gravity" of the alpha band power distribution within each signal epoch. This metric, defined by the following equation, effectively reflects the time-varying behavior of the Individual Alpha Frequency:

$$f_{\text{centroid}} = \frac{\sum_f f \cdot \text{PSD}(f)}{\sum_f \text{PSD}(f)} \tag{23}$$

- **Alpha asymmetry index**
  Some scientific studies based on EEG signal analysis provide evidence that the left anterior region of the brain is involved in emotions that drive us toward approach behaviors, such as enthusiasm, desire, or curiosity, whereas the right anterior region is associated with withdrawal-related emotions like sadness and fear. The EEG Asymmetry Index is a robust metric used to evaluate stress, as it reflects the emotional activation of a person. Numerous studies have reliably used it to distinguish different psychological states, as it varies depending on the emotion experienced.

Specifically, the Alpha Asymmetry Index (AAI) is defined as the difference between the natural logarithm of the alpha power in the right frontal lobe ($P_{alpha,right}$)and the left frontal lobe ($P_{alpha,left}$), as shown in the equation:

$$AAI = \ln\left(\frac{P_{\text{alpha,right}}}{P_{\text{alpha,left}}}\right) \tag{24}$$

The most commonly used EEG electrodes positions for assessing the alpha asymmetry are F3 and F4, as they are located over the dorsolateral prefrontal cortex, a brain area directly involved in stress regulation [54].

- **Hjorth Parameters**

  The Hjorth parameters are widely used to describe the temporal variations of the statistical properties of EEG signal. In addition to providing an overview of time-domain characteristics, they also have an equivalent in the frequency domain as they associated to the statistical moments of the signal's power spectrum. These parameters can be arbitrarily calculated in either the time or frequency domain, this possibility is ensured by the Paserval's Identity, which states that the total power in the frequency domain is equal to the average power in the time domain.

  The Hjorth parameters are as follows:

  – *Activity*: it provides a measure of the squared standard deviation of the signal's amplitude, often is referred to as the variance or mean power. Activity is strictly related to the zero order statistical moment of the signal's power spectrum:

$$\text{Activity} = \frac{1}{N}\sum_{i=1}^{N}(X_i - \bar{X})^2 \tag{25}$$

Where:

* N is the total number of signal samples,
* X_i is the value of i-th signal sample,
* $\bar{X}$ is the mean value of the signal.

– *Mobility*: it is defined as the ratio between the standard deviation of the signal's first derivative and the standard deviation of the signal itself. This parameter is independent of the signal's amplitude and depends only on the shape of the waveform. Mobility provides information about the rate of variation of the EEG signal and is associated with the second order statistical moment of its power spectrum:

$$\text{Mobility} = \sqrt{\frac{\frac{1}{N-1}\sum_{i=2}^{N}(X_i - X_{i-1})^2}{\frac{1}{N}\sum_{i=1}^{N}(X_i - \bar{X})^2}} \tag{26}$$

– *Complexity*: it is defined as the ratio between the mobility of the signal's first derivative ($\dot{X}$) and the mobility of the signal itself (X). Complexity gives insight into the sharpness of the waveform and quantifies the degree of deviation from a pure sine wave, which has a complexity value of 1. This parameter corresponds to the fourth order statistical moment of the EEG signal's power spectrum in the frequency domain:

$$\text{Complexity} = \frac{\text{Mobility}(\dot{X})}{\text{Mobility}(X)} \tag{27}$$

Together, these three parameters characterize the EEG signal in terms of amplitude, temporal dynamics, and morphological complexity [55].

- **Phase Locking Value (PLV)**
  The Phase Locking Value (PLV) is one of the most commonly used metrics to measure the level of phase synchronization between two narrow-band signals. If the two signals are completely independent, the PLV will be zero; conversely, if the signals are highly correlated, the PLV will approach one.

$$PLV(t) = \left| \frac{1}{N} \sum_{i=1}^{N} e^{j(\theta_1(t_i) - \theta_2(t_i))} \right| \tag{28}$$

  Where $\theta_1(t_i)$ and $\theta_2(t_i))$ are the instantaneous phase value of both signals at time instant t_i.

  In this study, PLV is used as a functional connectivity metric to evaluate potential variations in synchronization between different pairs of electrodes. When assessing synchronization across channels, it's crucial that the recorded signals don't share a common reference. The presence of a shared reference between channels can lead to artificial synchronization, thus overestimating the PLV [56].

The metrics described so far belong to traditional EEG analysis technique commonly used to characterize the signal. In the following paragraphs complexity metrics will be introduced, which allow to investigate the dynamics hidden in a complex signal like the EEG recorded at the cortical level.

The complexity metrics reflect on two important aspects of a dynamic system, its predictability and its regularity. The predictability of a dynamic system refers to the temporal evolution of the system's states, while the regularity describes the overall amount of pattern repetition within the system's trajectory. Although both concepts refer to different aspects, they are strictly correlated in practice [57].

Specifically, the metrics used to estimate EEG signal complexity in terms

of predictability, are represented by Higuchi Fractal Dimension (HFD) and by Katz Fractal Dimension (KFD), while regularity is estimated by Spectral Entropy (SE).

- **Higuchi Fractal Dimension (HFD)**
  The method proposed by Higuchi is one of the most diffused and effective techniques for estimating the fractal dimension of a time series, such as an EEG signal. The analysis steps for computing Fractal Dimension (FD) using Higuchi's method are as follows:

  Let's start considering a time series composed of a finite number of samples N:

$$(X(1), X(2), X(3), \ldots, X(N)) \tag{29}$$

  This series is decomposed into a set of subsequences X_k^m, each representing a under-sampling of the original time series:

$$X_k^m = \{X(m), X(m+k), X(m+2k), \ldots, X\left(m + \left\lfloor \frac{N-m}{k} \right\rfloor \cdot k\right)\} \tag{30}$$
$$\text{con } m = 1, 2, \ldots, k$$

  Here m and k represent the starting offset and the sampling interval, respectively.

Each subsequence X_k^m is associated with a length measure, computed as the sum of absolute differences between consecutive points of the under-sampled series normalized by a scale factor to allow comparison across different scales:

$$L_m(k) = \left(\sum_{i=1}^{\lfloor \frac{N-m}{k} \rfloor} \left| X(m+ik) - X\big(m+(i-1)k\big) \right| \right) \cdot \frac{N-1}{\lfloor \frac{N-m}{k} \rfloor \cdot k} \quad (31)$$

The term in the parentheses represents the normalization factor, which ensures that signal lengths computed at different scales are comparable. For each sampling interval k, it is obtained m values of signal length. The average of these values is defined as the curve length for interval k, denoted as $L_m(k)$ [58].

The fractal dimension of the original time series is then estimated as the slope of the line obtained by performing a linear regression in a log-log plot of $L(k)$ versus k:

$$HFD = -\frac{\log(L(k))}{\log(k)} \quad (32)$$

Where $1 < HFD < 2$. In conclusion, the HDF provides a multi-scale analysis of the signal allowing to evaluate how the signal's length changes as the observation scale increases.

- **Katz Fractal Dimension (KFD)**
  The KFD is a robust and computationally efficient method for quantifying the complexity of a signal. The technique, introduced by Michael J. Katz [59], interprets an arbitrary waveform as a geometric figure to which a traditional fractal dimension can be assigned:

$$FD = \frac{\log(L)}{\log(d)} \tag{33}$$

  Where L represents the total length of the waveform, calculated as the sum of the Euclidean distances between successive points:

$$L = \sum_{i=1}^{N-1} \text{dist}(i, i+1) \quad \text{with } i = 0, 1, \ldots, N \tag{34}$$

  while d represents the planar extent of the curve. For a waveform, which is an ordered set of points pairs with a natural starting point, d is defined as the distance between the first point of the time series and the farthest point from it:

$$d = \max(\text{dist}(1, i)) \tag{35}$$

  The fractal characterization assumes that the dimension of a geometric figure is independent of the scale at which is represented. Therefore, normalization is required. In the case of a waveform, a scale factor a is introduced, defined as the average distance between all points in the time series. The KFD is finally computed as:

$$KFD = \frac{\log(L/a)}{\log(d/a)} \tag{36}$$

- **Spectral Entropy**

  Spectral entropy (SE) is a low computational cost metric that quantifies the uncertainty of a signal in the frequency domain, based on the concept of entropy introduced by Shannon [60]. The underlying idea is that, starting from the signal's power spectral density (PSD), it is possible to define a probability distribution function ($p(f)$) as follows:

$$p(f) = \frac{\mathrm{PSD}(f)}{\sum_f \mathrm{PSD}(f)} \tag{37}$$

  Once the probability distribution function is defined, the spectral entropy can be computed as:

$$SE = -\sum_{i=1}^{N} p(f_i) \log p(f_i) \tag{38}$$

  where $p(f_i)$ represents the probability associated with the frequency component f_i, and N is the total number of frequency bins considered in the signal's spectrum.

  SE reaches high values when the signal has a broad and uniform power distribution in the frequency domain, such as in the case of white or colored noise. Conversely, SE takes on low values when the signal's power is concentrated around a specific frequency, as with sinusoidal signal.

4.4.3 K-means Clustering on Principal Components Space

In this section, the analysis method implemented to address the main experimental question of this thesis work will be described:

> *"Can EEG signals show real changes in brain activity or physiological state during or after listening to BB?"*

Following a preliminary analysis of the extracted features, described in the previous section, the following critical issues were identified:

- An univariate analysis of the signals recorded during the different phases of the acquisition protocol, aimed at highlighting potential effects of BB, turned out to be a laborious and inconclusive strategy.
- The response to BB is highly heterogeneous, meaning that not all subjects respond to the stimulation in the same way.

To better interpret the characteristics of cortical activity and detect potential variations from the baseline condition during the administration of the BB stimulus, a multivariate analysis technique was adopted, specifically the Principal Component Analysis (PCA). Subsequently, a clustering algorithm was implemented between baseline and stimulation or post stimulation conditions.

All steps involved in implementing and optimizing a fully automated algorithm for assessing the discrimination between different experimental conditions will be described below, the flowchart representing all the steps is shown in Figure 28.

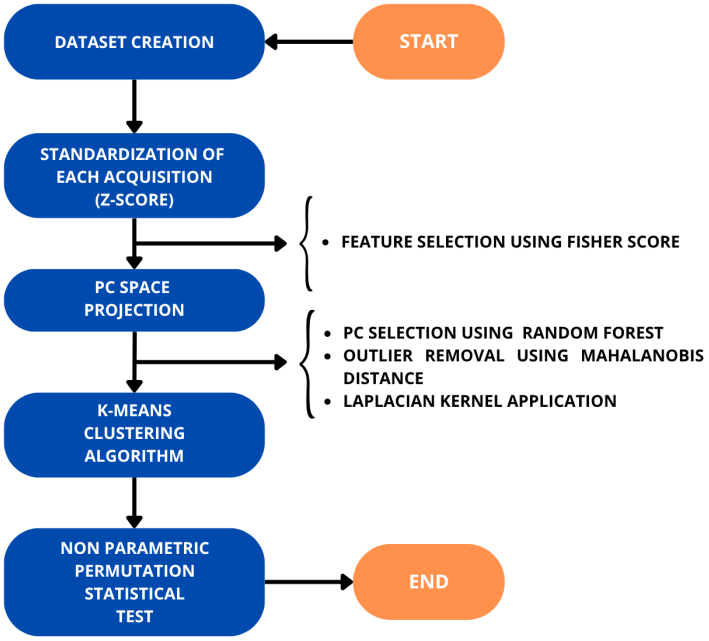

Figure 28: Analysis pipeline flowchart.

The information characterizing cortical activity during each phase of each acquisition session was organized into a data structure. Specifically, for each subject, three matrices were created, one for each acquisition session in the experimental protocol.

Each matrix has a bidimensional structure of size $N \times M$, where N is the total number of observations across all three conditions (baseline, stimulation, post-stimulation). Each observation correspond to a 15 second EEG segment. The number of columns M is determined by the product of the number of acquisition channels and the number of extracted features describing the cortical activity.

At this point, to better understand and manage the set of features that represent the cortical response to the stimulation, PCA was applied. In this context, PCA offers two main advantages:

- It reduces dimensionality of the data, enabling better management of the multivariate dataset by identifying an orthonormal basis onto which data can be projected. Each observation is represented along the principal components as a linear combination of the original variables.
- Projecting the observations onto the fist two or three principal components allows to represents the original dataset in a lower-dimensional space, where a visual assessment of potential separation between experimental conditions is possible. This offers a useful preliminary analysis to whether the BB stimulation induces noticeable changes in cortical activity compared to the baseline.

In this study, the comparison between experimental conditions is carried out on two levels:

1. At the level of individual acquisition, by considering each recording session separately for each subject.
2. At the level of the entire subject, by integrating information on cortical activity across different acquisition sessions.

Specifically, since the aim is to understand how cortical activity changes during and after the administration of BB, comparisons were performed in pairs, considering separately the baseline-stimulation and the baseline-post stimulation conditions.

The PCA technique was applied separately to each subject. This means that the vector space used to project the different EEG signal observations was generated from a matrix obtained by concatenating, along the row dimension, the matrices corresponding to the three acquisitions for the same subject.

Creating a global vector space that represents the entire subject's dynamics allows for the evaluation of the temporal evolution of the brain's response to BB, making the comparison between acquisitions more robust. Applying PCA independently to each acquisition would be equivalent to representing the temporal variation of an event using a different reference system at each sampling point.

Conversely, projecting the observations from the different phases of the acquisition protocol, across all three acquisition sessions for a given subject, into a reference space enables the evaluation of the reproducibility of the cortical response to the stimulation. The simultaneous comparison across the three acquisitions makes it possible to determine whether consistent changes occurred relative to the baseline condition, before listening to BB, and to verify whether the stimulation causes the EEG signal observations tend to align along coherent directions in the principal components space.

Before applying PCA, each matrix underwent a standardization process. Specifically, the standardization was performed separately for each acquisition, meaning that each value in the original matrix was transformed as follows [61]:

$$z_{ij} = \frac{x_{ij} - \mu_j}{\sigma_j} \tag{39}$$

Where:

- x_{ij} is the value of variable j for observation i in a given acquisition;
- μ_j is the mean of variable j computed across all observations in that acquisition;
- σ_j is the standard deviation of variable j for the same set of observations.

This standardization ensures that all features associated with a single acquisition are represented on a comparable scale and exhibit a distribution with zero mean and unit standard deviation. This step is essential, as it prevents differences in scale across variables from affecting the PCA projection.

Following the projection into the PCA space, to quantitatively assess the degree of separation between the experimental conditions pairs, both at the level of individual acquisitions and for the entire subject, the K-means clustering algorithm was applied [62].

Since the aim was to determine whether the observations from the stimulation and post stimulation conditions form distinct clusters compared to the baseline, the K-means algorithm was initialized with $K = 2$, corresponding to the number of conditions being compared. The initial centroids were set based on the mean characteristics of the two distributions to facilitate the convergence toward a solution, which was visually observed in the PC space.

Once clustering was completed, a supervised evaluation of the results was conducted by comparing the cluster assignments returned by k-means with the true condition labels of the observations. The separation performance was measured using accuracy, defined as:

$$\text{Accuracy} = \frac{1}{N} \sum_{i=1}^{N} \delta(\hat{y}_i, y_i) \tag{40}$$

Where:

- N is the total number of observations;
- $\hat{y}_i$ is the predicted label from clustering for observation i;
- y_i is the true label for observation i;
- $\delta(\hat{y}_i, y_i)$ is the Kronocker delta function, equal to 1 if the labels match and 0 otherwise.

The analysis method described so far, based on uniform data processing for all subjects, provided a general overview of the potential to separate the different experimental conditions. However, since the objective is to evaluate changes in cortical activity relative to each subject's own baseline, an optimization pipeline is needed. This pipeline aimed to maximize the separation between the different phases of the experiment while considering only intra-subject variability. Given that this form of sensory stimulation, perception may play a key role. This implies that the response to the stimulation could be highly subjective, shaped by the individual's interpretation. Consequently, brain activity may not change uniformly across subjects, making a personalized approach necessary to adapt the analysis to each individual.

The optimization pipeline was implemented with the goal of enhancing clustering performance and is structured as follows:

- **Feature selection using Fisher Score**

  The way in which the cerebral activity responds to BB stimulation can vary significantly between subjects. Consequently, not all the features extracted from the EEG signal are equally informative for each individual. Furthermore, the response to stimulation may change over time. Therefore, a feature selection step based on Fisher Score was applied [63]:

$$\text{Fisher Score} = \frac{(\mu_1 - \mu_2)^2}{\sigma_1^2 + \sigma_2^2} \tag{41}$$

  where μ_1 and μ_2 represent the mean values of the i-the feature distributions for the two classes being compared, and σ_1 and σ_2 are their respective standard deviations.

  The Fisher score is a robust metric that provides insight into a feature's ability to discriminate between classes. It was applied to the matrices

containing the features of the two experimental conditions under comparison, separately for each acquisition. A threshold of 0.8 was set to select only the most informative features; specifically, features with a Fisher Score higher than 0.8.

As a result, a set of features was selected for each of the three acquisitions for every subject. However, as previously mentioned, to ensure robust comparison across acquisitions, a unified PC space was needed. Therefore, for each subject, PCA was performed on a unified set of features obtained by merging those selected by the Fisher Score across all three acquisitions, as shown in Figure 30.

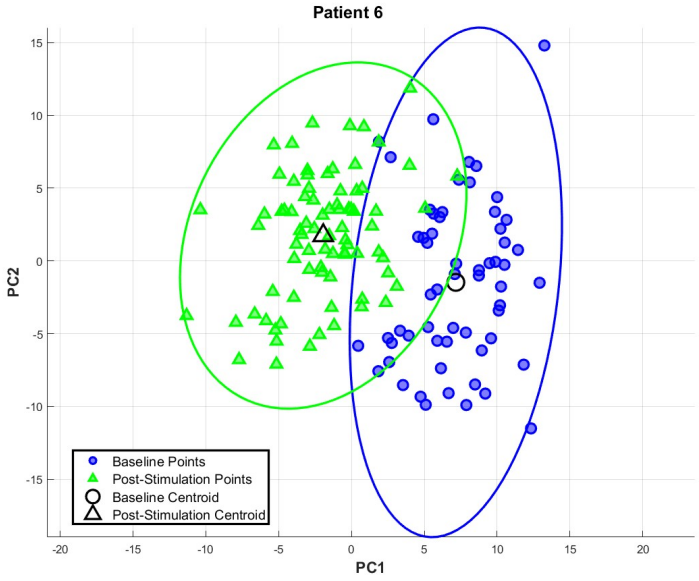

Figure 29: Projection of data on PC space relative to a single subject.

This approach has two main advantages: it enables the analysis to be performed on a lower-dimensional but highly informative dataset, and it ensures that each acquisition is analyzed in a feature space that includes the most relevant characteristics for that specific recording.

- **Principal Component Selection using Random Forest**

  After projecting the observations into the principal component space, a Random Forest algorithm was employed to identify the most informative principal components, those along which class separation was more pronounced [64].

  This step was necessary because, although PCA orders the components by explained variance, high variance doesn't necessarily imply high discriminative power.

  Random Forest assigns an importance score to each principal component based on its ability to distinguish between classes. Components ranked in the top 50% of importance were selected for further analysis.

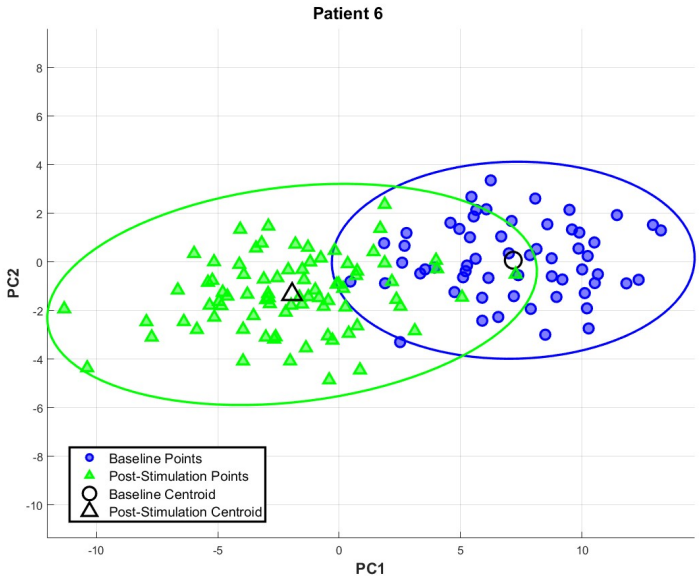

Figure 30: Projection of data on PC space after principal components selection.

- **Outlier removal with Mahalanobis distance**

  Once the analysis space was optimized for each subject, the next step was to identify observations that deviated significantly from the average behavior of their respective class. To detect such outliers, the Mahalanobis distance was used, which is a widely adopted method for identifying anomalies in multivariate spaces, such as the one created through PCA.

  Mahalanobis distance was calculated between each observation and the centroid of its class distribution [65]:

$$D_M(x_i, \mu_C) = \sqrt{(x_i - \mu_C)^T \Sigma_C^{-1} (x_i - \mu_C)} \tag{42}$$

  Where:

  - $x_i \in R^P$ is the i-th observation from class C in a P-dimensional space,
  - μ_C is the centroid of class C,
  - Σ_C is the covariance matrix of class C.

  For each condition a vector of Mahalanobis distances was computed. Only the between the observations falling within the 90th percentile of this distribution were retained, effectively excluding those that were too far from the class's average behavior.

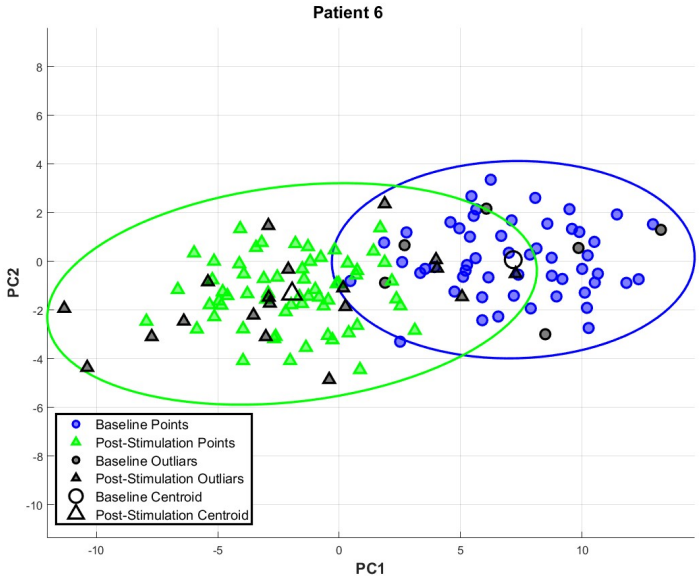

Figure 31: Projection of data on PC space with the outlier highlighted.

- **Laplacian Kernel Application**

  An additional improvement in the separation between different experimental conditions was obtained by applying a non linear transform to the observations projected in the PC space, using a kernel function [66]. Specifically, a Laplacian Kernel was used, defined as:

$$K(z_i, z_j) = \exp\left(-\frac{\|z_i - z_j\|_{L_1}}{\sigma}\right) \tag{43}$$

  Where:

  - $\|z_i - z_j\|_{L_1}$ represents the L_1 norm calculated between all the possible pairs of observations z_i and z_j in the PC space,
  - σ is the scale parameter that controls the width of the kernel.

  The Laplacian Kernel, once the value of σ is set, acts on the basis

of the $\|z_i - z_j\|_{L_1}$ distance between observations: it tends to bring closer those points that are already near to each other and amplify the distance between those that are further apart. This non linearity introduced by the kernel allows for increased separability between the different experimental conditions, as shown in Figure 32.

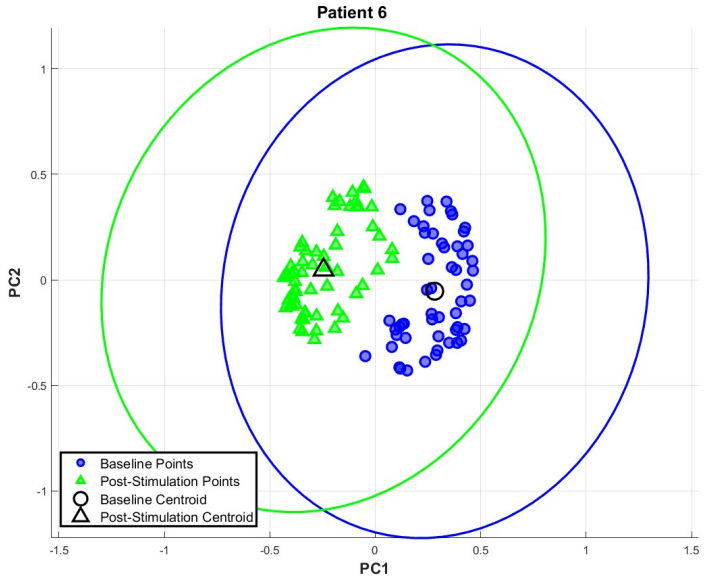

Figure 32: Laplacian kernel applied to the projection of data on the PC space.

These transformations generate a new feature space, optimized for each subject, in which the k-means clustering algorithm is applied to quantify the separation between stimulation and post-stimulation conditions relative to the baseline, as shown in Figure 33.

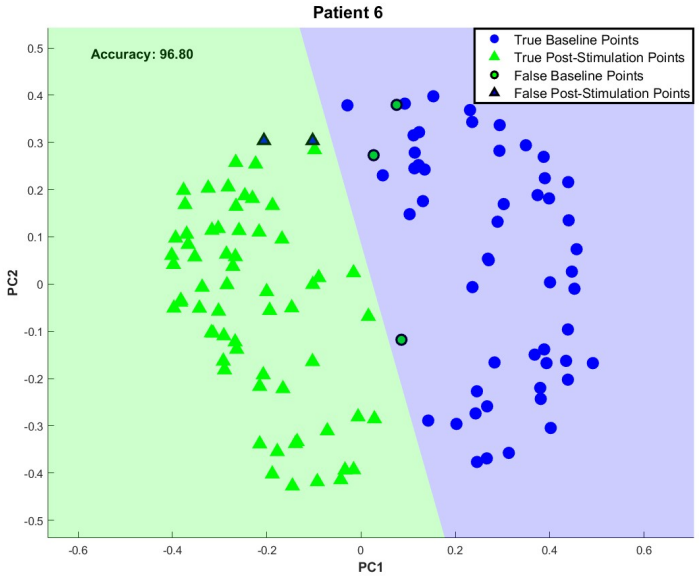

Figure 33: K-means clustering algorithm output.

To demonstrate that the observed separation isn't due to randomness, but rather likely reflects a cortical response to the BB stimulation, a non parametric permutation test was performed to assess the statistical significance of the clustering result.

This test involves randomizing the class labels that are associated with each observation N times, while preserving the original data structure, that is the location of each observation in the analysis space.

For each permutation, a new clustering accuracy value is computed using the shuffled labels. As with any statistical hypothesis test, the significance is expressed by the p-value. Specifically, for a permutation test the p-value is defined as:

$$p = \frac{1}{N} \sum_{n=1}^{N} I(x_n^* \geq x_0) \tag{44}$$

Where:

- x_n^* is the clustering accuracy obtained from the n-th permutation,
- x_0 is the original clustering accuracy,
- $I(\cdot)$ is the indicator function, equal to 1 if the condition is true, otherwise 0.

The resolution of the estimated p-value is $1/N$, meaning that the larger the number of permutations, the better the precision of the p-value estimated. In this study, $N = 10.000$ permutations were performed.

The Null Hypothesis (H_0) assumes that the labels are interchangeable, implying that there is no actual effect related to the BB stimulation.

If the test yields a low p-value ($p < 0.05$), the null hypothesis is rejected, supporting the conclusion that the observed class separation reflects a real and systematic effect induced by the stimulation [67].

4.4.4 Alpha Rhythm Analysis

One of the goals of this thesis is to investigate whether the frequency band of the EEG signal affected by stimulation undergoes any modulation that can be attributed to the action of BB. This section describes the analysis pipeline developed for the characterization of the alpha rhythm.

The alpha rhythm, even in the absence of external stimulation, is characterized by periodic amplitude fluctuations, commonly described as 'waxing and waning' or 'beats' [68] [69].

Therefore, by observing the oscillations of the alpha rhythm, one can notice that they appear as a succession of 'spindles', where the amplitude gradually increases, reaches a peak and then decreases. It has been hypothesized that variations in the characteristics of the alpha spindles reflect changes in the underlying neural dynamics; thus, to verify whether BB interfere with the spontaneous modulation of the alpha rhythm amplitude, alpha spindles were extracted and characterized both morphologically and statistically. Finally, a non linear analysis was conducted to highlight possible variations in the dynamics of amplitude fluctuations, with the specific aim of providing insights into changes in the temporal structure of the alpha rhythm.

To extract detailed information on how the type of stimulation interacts with the subject's natural alpha rhythm, an automated procedure for alpha spindle extraction was implemented.

The signal $x(t)$, representing the cleaned EEG trace, was filtered using a 4th order zero lag anti causal Butterworth bandpass filter between 8 and 12 Hz, obtaining a narrow band process $x^{\alpha}(t)$, representing the alpha activity. The real signal $x^{\alpha}(t)$ was then converted to a complex analytic signal:

$$z(t) = x^{\alpha}(t) + j\hat{x}^{\alpha}(t) \tag{45}$$

where $\hat{x}^{\alpha}(t)$ represents the Hilbert transform of the signal $x^{\alpha}(t)$:

$$\hat{x}^{\alpha}(t) = \frac{1}{\pi} \cdot (\text{V.P.}) \int_{-\infty}^{+\infty} \frac{x^{\alpha}(\tau)}{t-\tau}\, d\tau \tag{46}$$

Where $V.P.$ is Cauchy principal value.

From the complex signal, the envelope of the alpha rhythm was obtained:

$$env(t) = |z(t)| = |x^{\alpha}(t) + j\hat{x}^{\alpha}(t)| \tag{47}$$

A mobile average filter with 200 ms window was then applied to the envelope to retain the slower components of amplitude modulation while attenuating high frequency fluctuations. Figure 34 shows a segment of the alpha rhythm with its envelope superimposed.

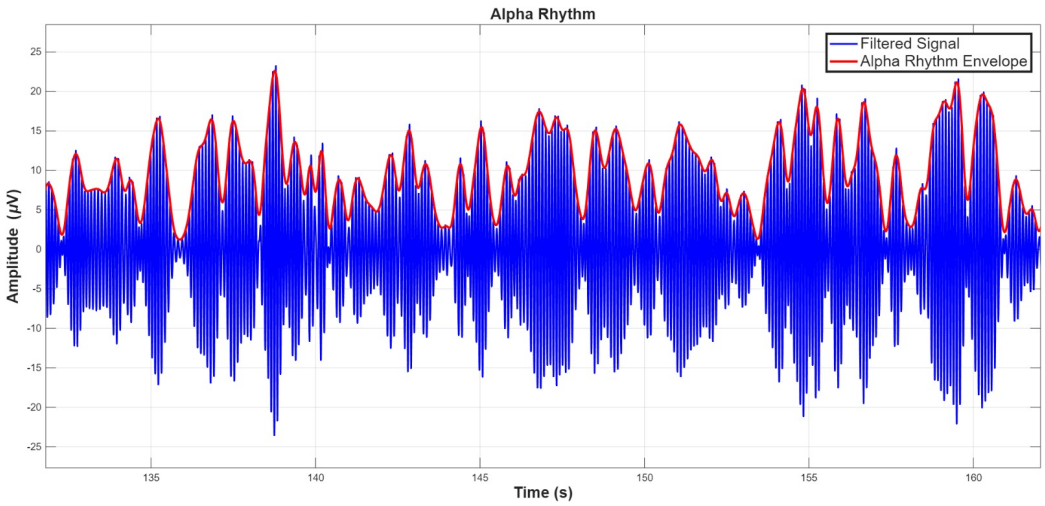

Figure 34: Alpha Rhythm's envelope, in red, superimposed on the filtered signal, in blue.

Once the envelope of the alpha rhythm amplitude was obtained, the pipeline for alpha spindles extraction was carried out.

An alpha spindles is defined as a portion of the alpha rhythm characterized by 'waxing and waning' amplitude fluctuations, where the signal activity is above average. The algorithm identifies the alpha spindles based on these characteristics.

The first step involved calculating the first derivative of the envelope to detect

local maxima (peaks) and minima (valleys) by analyzing the zero crossings.

$$\text{If } \frac{d}{dt}[env(t-1)] > 0 \wedge \frac{d}{dt}[env(t)] < 0 \Rightarrow t \text{ is a peak}$$

$$\text{If } \frac{d}{dt}[env(t-1)] < 0 \wedge \frac{d}{dt}[env(t)] > 0 \Rightarrow t \text{ is a valley}$$

To consider the detected peaks and valleys as valid, an amplitude threshold was applied, specifically a moving threshold ,corresponding to the mean value of the alpha rhythm envelope within a 20 second window. Peaks were accepted if their amplitude was higher than $\tau(t)$, while valleys were considered if their amplitude was below $k \cdot \tau(t)$ with $k = \frac{\sqrt{2}}{2}$, ensuring a sufficient separation between local maxima and minima. Figure 35 shows the mobile threshold as well as the local peaks and valleys.

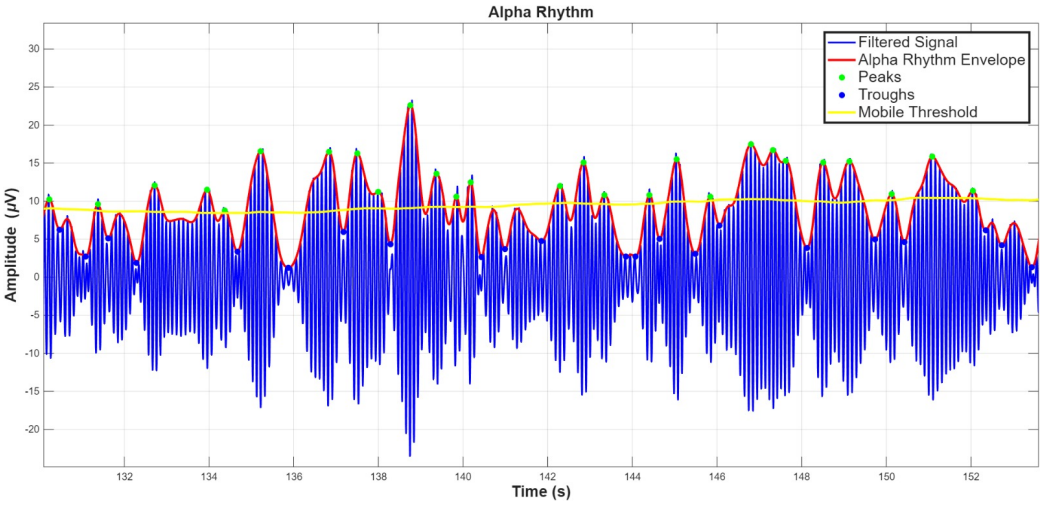

Figure 35: Local peaks and valleys of the envelope with the mobile threshold for alpha spindles identification.

At this point, each alpha spindle was extracted by considering the portions of the alpha rhythm between two consecutive valid valleys, containing at least one valid peak. This ensures that the extracted time series exhibit the typical 'waxing and waning' morphology of the alpha spindles. Figure 36 shows the extracted alpha spindles in a segment of the Alpha Rhythm.

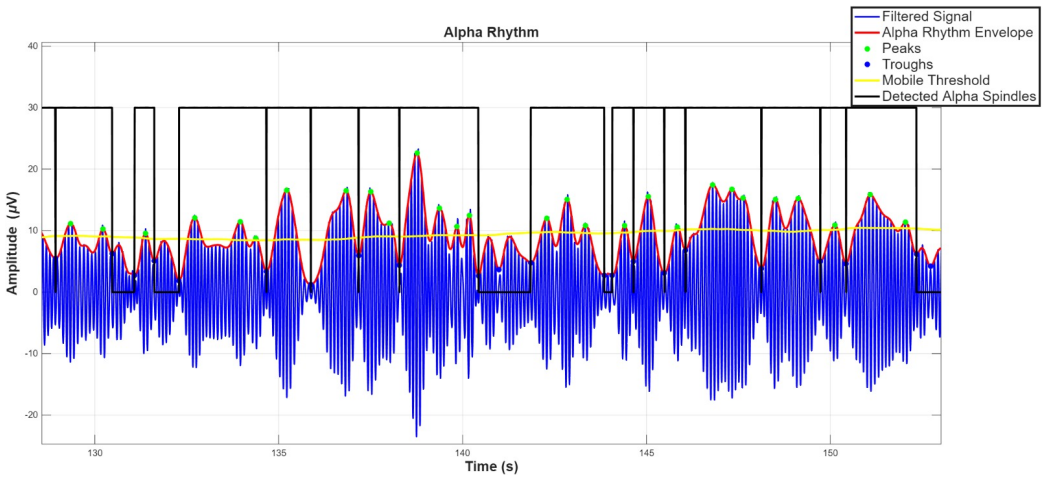

Figure 36: Alpha spindles extracted from a segment of the Alpha rhythm.

Once the alpha spindles were extracted,the next step was their morphological characterization. Alpha spindles were described using the following parameters:

- **Duration**: the time interval, expressed in seconds, between two consecutive valleys that define the start and end of the event:

$$\text{Alpha Spindle Duration} = t_{\text{end},i} - t_{\text{start},i} \tag{48}$$

  Where:

  - $t_{\text{start},i}$ is the starting instant of spindles i,
  - $t_{\text{end},i}$ is the ending instant of spindles i,

- **Amplitude**: the mean value of the amplitude envelope of the alpha rhythm within each oscillatory event:

$$\text{Amplitude} = \frac{1}{N_i} \sum_{n=t_{\text{start},i}}^{t_{\text{end},i}} env[n] \tag{49}$$

  Where:

  - $env[n]$ represents the amplitude envelope of the alpha rhythm
  - $N_i = t_{\text{end},i} - t_{\text{start},i} + 1$, is the number of samples in spindle i.

- **Incidence rate**: the occurence frequency of oscillatory events, expressed as the total number of detected alpha spindles relative to the total signal duration in seconds:

$$\text{Incidence rate} = \frac{N}{T} \tag{50}$$

  Where:

  - N is the total number of detected spindles
  - T is the total duration of the recorded alpha rhythm, expressed in seconds.

Since the alpha rhythm manifests as a succession of transient oscillatory events, variations in the average morphological features of the alpha spindles may influence the behavior of the EEG oscillations in the alpha band. In particular, an increase in any of these parameters would reflect a global increase alpha rhythm's power. From a physiological perspective, each parameter highlights a specific aspect of the underlying neuronal dynamics [70].

In addition to the morphological characterization, the alpha spindles were also statistically described through the Alpha Control Ratio (ACR):

- **Alpha Control Ratio**
  The Alpha Control Ratio (ACR) is defined as the ratio between the average spindle duration and the standard deviation of the spindle durations:

$$\text{Alpha Control Ratio} = \frac{\frac{1}{N}\sum_{i=1}^{N} d_i}{\sqrt{\frac{1}{N+1}\sum_{i=1}^{N}(d_i - \bar{d})^2}} = \frac{\bar{d}}{\sigma_d} \tag{51}$$

  Where:

  - d_i is the duration of spindle i,
  - $\bar{d}$ is the mean spindle duration,
  - σ_d is the standard deviation of the spindle durations.

  The alpha control ratio, as defined, is a indicator of the alpha rhythm variability. Higher ACR values indicate a more regular alpha rhythm, associated with a more homogeneous distribution of spindles durations. Conversely, lower values indicate a greater variability in the generation of oscillatory events [71].

Following the same methodology applied to the full EEG signal, a complexity analysis was also conducted on the amplitude envelope of the alpha rhythm $x^{\alpha}(t)$ using the 'Detrend Fluctuation Analysis'.

- **Detrend Fluctuation Analysis (DFA)**
  The DFA method, first introduced by Peng and all [72], quantifies intrinsic long- range temporal correlations within a time series, providing valuable information about the complex dynamics of amplitude fluctuations in the alpha rhythm.

The analysis steps are the following:

1. From the amplitude envelope of the alpha rhythm, the integrated signal $Y(t)$ is computed:

$$Y(t) = \sum_{t'=1}^{t} env(t') \tag{52}$$

2. The integrated time series is divided into non overlapping segments of length τ window, where the values are logarithmically spaced. The τ values space between 200 ms (the minimum duration of an alpha burst) and half the total signal length.

3. The local trend is subtracted from the integrated signal to obtain the detrended signal series $\varepsilon_\nu(\tau)$:

$$\varepsilon_\nu(\tau) = Y(\tau) - Y_\nu(\tau) \tag{53}$$

4. The mean squared fluctuation $F^2(\tau, \nu)$ of each segment is computed:

$$F(\tau) = \sqrt{\frac{1}{N_\tau} \sum_{\nu=1}^{N_\tau} F^2(\tau, \nu)} \tag{54}$$

   Where N is the number of elements in the segment ν.

5. To obtain a representative value of the alpha rhythm in the τ scale, $F^2(\tau, \nu)$ is averaged over all segments:

$$F^2(\tau, \nu) = \frac{1}{N} \sum_{\tau=1}^{N} [\varepsilon_\nu(\tau)]^2 \tag{55}$$

Where N_τ is the number of segments of the alpha rhythm at the τ scale. Typically the relationship between $F(\tau)$ and τ is linear on a double logarithmic scale and can be described by:

$$\log F(\tau) = \alpha \cdot \log \tau + C \tag{56}$$

Where the angular coefficient α is the scaling exponent of the original series. Scaling exponents in the range $0.5 - 1$ indicate the presence of persistent long range correlations. A signal with no correlations, such as white noise, has a scaling exponent of 0.5 [73].

4.4.5 ECG Analysis

A dedicated algorithm computed by the research group, operating independently of the Polar band, enables the visualization and storage of relevant signals into Excel tables. In particular, the first column contains the timestamp in milliseconds, while the following columns record either the Heart Rate, the accelerations along the three axes of the reference system used by the heart rate monitor, or the ECG signal.

The Matlab software enables, through a simple command, the loading of these Excel files, recreating a data structure identical to that of the original *.csv* file.

Initially, the acquisition algorithm didn't specify the sampling frequency. However, using the timestamp information, it was observed that the sampling rate was not constant, fluctuating around 130 Hz. Therefore, all signals were resampled at 125 Hz to obtain evenly spaced samples both in time and among different subjects. The analysis of the chest-strap output focused especially on the ECG signal, as this was only a secondary aspect of the thesis, whose main focus was on the effects of BB stimulation on EEG signals.

Once the ECG signals were loaded and resampled, they were realigned with the respective EEG signals to ensure that the analyzed time intervals matched. Specifically, the first timestamp of the *.easy* file was taken as reference, with a one-second delay applied, considering the EEG sampled at 500 Hz as it was preferable to start from the first complete second. The duration of each phase was then added to the initial timestamp, minus two seconds, to compensate for the initial delay and to ensure that only complete seconds were considered, thus defining the temporal boundaries of interest. Once the temporal limits corresponding to the different acquisition phases were established, the ECG signals were divided into three parts according to the phases and saved into a data structure.

The realigned signals were then processed by Pan Thompkins algorithm, which extracted the QRS complexes from the ECG signals, allowing for the calculation of features based on these intervals by obtaining the positions and the amplitude values of the R waves.

Specifically, the algorithm consists of a series of three digital filters: the first is a bandpass with integer coefficients composed of cascaded low pass, with a cutoff frequency of 15 Hz, and high pass, with a cutoff frequency of 5 Hz, filters to reject noise the second is a derivative filter and the third involves squaring the signal's amplitude followed by passing it through a moving window integrator. Finally, adaptive thresholds and temporal control of the interval between peaks are applied to accurately detect the positions of the QRS complexes, every step is shown in Figure 37 [74].

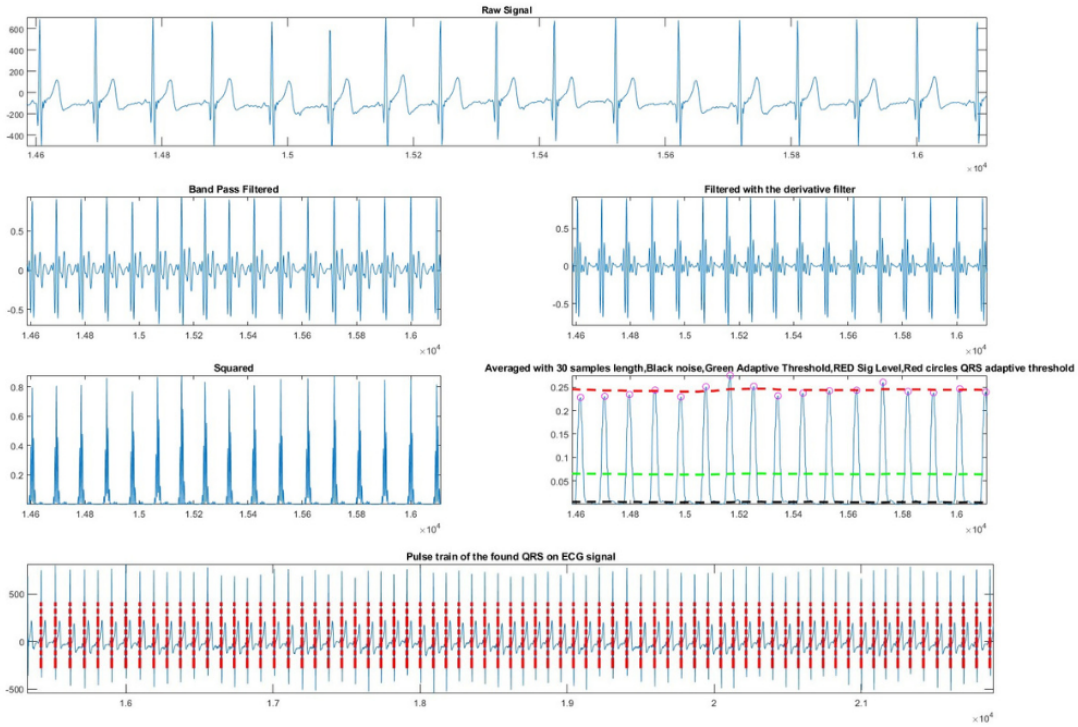

Figure 37: Effects of each Pan Thompkins algorithm step on the ECG data.

With the position of the R peaks identified, the main feature extracted based on the R-R intervals was as follows:

- **Heart Rate**
  The Heart Rate is calculated from the time interval between two consecutive R peaks in the ECG signal, known as the $R-R$ interval. This interval is expressed in seconds and represents the time between two successive heartbeats. The formula used to calculate the heart rate, expressed in beats per minute (bpm), is:

$$\mathrm{HR} = \frac{60}{\mathrm{RR}} \tag{57}$$

Where HR is the heart rate and RR is the average time interval computed over $R - R$ intervals extracted from the ECG signal. This approach provides immediate and precise estimate of heart rate based on the detected R peaks [75].

5 Results and Discussion

In this section, the results obtained from the EEG and ECG signals recorded during the different acquisitions of the experimental protocol are presented.

The results, which will be the focus of the following sections, are organized in a way that provides systematic answers to the experimental questions introduced at the beginning of this work.

The discussion will first address the results related to the clustering task, and then move on to analyzing the impact of the stimulation on brain oscillatory mechanisms, with particular attention to the modulation of the alpha rhythm.

After completing the analysis concerning the effects of continuous stimulation through BB on cerebral activity, attention will shift onto the analysis of the results related to the activation of the autonomic nervous system.

5.1 Clustering Output

The implementation of a clustering algorithm operating in a multivariate space, generated following the principal components analysis, represents the strategy adopted to address one of the central questions of this study.

Clustering was used with the aim of verifying whether continuous stimulation through BB is capable of influencing cortical activity to such an extent that observations from the stimulation or post stimulation phases were clearly distinguishable from those associated with the baseline condition.

Figures 38 and 39 report the accuracy percentages achieved by the k-means clustering algorithm in correctly classifying observations from the experimental conditions being compare. Specifically, Figure 38 refers to the comparison between the stimulation and baseline phases, while Figure 39 presents the results of the comparison between post stimulation baseline phases.

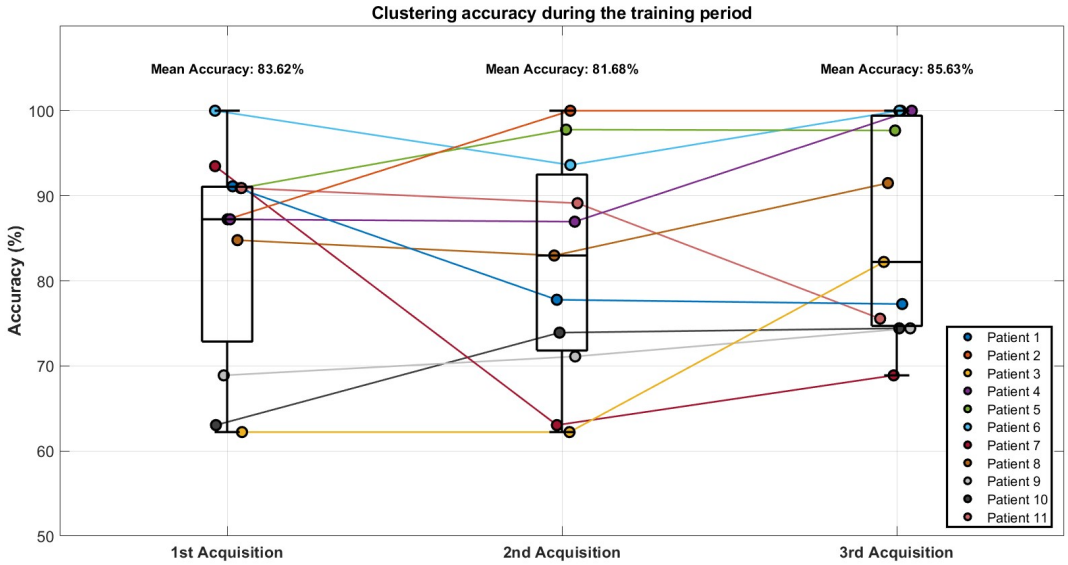

Figure 38: Stimulation accuracy across the acquisition sessions.

For each of the three acquisition sessions planned in the experimental protocol, a boxplot is shown representing the distribution of accuracy values for each participant. Markers corresponding to the same subject are connected across the different acquisitions, providing not only information related to individual sessions but also an overview of the evolution of each participant's response to the stimulation.

Observing Figure 38, which shows the comparison between the stimulation and baseline phases, it can be seen that the accuracy values, indicating how well each phase is correctly classified, are very high across all sessions, with a mean accuracy of 83,63% for the first acquisition, 81,68% for the second and 85,63% in the third and final one.

However, a clear inter subject variability is evident in all three acquisition sessions: for some subjects, the distinction between stimulation and rest conditions is very clear, with accuracy values close to 100% while for others

the separation is much less pronounced, with significantly lower accuracy values.

In the second acquisition, recorded at the end of the training period, and in the third one, the distribution of accuracy values appears more dispersed compared to the first acquisition, where participants experienced the stimulation for the first time.

Between the second and third acquisition sessions, an average of four days passed during which participants were asked to suspend daily stimulation sessions.

What emerges from comparing the clustering performances in discriminating between the two experimental phases is that, after the interruption of the training period, there is an improvement or no change in accuracy, which except for one subject remains at least unchanged compared to that observed during the second acquisition.

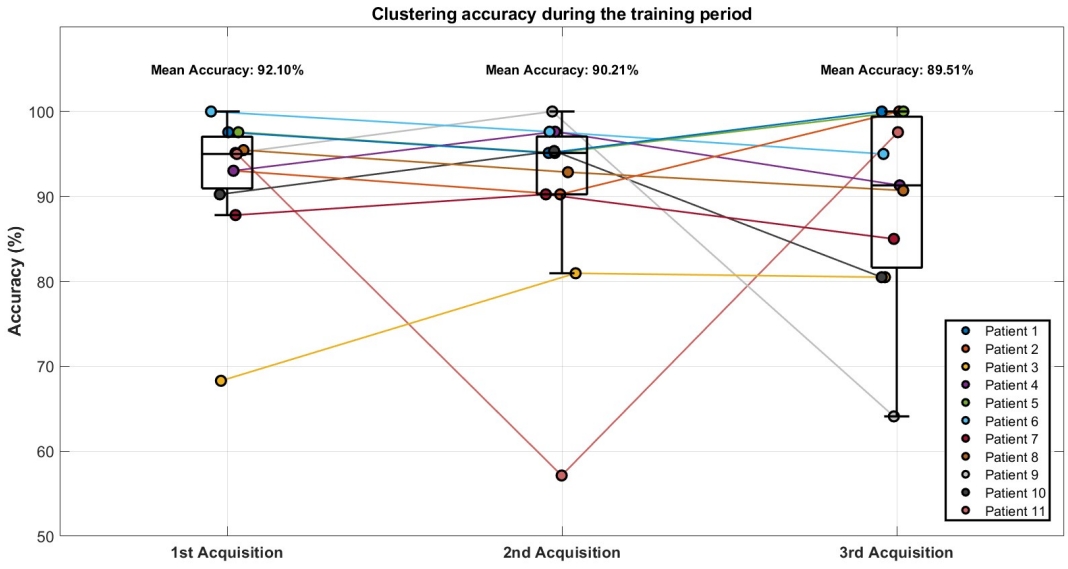

Figure 39: Post-Stimulation accuracy across the acquisition sessions.

During each data acquisition session, in addition to recording the subject's response while listening to the audio track containing BB, an additional seven minutes of EEG signal were recorded, corresponding to the post stimulation phase.

The goal of acquiring EEG recordings after the stimulation phase is to understand whether the effect induced by BB is transient, limited solely to the exposure period, or whether the evoked mental state persists over time.

In this regard, similarly to what was described for the stimulation phase, Figure 39 shows the distributions of accuracy values with which the k-means algorithm correctly separates the post-stimulation and baseline observations across all three different acquisition sessions.

What emerges from the figure is that, also in this case and across all three sessions, the clustering algorithm is able to distinguish the two phases with high precision.

Furthermore, when analyzing the temporal trend of the clustering algorithm's performance, it is observed that accuracy values remain essentially stable between the first and second acquisition sessions. Moreover, in most cases, the precision with which the post stimulation condition is separated from the resting condition exceeds 90%. The only notable exception is subject 11, for whom a sharp decrease in model accuracy is recorded between the two sessions. During the third acquisition, although the overall accuracy remains high a greater dispersion in the distribution of accuracy values is observed.

As mentioned in the previous sections, the comparison between the phases of the experimental protocol in this study was carried out on two levels. The first level focused on analyzing each acquisition session individually, examining the separability between phases the observations within a single session, which results have been just presented. The second level of analysis aimed to provide a broader evaluation of the capability of BB to influence

brain activity by altering cortical dynamics relative to the baseline condition.

To obtain a more comprehensive and robust understanding of the effects of BB on neural activity, all observations from the experimental conditions under comparison were projected into a shared multivariate space that included data from all three acquisition sessions.

Figure 40 shows the distributions of accuracy value with which the k-means clustering algorithm was able to separate the experimental conditions. The boxplot on the left corresponds to the comparison between the stimulation and the baseline phase, while the one on the right shows the results for the comparison between the post stimulation phase and the baseline phase.

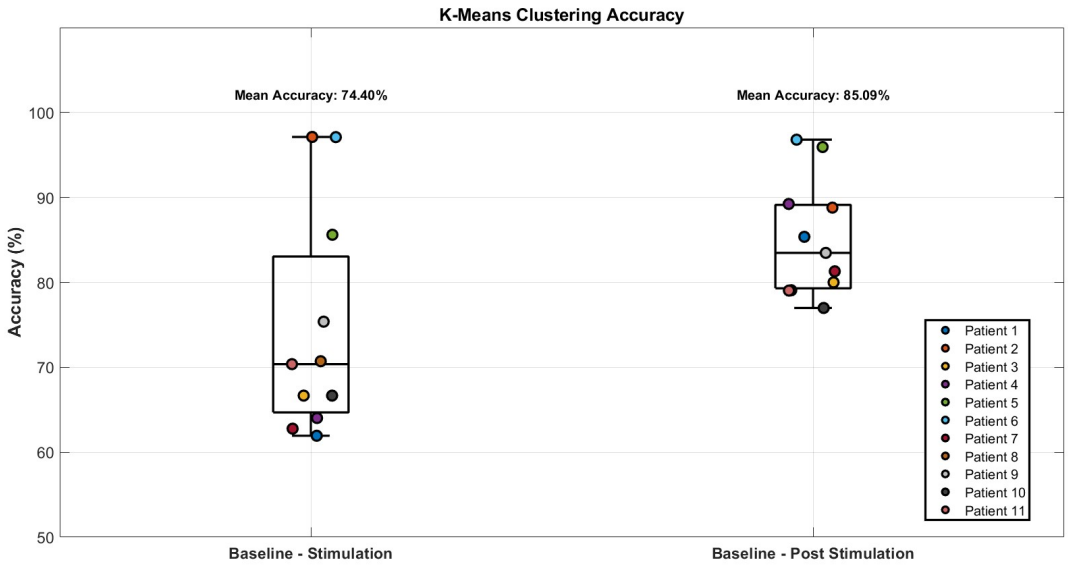

Figure 40: Accuracy of baseline vs. stimulation and baseline vs. post stimulation for the entire subject, comprehending all three sessions.

The analysis of the results reveals a significant difference in the clustering algorithm's ability to distinguish both the stimulation and post stimulation

conditions from the baseline. Specifically, the average accuracy obtained when comparing the stimulation condition to the baseline is 74,40%, while the comparison between the post stimulation condition and the baseline yields a noticeable higher average accuracy of 85,09%.

This result, supported from the observation that at the single acquisition level analysis the clustering algorithm show a superior capacity to separate the observations relative to post stimulation respect to stimulation, suggesting that the induced effect by BB, not only persists in time but can consolidate after the exposition period to the stimulus.

One possible explanation for this result may lie in the cognitive processes involved during the stimulation phase. Due to the sensory nature of the stimulus, participants may perceive the binaural beats differently while listening to the audio track. This perception introduces variability in the actual effect of the stimulation, influenced by factors as attention, subjective interpretation of the sound, or the degree of engagement. Conversely, during the post stimulation phase, the perceptual component is no longer present, and what is observed may be a cleaner expression of the effect of BB, no longer influenced by perceptual processes activated during listening.

Despite the observed differences between the stimulation-baseline and post stimulation-baseline comparisons, the algorithm's ability to reliably separate the different experimental conditions, even when considering a much larger dataset spanning temporally distant acquisition sessions, suggests that the effects of BB on neural activity modulation are robust and sufficiently stable to emerge beyond individual sessions. Furthermore, the fact that such changes are evident even in aggregate analysis, which is inherently more complex and subject to increased variability, indicates that the effects of BB are strong enough to ensure good separability between conditions even in the presence of noise introduced by inter subject and temporal variability.

To support the validity of the results discussed so far, the outcomes of the permutation test are presented below. This test was conducted to evaluate the statistical significance of the separation between the different experimental conditions, both at the level of individual acquisitions and at the entire subject.

Figures 41 and 42 specifically illustrate the results of the statistical test applied to single acquisition session. In particular, Figure 41 refers to the stimulation condition compared to baseline, while Figure 42 refers to the post stimulation condition compared to baseline.

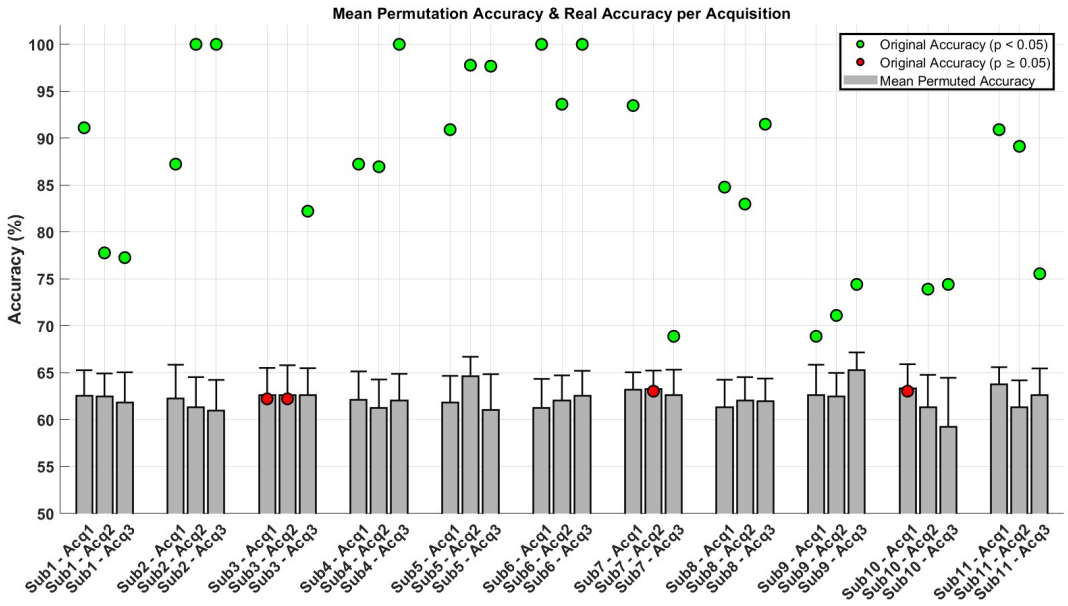

Figure 41: Permutation accuracies for baseline vs stimulation across all the acquisition and subjects.

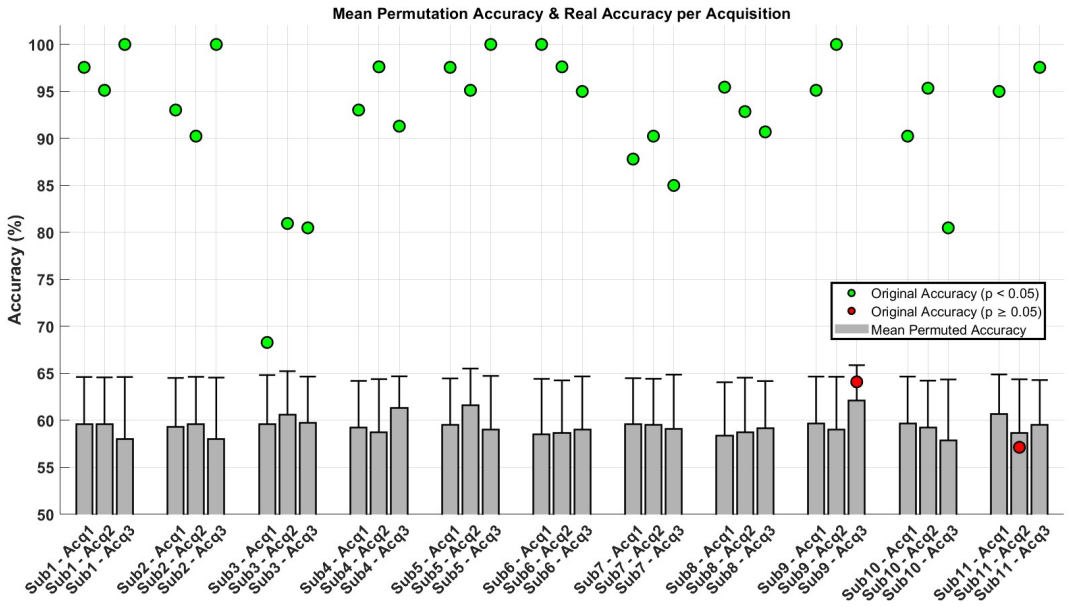

Figure 42: Permutation accuracies for baseline vs post stimulation across all the acquisition and subjects.

In each figure, every barplot represents the distribution of accuracy values obtained through the random permutation of the class labels of between the two conditions being compared. The original accuracy value, calculated without permuting the labels, and indicating how well the clustering algorithm correctly assigns observations to their actual class, is marked with a green dot if the corresponding p-value is less than 0.05, indicating statistically significant separation. If the p-value exceeds the significance level, the original accuracy value is shown in red.

In a similar manner to the analysis conducted for individual acquisitions, Figures 43 and 44 report the results of the statistical test performed on the clustering outcome obtained from aggregating observations across all three acquisition sessions. Specifically, Figure 43 corresponds to the comparison between stimulation and baseline, while Figure 44 shows the results for the comparison between post stimulation and baseline.

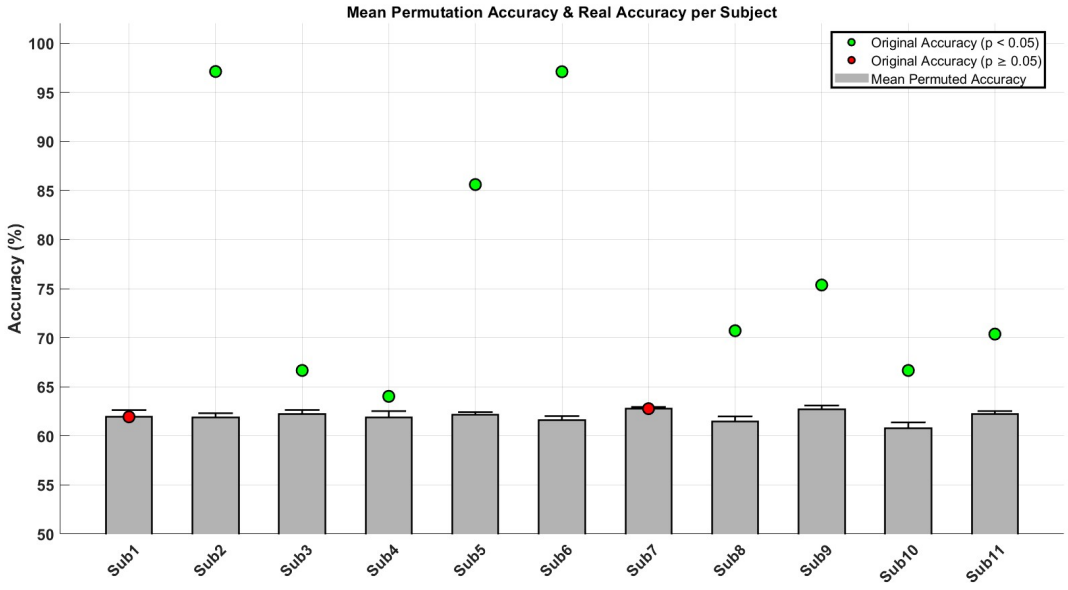

Figure 43: Permutation accuracies for baseline vs stimulation of the entire subjects.

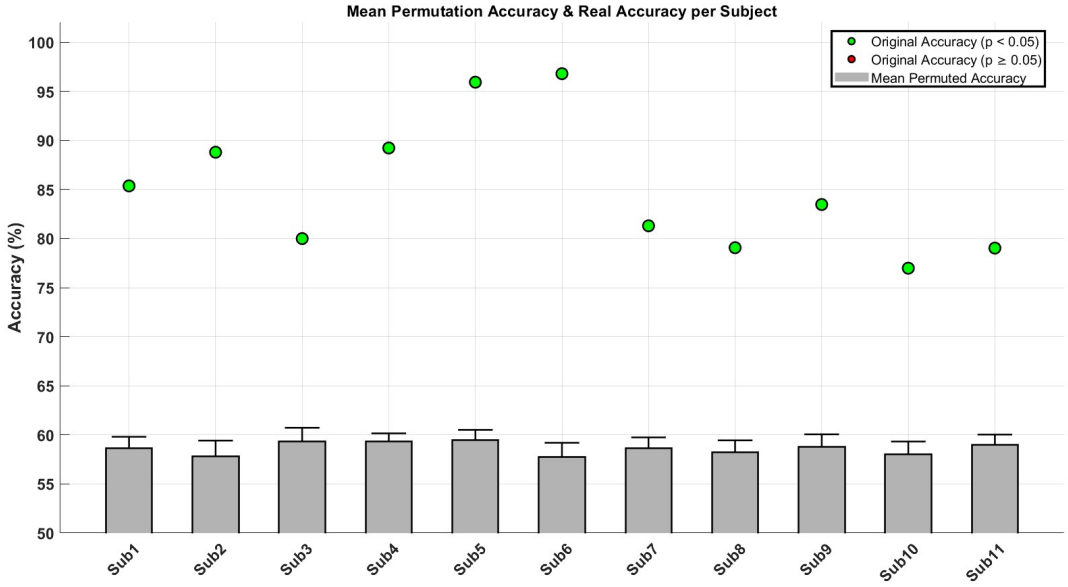

Figure 44: Permutation accuracies for baseline vs post stimulation of the entire subjects.

The statistical test results show that, for the single acquisition analysis, the separation between stimulation and baseline is statistically significant in 29 out of 33 cases. Regarding the post stimulation vs baseline comparison, statistical significance is confirmed for all acquisitions except for the third session of subject 9 and the second session of subject 11. Notably, the few cases where statistical significance isn't reached correspond to acquisitions with low clustering performance in classifying the observations correctly.

When analyzing data at the subject level, statistical significance is consistently achieved when comparing the post stimulation condition to baseline. In contrast, for the stimulation condition, significance isn't reached in two subjects, being observed in 9 out of 11 cases.

The results suggest that the observed separability between the stimulation and post stimulation conditions, compared to the baseline, isn't due to ran-

dom phenomena. On the contrary, it can be confidently stated that BB have a consistent and measurable impact on cortical activity, sufficient to enable a clear distinction between experimental phases. This effect appears to be particularly evident and robust during the post stimulation condition.

5.2 Alpha Rhythm Modulation

In this section the results of the analysis aimed at understanding how BB stimulation influences the spontaneous modulation of the alpha rhythm are presented and discussed.

To verify whether the administration of BB induces a significant change in the dynamics of the alpha rhythm, a statistical analysis was performed on both the morphological parameters used to characterize the extracted alpha spindles and the temporal complex metrics related to signal amplitude fluctuations. These metrics were compared across the different experimental conditions.

Specifically, a statistical approach was chosen that would provide an overall view of how BB affected the alpha rhythm. This was done through a repeated-measures analysis, incorporating within each experimental condition the values derived from all three acquisition sessions of each subject.

The analysis focused on pairwise comparisons between conditions: stimulation vs baseline, post stimulation vs baseline and stimulation vs post stimulation. The observations from the different experimental phases were treated as paired data, as they originate from the same subjects and are therefore intrinsically correlated. The use of repeated measures tests was necessary to account for the dependent structure of the data, which includes within subject correlations introduced by the experimental design.

The choice of statistical test for comparing the different experimental con-

ditions was based on the assessment of normality of each distribution. To this end, the Lillieforst test was applied separately to each distribution corresponding to the baseline, stimulation and post stimulation conditions. When comparing pairs of conditions, a paired t-test was used if both distributions met the assumption of normality. If at least one of the distributions violated this assumption, a non parametric paired test, specifically the Wilcoxon signed rank test, was used instead.

Finally, statistical significance was evaluated based on the p-value. Differences between conditions were considered significant at $p < 0.05(*)$, highly significant at $p < 0.01(**)$ and very highly significant at $p < 0.001(***)$.

Figure 45, shown below, is divided into three panels, each representing a different metric used to characterize the alpha rhythm over the frontal channels F3 in light blue and F4 in orange, across the three experimental phases: baseline, stimulation post stimulation.

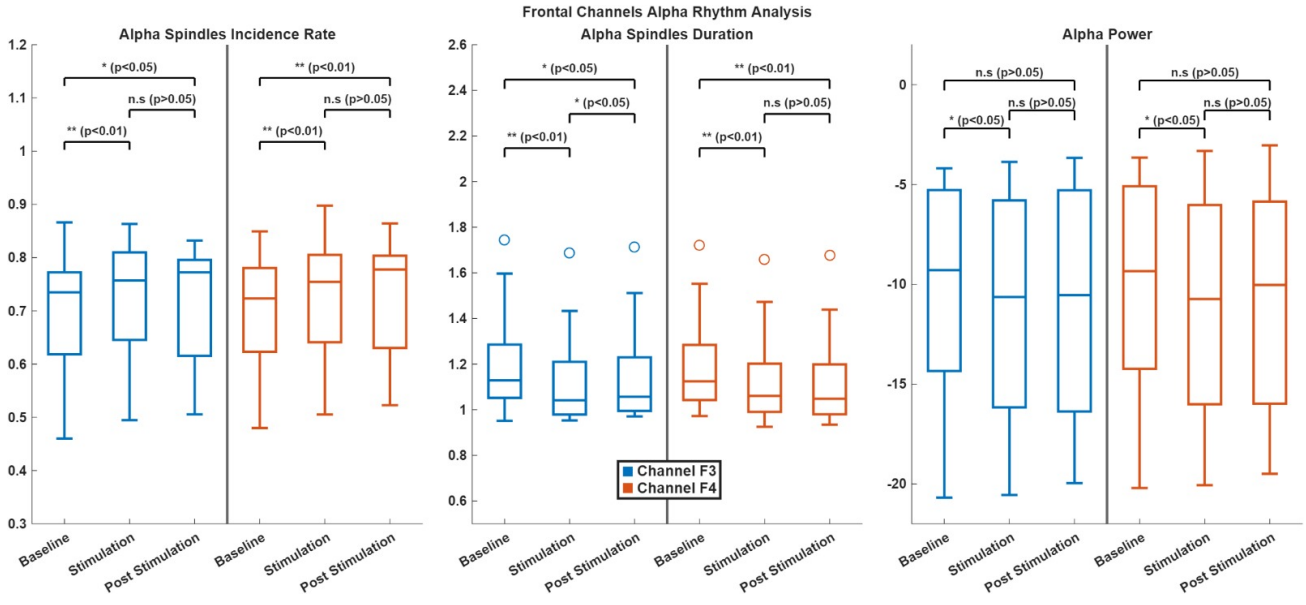

Figure 45: Alpha rhythm parameters extracted on the frontal channels.

In detail, a significant increase in the incident rate of alpha spindles was observed during the stimulation phase compared to the baseline, in both F3 and F4 channels. This increase tends to persist, particularly in channel F3, even during the post stimulation phase. At the same time, a significant reduction in the mean duration of alpha spindles was observed during and after the stimulation in both channels. This suggests a decreased stability in the spontaneous oscillatory processes generated by neuronal activity, favoring shorter and more transient events.

Another noteworthy finding concerns the significant reduction in alpha band power of the EEG signal during stimulation. While this reduction persists into the post stimulation phase for channel F3, a return toward baseline values is observed in channel F4.

No significant changes were found in the mean amplitude of the alpha spindles, suggesting that the effect of the stimulation primarily acts on the frequency of occurrence and duration of the oscillatory events associated with the alpha rhythm, rather than their intensity.

Overall, the results suggest that the BB stimulation can significantly modulate the morphology of the spindles underlying the amplitude fluctuations of the alpha rhythm, and alter its overall energetic content.

Furthermore, an important observation is that the modulation of the alpha rhythm does not appear to be transient, but rather prolonged over time: indeed, no statistically significant differences were found between the stimulation and post stimulation conditions.

To provide a comprehensive overview of the morphological analysis of alpha spindles, the graphs showing the variation of each metric used to characterize the alpha spindles across the different experimental conditions are reported in Appendix.

The discussion on the modulation of the oscillatory activity of the alpha rhythm concludes with the analysis of the temporal complexity of its amplitude, performed using the Detrend Fluctuations Analysis.

The Figure 46 displays the trend of the DFA exponent α calculated from the alpha rhythm envelope extracted from all eight EEG recording channels. It reveals that, during the stimulation phase, the DFA exponent α undergoes a significant reduction across all channels, suggesting a widespread modification, extending throughout the entire cortical region, of the temporal organization of alpha fluctuations as a result of the stimulation. Interestingly, and consistent with the morphological analysis, the most pronounced changes are again observed in the F3 and F4 channels, located in the frontal region.

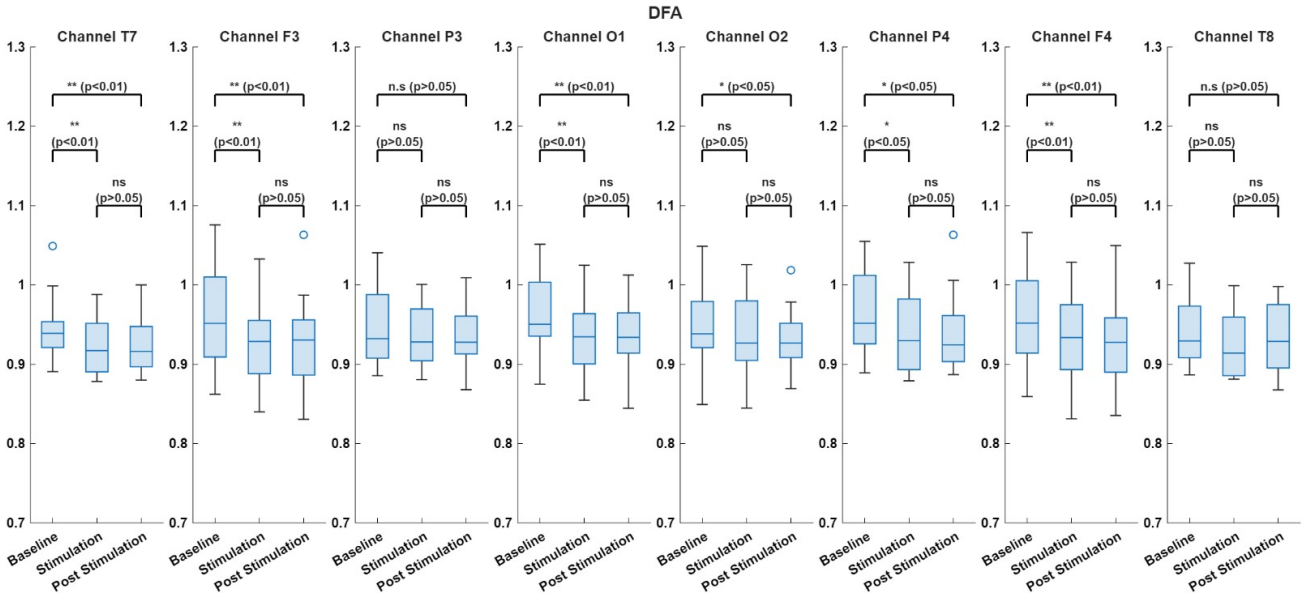

Figure 46: DFA parameter extracted on all the electrodes.

Moreover, the DFA exponent remains lower than baseline levels even during the post stimulation phase, indicating a lasting effect that persists after the acoustic stimulation ends. This is confirmed by the fact that, in almost all

channels except for T8, the distribution of α values during post stimulation differs significantly from those observed during baseline.

Similarly, the absence of statistically significant differences between the stimulation and post stimulation phases in all channels suggests that these two conditions tend to adopt a similar configuration.

Overall, the findings indicate that BB stimulation significantly alters the temporal structure of spontaneous alpha oscillations in a widespread manner across all examined brain regions, with effects that persist beyond the stimulation period. Specifically, the reduction in the DFA exponent suggest a reorganization of the fluctuation dynamics of the alpha rhythm, making them more irregular and less predictable under the influence of stimulation.

5.3 Heart Rate Variability

The ECG signal analysis focused specifically on extracting the heart rate of the subjects by identifying the R peaks using the Pan Thompkins algorithm.

This analysis was conducted alongside the EEG signal investigation to assess whether other physiological signals were influenced by BB stimulation. In particular, evaluating the heart rate can provide insight into potential changes in the subject's psychophysiological state. For instance, an increase in heart rate may indicate a stress response, whereas a decrease may suggest a relaxation effect.

The Heart Rate considered was the average value calculated over the entire duration of each experimental phase. Figures 47, 48 and 49 display the evolution of this parameter across the three phases of each acquisition.

In Figure 47, representing the first acquisition, all participants, except for two, showed heart rates within a normal physiological range that remained stable over time. The two exceptions started with elevated heart rates that progressively decreased throughout the session. This may attributed to a

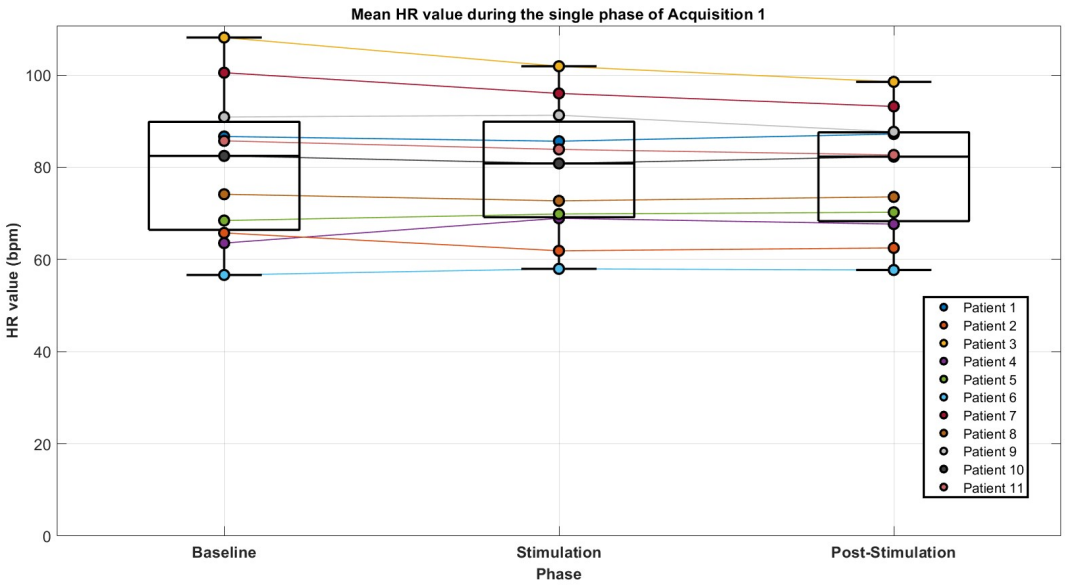

Figure 47: Heart Rate across the phases of the first acquisition session.

white coat effect, where the initial stress related to the experimental context gradually faded, not necessarily due to BB stimulation but rather to natural adaption.

In Figure 48, referring to the second acquisition, all patients maintained a stable heart rate throughout the session, with no significant fluctuations attributable to BB stimulation.

Similarly, Figure 49, which presents data from the third acquisition, shows a consistent heart rate trend across all subjects, again without meaningful changes that could be linked to the stimulation.

In conclusion, based on the heart rate data across the different acquisitions, there is no clear evidence of a physiological effect induced by binaural beats stimulation.

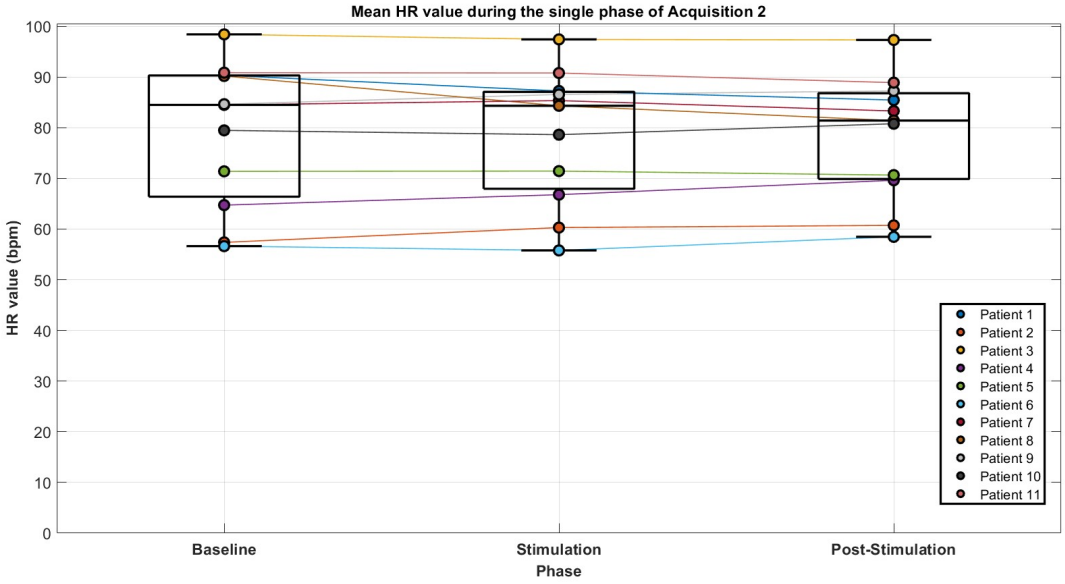

Figure 48: Heart Rate across the phases of the second acquisition session.

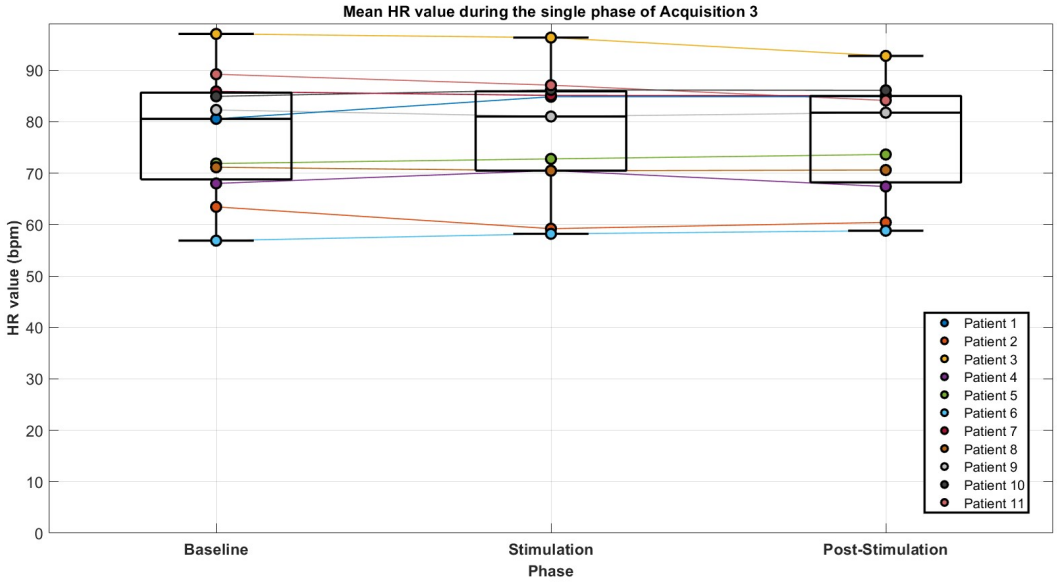

Figure 49: Heart Rate across the phases of the third acquisition session.

6 Conclusion

In this chapter, a clear and structured overview of the effects induced by binaural beat stimulation will be presented, based on the results obtained through the adopted analysis protocol. First, precise answers will be provided to the initial research questions. This will be followed by a critical interpretation of the findings, comparing them with the existing literature on the topic and highlighting the specific contribution of this study within the broader context of research on binaural beats. Finally, the limitations of the study will be discussed, and possible directions for future developments will be proposed, with the aim of advancing the understanding of the effects of BB on cortical electrical activity.

6.1 Answer to Experimental Question

> *"Can EEG signals show real changes in brain activity or physiological state during or after listening to BB?"*

The results obtained from the analysis method described in the Materials and Methods section show that both during and after the administration of BB, cortical electrical activity exhibited behavior that differed from that recorded during the baseline condition. Moreover, the ability to discriminate between the different experimental conditions wasn't limited to single-sessions analyses; excellent results were also obtained when the analysis was extended to include data from all three acquisition sessions.

The effectiveness of the multivariate approach in identifying a cerebral response to the stimulation suggests that the observed variations in cortical activity cannot be attributed to a single feature of the EEG signal. Instead, they point to a more complex modulation mechanism that emerges from the combination of multiple variables describing brain activity as a whole.

The results also highlighted an interesting aspect: the high heterogeneity in cortical responses to this type of stimulation. No consistent patterns emerged in how EEG signal characteristics changed in response to BB. Furthermore, there was no consistency either across subjects or across different sessions for the same individual in terms of which features showed the most significant variations between experimental conditions. The features contributing to the cortical response to binaural beat stimulation varied and didn't necessarily originate from the same brain areas.

Another surprising finding is that the separation between experimental conditions was even more pronounced when comparing the post stimulation phase to the baseline, compared to the separation observed during the stimulation phase itself. This result was confirmed both in analyses conducted on individual acquisitions and those extended across the full dataset for each subject.

This result suggests that during stimulation, cognitive processes related to auditory processing are activated, with their intensity and nature varying significantly among individuals. These differences are presumably linked to how the BB are perceived and to the level of engagement the stimulus produces. Once the stimulation ends and the audio stops, the mechanisms tied to active sound perception cease. Therefore, the post stimulation phase may more directly reflect the effects of BB on each subject's neural activity.

From a physiological perspective, the analysis of heart rate variability didn't reveal significant changes indicative of parasympathetic system activation or deactivation. This could be attributed to the experimental setup: participants were seated comfortably and relaxed, with eyes covered, in a low stimulation environment. Under such conditions, it is plausible that the autonomic nervous system was already in a relatively calm and stable state, reducing the likelihood of observing marked variations induced by the stimulation.

> *"Is the BB effect on the cerebral rhythm immediate or does it require a training period in which the subject can synchronize more efficiently with the rhythm of the beats?"*

Since the effects of stimulation through BB aren't yet clearly understood, the effectiveness of the daily stimulation period was evaluated based on the variation in the degree of separability between experimental conditions, measured through the accuracy of the clustering algorithm.

From the analysis of the results, both in the comparison between the stimulation and baseline phases, and between the post stimulation and baseline phases, it emerges that excellent separation between different experimental conditions was achieved as early as the first recording session, in which subjects experienced BB stimulation for the first time.

Examining the evolution of accuracy values across the different acquisition sessions, no clear evidence emerges to suggest that the effectiveness of BB stimulation requires a prolonged exposure period to induce a stronger brain response. What can be observed is a greater heterogeneity in the degree of the separability between stimulation and baseline phases when comparing the first and second sessions: some subjects show improvement, other deterioration, and others no significant change.

The fact that the largest variations occur during the stimulation phases, while in the post stimulation phase, except for a single case, the differences between sessions are minimal, suggests that the training period may have influenced how each subject perceives and processes the binaural betas. This subjective change in the mode of stimulus processing could explain the greater variability observed in the distribution of accuracy values during the stimulation phase.

However, it wasn't possible to determine with certainty whether daily listening to BB progressively enhances the response to stimulation, or whether, on

the contrary, it leads to a saturation effect, thereby reducing the impact of BB and the ability to distinguish between experimental conditions.

The comparison between the initial and final acquisition sessions was expected to clarify whether the effectiveness of the stimulation depends on consistent training, or whether the effects persist even after the daily exposure is discontinued. Nevertheless, even in this case the results appear inconclusive and difficult to interpret, making it complex to establish with certainty whether repeated listening enhances the response over time, or instead causes a saturation effect that reduces efficacy.

> *"Does BB stimulation modulate the cerebral rhythm in the target frequency band?"*

The results of the analysis conducted on the modulation of alpha rhythm amplitude fluctuations induced by BB reveal that both during and after the stimulation, significant changes occur in the morphological characteristics of the alpha spindles, particularly in the frontal region, especially in channels F3 and F4. Specifically, the observed increase in the incidence rate of alpha spindles along with a reduction in their average duration, suggests a possible attempt to synchronize the alpha rhythm in the frontal channels with the BB. These beats manifest as short duration amplitude modulations that occur at a high temporal frequency. Furthermore, a reduction in the EEG signal's frequency content within the alpha band was observed, which proved to be statistically significant, specifically in the frontal channels. These findings appears to contrast with the hypothesis underlying the concept of brain entrainment, according to which stimulation at a specific EEG frequency should generate an increase in the power of the signal around the stimulation frequency. However, these findings support previous results from two existing studies in the literature, which showed that continuous, unmasked stimulation using pure beats primarily affects the frontal region of the cerebral cortex, and that stimulation within the alpha band leads to a reduction

in the overall power of the alpha rhythm [76] [25].

Finally, the α exponent derived from DFA appears to be a robust metric for identifying the effect of binaural beats on the alpha rhythm. The results showed a statistically significant reduction in this parameter across almost all brain areas from which the EEG signal was recorded, both during and after stimulation, suggesting that BB are capable of altering the temporal dynamics of alpha rhythm fluctuations. Specifically, it has been shown that in healthy subjects, a reduction in α exponent is observed during focused attention meditation tasks [77]. This finding suggests that stimulation through BB may effectively induce a state of relaxation and contribute to enhance attentional capacity.

In conclusion, the study carried out in this thesis contributed to clarifying some key aspects regarding stimulation with binaural beats, particularly when the stimulation frequency is calibrated to each subject's IAF. The results obtained from the analysis of EEG recording from the various participant highlighted an often overlooked aspect in studies involving BB: the subjectivity of individual response to stimulation. Moreover, the in depth analysis of the alpha rhythm allowed for a more accurate exploration of the brain entrainment mechanisms associated with binaural beat stimulation.

6.2 Limitations and Future developments

Despite the results obtained, this study presents several important limitations that should be considered for a potential methodological improvements and future investigations on the subject.

From a technical analysis perspective, one of the main issues concerns the lack of clear and widely accepted information regarding the specific cerebral response to binaural beat stimulation. This has made in particularly challenging to evaluate the long term effects of BB, as it is not yet clear which parameter should be used to demonstrate the effectiveness of the stimulation.

Additionally, the experimental design used to assess the training effects could be further improved. Firstly, the number of EEG and ECG recording sessions per subject should be increased by implementing daily monitoring. Furthermore, to conduct a longitudinal study capable of providing insights into how binaural beats affect the brain over increasing exposure time, the duration of the experimental protocol should be extended, lengthening both the training period and the phase in which home administration of BB is suspended.

Another valuable addition could have been the use of self assessment questionnaires, allowing participants to report their emotional responses to the stimulation. The integration of subjective data alongside the quantitative analysis of physiological signals would have allowed consideration of perceived effects during and after stimulation, which didn't emerge from the neuro physiological analysis alone.

Another limitation of the study concerns the equipment used to record EEG signals. Employing a high density acquisition system with a larger number of electrodes would have enabled a more detailed topographic analysis. This, in turn, would have allowed for the full exploitation of the ICA algorithm's potential to identify with greater accuracy the brain ares involved in the response to stimulation. Moreover, higher spatial resolution would have supported a more in depth analysis of changes in functional connectivity across different cortical regions.

It is also important to highlight the lack of standardization in the audio playback system. Each participant used their own personal devices, earphones and smartphones, to listen to the BB, inevitably introducing variability in sound quality and volume intensity. However, this choice was dictated by the longitudinal nature of the study, which required daily BB administration, making it essential to adopt a flexible protocol that could be easily integrated into the participants' daily routines.

In addition to the limitations related to the instrumentation and experimen-

tal design, another crucial aspect concerns the lack of shared guidelines in the scientific community regrading the optimal parameters to be used when designing audio tracks containing BB, in order to maximize the effectiveness of the stimulation. Specifically, there is no consensus on the ideal values for the carrier frequency, the beat frequency, or the degree of lateralization, depending on the intended neuro physiological target, such as relaxation or enhanced attention.

Another area that requires further investigation concerns the mode of BB administration. It is still unclear whether stimulation should be continuous and prolonged, whether it is more effective when delivered in blocks, or whether in a intermittent, burst like presentation yields better results. Additionally, it would be interesting to explore whether integrating BB with background music or with white or colored noise could amplify or modulate the effects of the stimulation.

Given these open issues, future studies should focus on a systematic analysis of binaural beats, with the aim of clarifying the mechanisms of action and identifying the optimal conditions for effective stimulation. In light of the results obtained in this work, which suggest a marked inter individual variability in the response to BB, it may be promising to move toward personalized stimulation protocols, possibly by employing biofeedback based approaches. Such methods could help tailor the technical parameters of the stimulation to the specific neuro physiological characteristics of each individual. Although this study already attempted to adapt the stimulation to the subject's characteristics using the IAF, implementing a real time adjustment of the parameters could further enhance the effectiveness of the BB.

Appendix

Subjects' IAF

Patient	IAF (Hz)	Earphones model
1	9,82	Airpods series 2
2	10,80	Airpods series 2
3	9,83	Airpods Pro
4	9,90	Airpods series 3
5	11,03	JBL 230 nc
6	9,84	Airpods series 3
7	10,88	Airpods series 3
8	10,51	Airpods series 2
9	10,54	QCY T1C
10	10,15	Apple EarPods
11	11,16	Airpods series 2

Table 1: Subject's IAF and earphones used.

Validation of optimization steps

The optimization pipeline, described in detail the Material and Methods section, was applied to a surrogate dataset with a number of elements comparable to that of the original dataset. Specifically, three different conditions were analyzed.

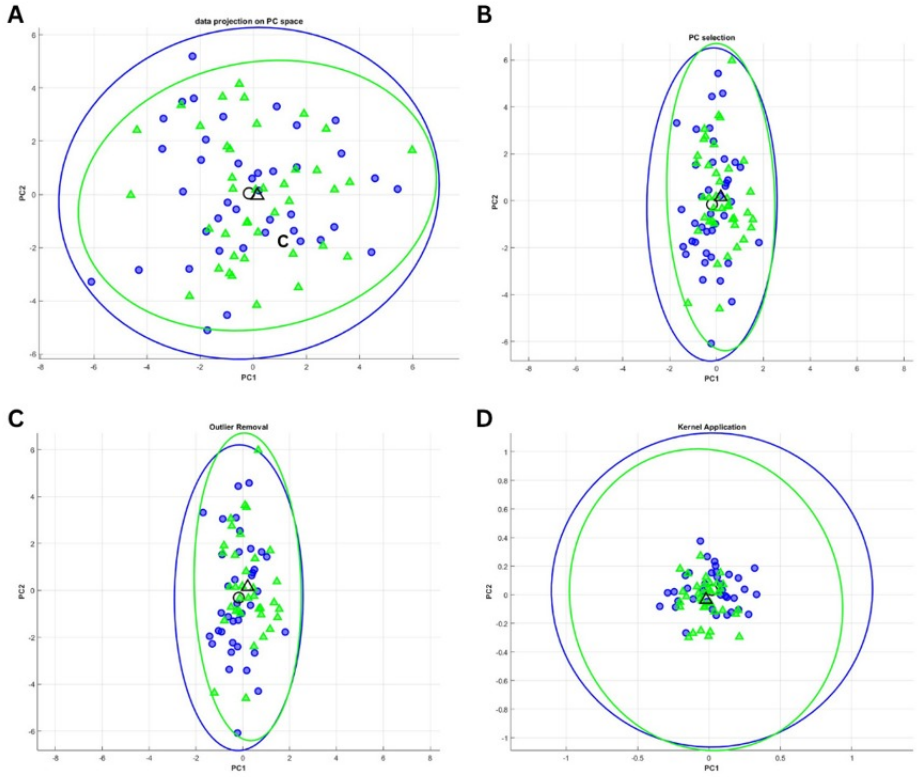

Figure 50: Optimization steps onto PC space for two $N_0(0,1)$ distributions.

In the first case, the analysis algorithm was applied to a dataset in which the two classes were represented by two standard normal distributions $N_0(0,1)$, with no structural differences. As shown in Figure 50, particularly observing panel A, the projection of the data onto the PC space reveals a complete overlap between the two distributions. After the optimization steps, which modify how the different observations of the two groups are represented within the PC space, the overlap between the two classes remains evident. This demonstrates that the proposed algorithm doesn't produce artificial separations between classes when no real differences exist between the distributions being compared. To complete the control analysis and further validate the

method, two additional tests on surrogate dataset were conducted, aiming to verify that the algorithm is capable of detecting a separation in the projection within the PC space real differences exist in the characteristics of the two compared distributions.

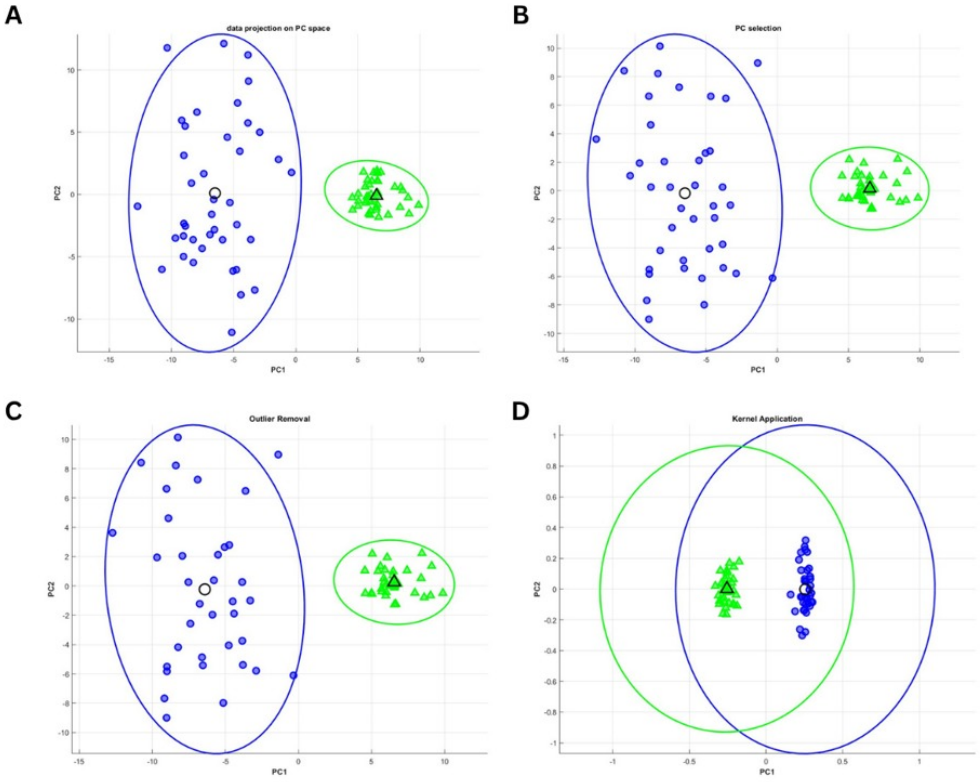

Figure 51: Optimization steps onto PC space for $N_1(0,2)$ and $N_2(1,1)$.

In the second condition, two gaussian distributions $N_1(0,2)$ and $N_2(1,1)$ were compared, characterized by different means and standard deviations, and represented in blue and green respectively in Figure 51. As shown in panels A-D, the optimization pipeline preserves the separation between the two classes throughout the various steps, confirming the sensitivity of the method to the presence of structural differences in the distributions.

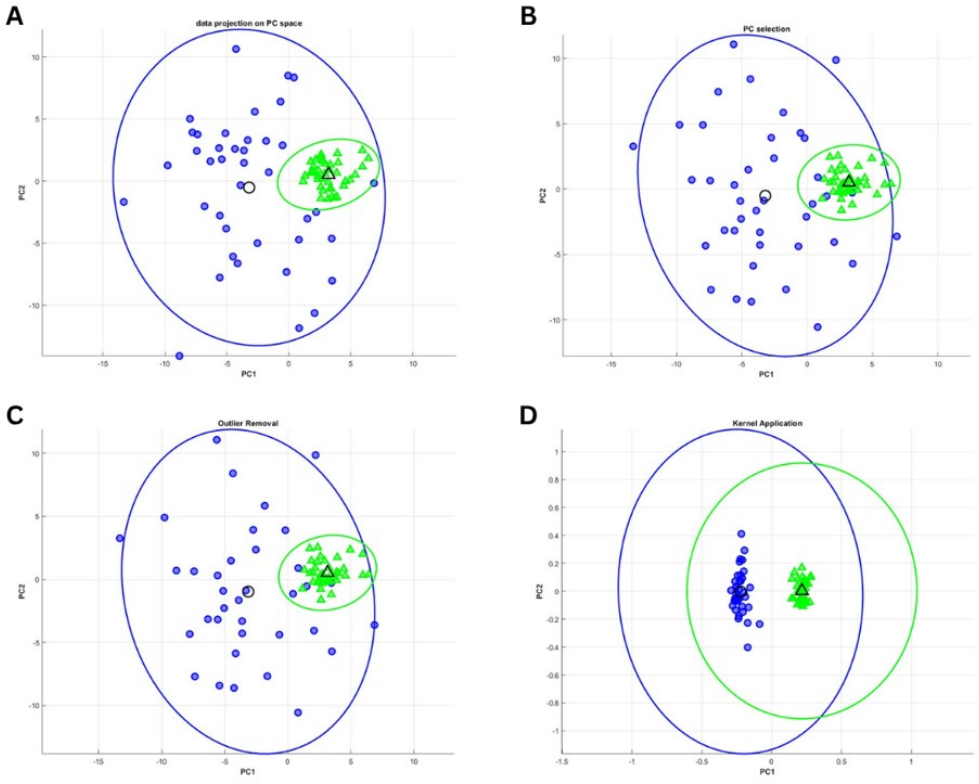

Figure 52: Optimization steps onto PC space for $N_1(0, 2)$ and $N_2(0.5, 1)$.

In the third condition, two gaussian distributions, $N_1(0, 2)$ and $N_2(0.5, 1)$, were analyzed. These were characterized by a lower degree of separation compared to the distributions examined in the previous case, and are represented in blue and green respectively in Figure 52. As shown in panel A of the figure, the simple projection of the data onto the space generated by PCA reveals a partial overlap between the two distributions, even though they are, by construction, statistically distinct. However, panels B-D show that the optimization pipeline is capable of detecting these structural differences and correctly assigning the observations their respective classes, grouping them around their true centroids. This result further confirms the sensitivity and

reliability of the method in discriminating between different classes, but only when the data distributions being compared are intrinsically characterized by a real structural difference.

In-depth analysis of Permutation test

To correctly interpret the results obtained from the statistical test, it is important to consider that the mean value of the accuracy distribution derived from the label permutations is subject to a systemic bias. This bias arises from the imbalance in sample size between the two compared classes, given that both stimulation and post stimulation conditions include a higher number of observations than the baseline condition.

Therefore, in order to demonstrate that the null (random) condition leads to an accuracy distribution systemically shifted above chance level, permutation tests were conducted under the constrain of balanced class sizes. Specifically, for each pairwise comparison, the class with the smaller number of observations was identified, and an equal number of samples were randomly selected from the larger class to ensure balanced distributions.

Figures 53 and 54 display the results of the permutation tests performed for the stimulation vs baseline and post-stimulation vs baseline comparisons, respectively, after balancing the class size. Panel A refers to the single acquisition analysis, whereas panel B presents the results based on the full-subject data.

What emerges is that, unlike the previous condition in which the classes were unbalanced, the mean of the accuracy distribution after permutation now centers around 50%, as expected under conditions of randomness. Moreover, in the comparison between stimulation and baseline, a reduction in the number of non significant cases is observed. This suggest that, in those cases, the class separability can be attributed more reliably to the effect of stimulation.

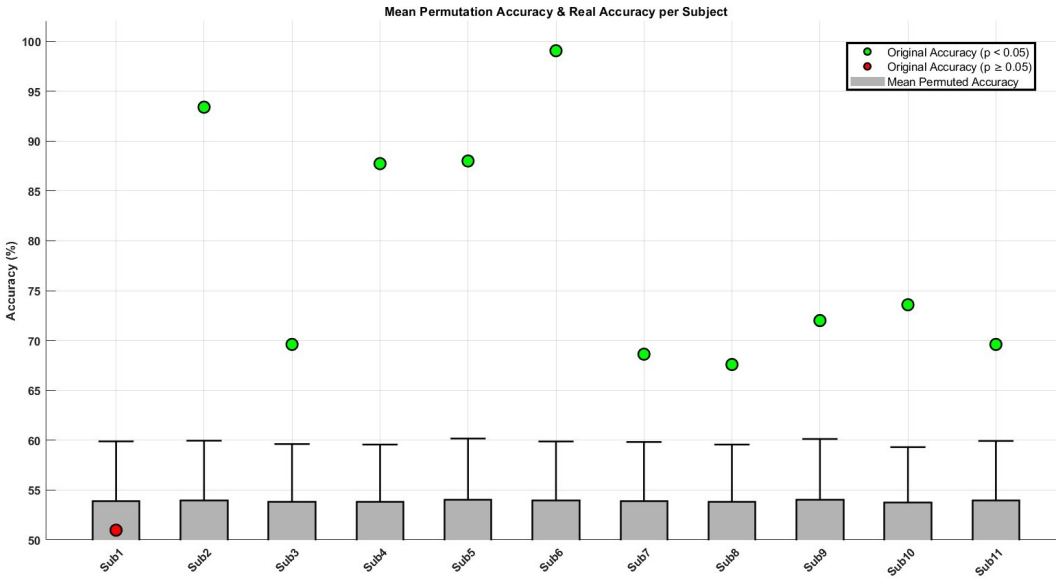

A

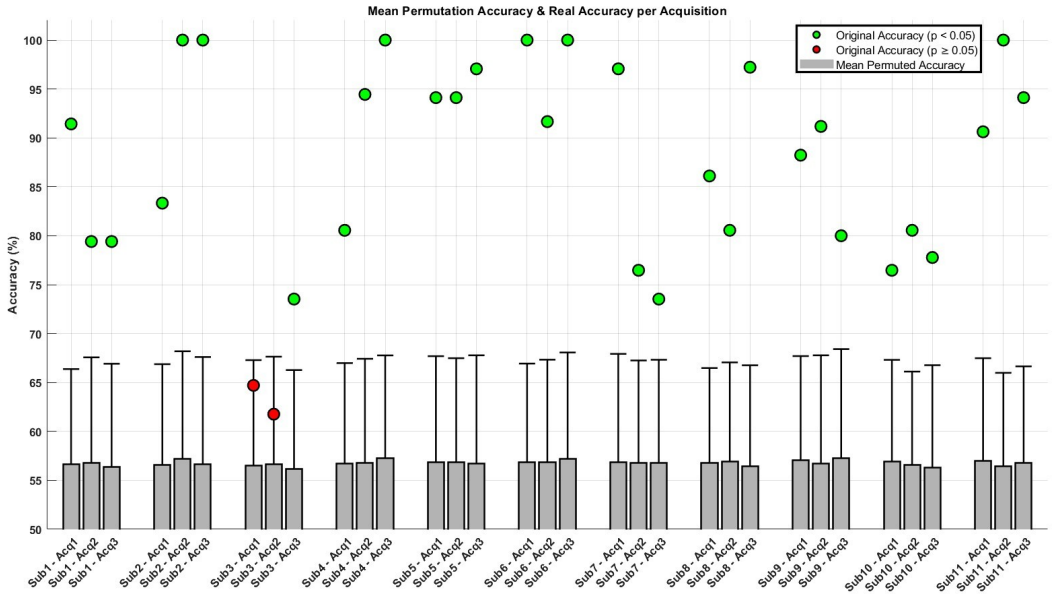

B

Figure 53: Permutation test applied to balanced classes of stimulation and baseline.

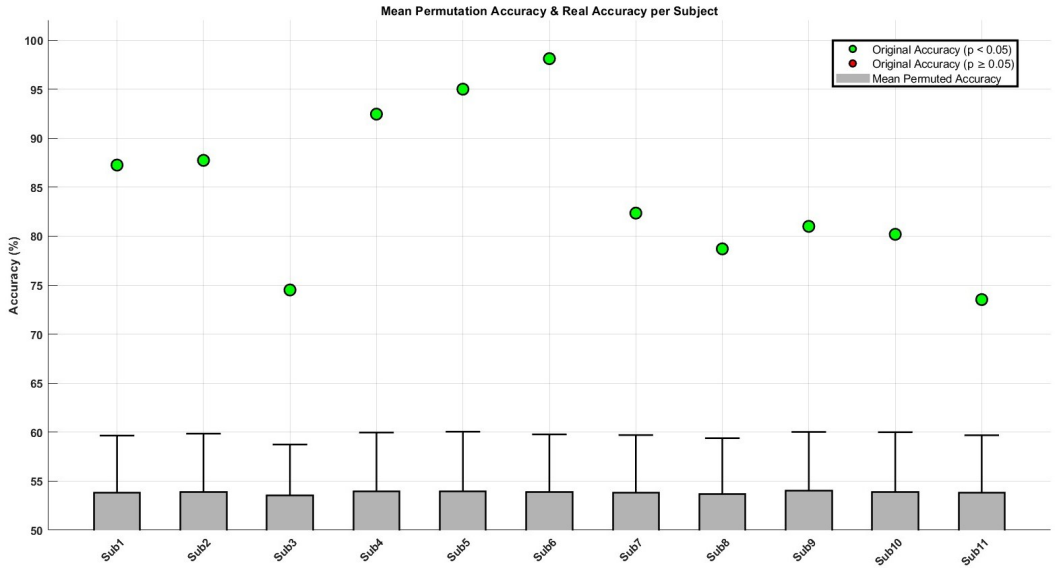

A

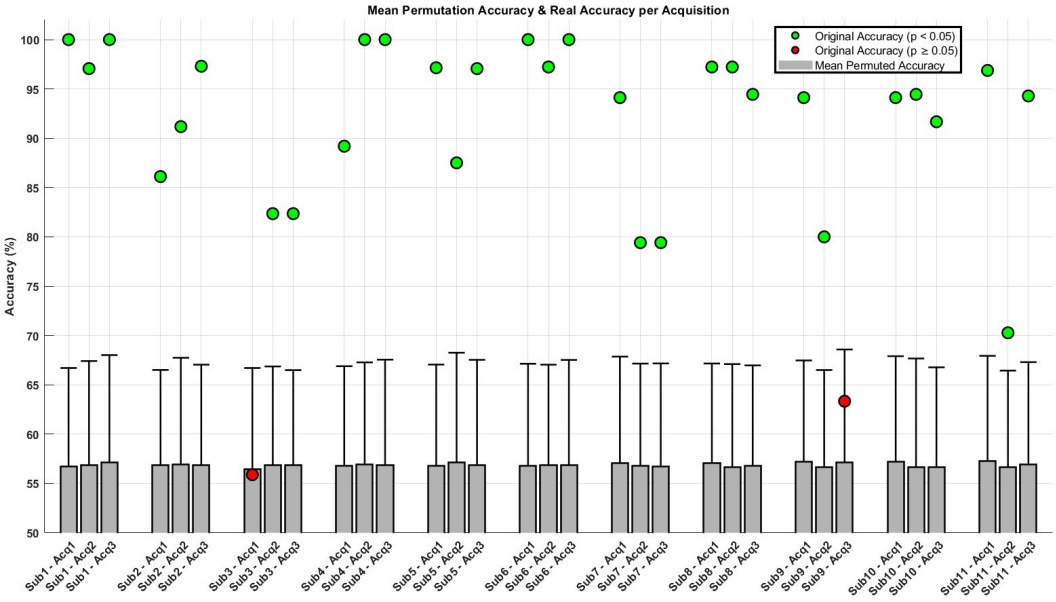

B

Figure 54: Permutation test applied to balanced classes of post-stimulation and baseline.

Topoplot of Alpha Rhythm Features

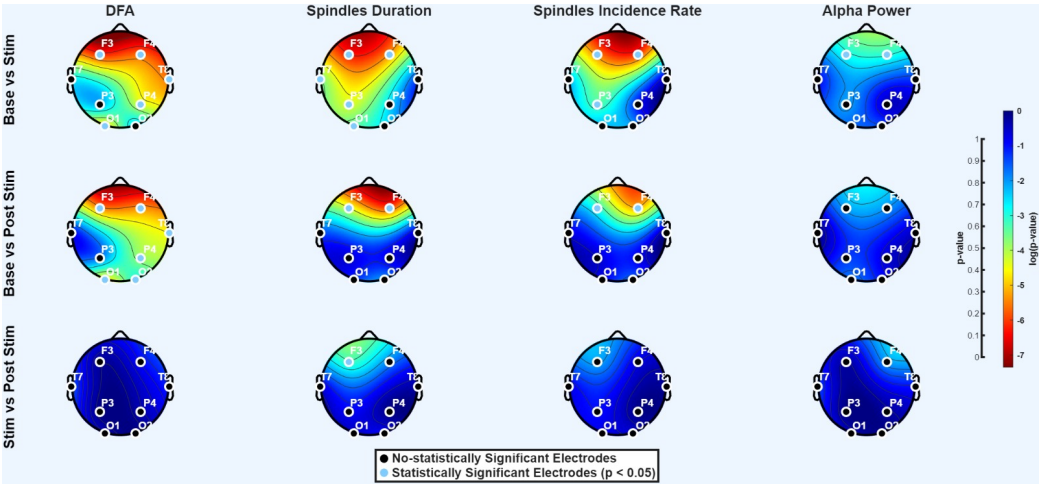

Figure 55: Topoplot of Alpha Rhythm Features showing statistical significance difference between different phases.

References

[1] Stephanie Willerth. Introduction to the nervous system. In *Engineering Neural Tissue from Stem Cells*, pages 17–38. Elsevier, 2017.

[2] George Varvatsoulias. Cerebral cortex and psychological functions: The role of lobes in the human brain. *GESJ: Education Science and Psychology*, (3(35)):58–67, 2015. CPsychol AFBPsS CSci Expert Witness, Applied Psychology Supervisor, Cognitive Behavioural Psychotherapist (BABCP Accredited), Newham College University Centre, Stratford Campus, Greater London, UK.

[3] Siuly Siuly, Yan Li, and Yanchun Zhang. *EEG Signal Analysis and Classification: Techniques and Applications*. Health Information Science. Springer, Cham, 2016.

[4] Syed Shah, Gopinath Gnanasegaran, Jeanette Sundberg-Cohon, and John R. Buscombe. The heart: Anatomy, physiology and exercise physiology. In *The Heart: Anatomy, Physiology and Exercise Physiology*. January 2009.

[5] David B. Geselowitz. On the theory of the electrocardiogram. *Proceedings of the IEEE*, 77(6):857–876, 1989. Supported in part by Grant HL 36625 from the National Institutes of Health.

[6] Ruth Maria Ingendoh, Ella S. Posny, and Angela Heine. Binaural beats to entrain the brain? a systematic review of the effects of binaural beat stimulation on brain oscillatory activity, and the implications for psychological research and intervention. *PLOS ONE*, 18(5):e0286023, 2023.

[7] T.L. Huang and C. Charyton. A comprehensive review of the psychological effects of brainwave entrainment. *Journal of Alternative and Complementary Medicine*, 31(3):123–145, 2025.

[8] Gerald Oster. Auditory beats in the brain. *Scientific American*, 229(4):94–102, 1973.

[9] May Elizabeth Chin. *Thresholds for the Binaural-Beat Stimuli as a Function of the Interaural Noise Correlation*. Ph.d. dissertation, Northwestern University, Evanston, Illinois, 1973. Field of Audiology.

[10] J.C.R. Licklider, J.C. Webster, and J.M. Hedlun. On the frequency limits of binaural beats. *The Journal of the Acoustical Society of America*, 22(4):468–473, 1950.

[11] David R. Perrott and Michael A. Nelson. Limits for the detection of binaural beats. *The Journal of the Acoustical Society of America*, 46(6):1477–1481, 1969.

[12] David R. Perrott and Alan D. Musicant. Rotating tones and binaural beats. *The Journal of the Acoustical Society of America*, 61(5):1288–1292, 1977.

[13] Jerry V. Tobias. Application of a "relative" procedure to a problem in binaural-beat perception. *The Journal of the Acoustical Society of America*, 35(9):1463–1469, 1963.

[14] David R. Perrott, Renee Briggs, and Sharon Perrott. Binaural fusion: Its limits as defined by signal duration and signal onset. *The Journal of the Acoustical Society of America*, 47(4B):1048–1054, 1970.

[15] S. Zschocke and H. Kursawe, editors. *Klinische Elektroenzephalographie*. Springer Medizin, Berlin, 3., aktualisierte und erweiterte auflage edition, 2012.

[16] Sandhya Basu and Bidisha Banerjee. Prospect of brainwave entrainment to promote well-being in individuals: A brief review. *Psychological Studies*, 65(4):322–329, 2020.

[17] Miguel Garcia-Argibay, Miguel A. Santed, and José M. Reales. Efficacy of binaural auditory beats in cognition, anxiety, and pain perception: a meta-analysis. *Psychological Research*, 83(2):357–372, 2019.

[18] Bernhard Ross and Marc Danzell Lopez. 40-hz binaural beats enhance training to mitigate the attentional blink. *Scientific Reports*, 10:7002, 2020.

[19] Susan Kennel, Ann Gill Taylor, Debra Lyon, and Cheryl Bourguignon. Pilot feasibility study of binaural auditory beats for reducing symptoms of inattention in children and adolescents with attention-deficit/hyperactivity disorder. *Journal of Pediatric Nursing*, 25(1):3–11, 2010. © 2010 Elsevier Inc. All rights reserved.

[20] Hector D. Orozco Perez, Guillaume Dumas, and Alexandre Lehmann. Binaural beats through the auditory pathway: From brainstem to connectivity patterns. *eNeuro*, 2020.

[21] Helané Wahbeh, Carlo Calabrese, Heather Zwickey, and Dan Zajdel. Binaural beat technology in humans: A pilot study to assess neuropsychologic, physiologic, and electroencephalographic effects. *The Journal of Alternative and Complementary Medicine*, 13(2):199–206, 2007.

[22] Werner Schmid, Peter Marhofer, Philipp Opfermann, Markus Zadrazil, Oliver Kimberger, Lydia Triffterer, Daniela Marhofer, and Wolfgang Klug. Brainwave entrainment to minimise sedative drug doses in paediatric surgery: a randomised controlled trial. *British Journal of Anaesthesia*, 125(3):330–335, 2020. Advance Access Publication Date: 8 July 2020.

[23] V. Gkolias, A. Amaniti, A. Triantafyllou, P. Papakonstantinou, P. Kartsidis, E. Paraskevopoulos, P.D. Bamidis, L. Hadjileontiadis, and D. Kouvelas. Reduced pain and analgesic use after acoustic binaural beats ther-

apy in chronic pain: a double-blind randomized control cross-over trial. *European Journal of Pain*, 2021. Article in press.

[24] Nantawachara Jirakittayakorn and Yodchanan Wongsawat. Brain responses to a 6-hz binaural beat: Effects on general theta rhythm and frontal midline theta activity. *Frontiers in Neuroscience*, 11:365, 2017. Published: 28 June 2017.

[25] T. Yamsa-ard and Y. Wongsawat. The relationship between eeg and binaural beat stimulation in meditation. In *Proceedings of the 2014 Biomedical Engineering International Conference (BMEiCON-2014)*, pages 1–5. IEEE, 2014. Email: traisak.y@gmail.com, yodchanan.won@mahidol.ac.th.

[26] Patrick A. McConnell, Brett Froeliger, Eric L. Garland, Jeffrey C. Ives, and Gary A. Sforzo. Auditory driving of the autonomic nervous system: Listening to theta-frequency binaural beats post-exercise increases parasympathetic activation and sympathetic withdrawal. *Frontiers in Psychology*, 5:1248, 2014. Published: 14 November 2014.

[27] Ruth Maria Ingendoh, Ella S. Posny, and Angela Heine. Binaural beats to entrain the brain? a systematic review of the effects of binaural beat stimulation on brain oscillatory activity, and the implications for psychological research and intervention. *PLOS ONE*, 18(5):e0286023, 2023.

[28] Neuroelectrics. Starstim 8: Wearable and wireless 8-channel tes-eeg system. `https://www.neuroelectrics.com/starstim-8`, 2025. Accessed: 2025-05-02.

[29] Polar Electro Oy. *Polar H10 Heart Rate Sensor User Manual*. Polar Electro Oy, 2025. Available at `https://support.polar.com/it/support/h10_heart_rate_sensor`.

[30] Pierre Comon. Independent component analysis, a new concept? *Signal Processing*, 36(3):287–314, 1994.

[31] Te-Won Lee, Mark Girolami, and Terrence J. Sejnowski. Independent component analysis using an extended infomax algorithm for mixed subgaussian and supergaussian sources. *Neural Computation*, 11(2):417–441, 1999.

[32] Julie Onton, Marissa Westerfield, Jeanne Townsend, and Scott Makeig. Imaging human eeg dynamics using independent component analysis. *Neuroscience and Biobehavioral Reviews*, 30(6):808–822, 2006.

[33] Ricardo Vigário, Jaakko Särelä, Veikko Jousmäki, Matti Hämäläinen, and Erkki Oja. Independent component approach to the analysis of eeg and meg recordings. *IEEE Transactions on Biomedical Engineering*, 47(5):589–593, 2000.

[34] Jean-François Cardoso and Bruno H. Laheld. Equivariant adaptive source separation. *IEEE Transactions on Signal Processing*, 45(2):434–444, 1996.

[35] A. J. Bell and T. J. Sejnowski. An information-maximization approach to blind separation and blind deconvolution. *Neural Computation*, 7(6):1129–1159, 1995.

[36] Aapo Hyvärinen, Juha Karhunen, and Erkki Oja. *Independent Component Analysis*. John Wiley & Sons, New York, 2001.

[37] Svante Wold, Kim Esbensen, and Paul Geladi. Principal component analysis. *Chemometrics and Intelligent Laboratory Systems*, 2:37–52, 1987. Printed in The Netherlands.

[38] Karl Pearson. Liii. on lines and planes of closest fit to systems of points in space. *Philosophical Transactions of the Royal Society of London.*

Series A, Containing Papers of a Mathematical or Physical Character, 187:301–320, 1901. Communicated by the Author.

[39] Harold Hotelling. Analysis of a complex of statistical variables into principal components. *Journal of Educational Psychology*, 24(6):417–441, 1933. A study made in part under the auspices of the Unitary Traits Committee and the Carnegie Corporation. The author is indebted to Professors Truman L. Kelley, L. L. Thurstone, Clark V. Hull, C. Spearman, and E. L. Thorndike for their contributions.

[40] Ian T. Jolliffe and Jorge Cadima. Principal component analysis: a review and recent developments. *Philosophical Transactions of the Royal Society A: Mathematical, Physical and Engineering Sciences*, 374(2065):20150202, 2016. One contribution of 13 to a theme issue 'Adaptive data analysis: theory and applications'.

[41] Tapas Kanungo, David M. Mount, Nathan S. Netanyahu, Christine D. Piatko, Ruth Silverman, and Angela Y. Wu. An efficient k-means clustering algorithm: Analysis and implementation. *IEEE Transactions on Pattern Analysis and Machine Intelligence*, 24(7):881–892, 2002. Manuscript received 1 Mar. 2000; revised 6 Mar. 2001; accepted 24 Oct. 2001. Recommended for acceptance by C. Brodley.

[42] Stuart Lloyd. Least squares quantization in pcm. *IEEE Transactions on Information Theory*, 28(2):129–137, 1982. hal-04614938.

[43] Jerry V. Tobias. Consistency of sex differences in binaural-beat perception. *International Audiology*, 4:179–182, 1965.

[44] David Vickael and Michael A. Nelson. Limits for the detection of binaural beats. 1969. Received 14 August 1969.

[45] Lauren Sidelinger, Mengsen Zhang, Flavio Frohlich, and Stacey B. Daughters. Day-to-day individual alpha frequency variability measured

by a mobile eeg device relates to anxiety. *European Journal of Neuroscience*, 2023.

[46] Andrew W. Corcoran, Phillip M. Alday, Matthias Schlesewsky, and Ina Bornkessel-Schlesewsky. Toward a reliable, automated method of individual alpha frequency (iaf) quantification. *Psychophysiology*, 55(3):e13064, 2018.

[47] May Elizabeth Chin. *Thresholds for the Binaural-Beat Stimuli as a Function of the Interaural Noise Correlation*. Ph.d. thesis, Northwestern University, Ann Arbor, Michigan, 1973. University Microfilms, A Xerox Company.

[48] Siddharth Sharma, Shreya Rewadkar, Harshada Pawar, and Vaibhav Deokar. Survey on binaural beats and background music for increased focus and relaxation. In *2017 International Conference on Emerging Trends & Innovation in ICT (ICEI)*, Pune, India, February 3–5 2017. Pune Institute of Computer Technology. Guide: Prof. Vina M. Lomte.

[49] Subhra Chakraborty, Raja Raman, Ramanujam Upadhayay, and Rahul. Implementation of optimized technique for enhancing eeg signal quality by improving signal to noise ratio. In *2024 International Conference on Intelligent Algorithms for Computational Intelligence Systems (IACIS)*, Bengaluru, India, 2024. IEEE.

[50] Md. Fazlul Karim Khondakar, Trishita Ghosh Troyee, Mahmudul Hasan, Md. Hasib Sarowar, Mehdi Hasan Chowdhury, and Quazi Delwar Hossain. A comparative analysis of different pre-processing pipelines for eeg-based preference prediction in neuromarketing. In *2023 IEEE Pune Section International Conference (PuneCon)*, Pune, India, 2023. IEEE. COEP Technological University, Dec 14-16, 2023.

[51] Nisreen Said Amer and Samir Brahim Belhaouari. Eeg signal processing for medical diagnosis, healthcare, and monitoring: A comprehensive

review. *IEEE Access*, 11:169654–169669, Dec 2023. Received 8 October 2023, accepted 4 December 2023, date of publication 12 December 2023, date of current version 21 December 2023.

[52] EEGLAB. Eeglab tutorial: Rereferencing background concepts. `https://eeglab.org/tutorials/ConceptsGuide/rereferencing_background.html`, 2023. Accessed: 2025-05-02.

[53] O. Bertrand, F. Perrin, and J. Pernier. A theoretical justification of the average reference in topographic evoked potential studies. *Electroencephalography and Clinical Neurophysiology*, 62(5):462–464, 1985. Accepted for publication: August 16, 1985.

[54] Giorgos Giannakakis, Dimitris Grigoriadis, Katerina Giannakaki, Olympia Simantiraki, Alexandros Roniotis, and Manolis Tsiknakis. Review on psychological stress detection using biosignals. *IEEE Transactions on Affective Computing*, 13(1):440–460, Jan.–Mar. 2022.

[55] Bo Hjorth. Eeg analysis based on time domain properties. *Electroencephalography and Clinical Neurophysiology*, 1970. Accepted for publication: January 30, 1970.

[56] Sergul Aydore, Dimitrios Pantazis, and Richard M. Leahy. A note on the phase locking value and its properties. *NeuroImage*, 74:231–244, 2013. 1053-8119/$-see front matter 2013 Elsevier Inc. All rights reserved.$

[57] Zen J. Lau, Tam Pham, S. H. Annabel Chen, and Dominique Makowski. Brain entropy, fractal dimensions and predictability: A review of complexity measures for eeg in healthy and neuropsychiatric populations. *European Journal of Neuroscience*, 56(2):2010–2027, 2022. Received: 3 May 2022, Revised: 20 July 2022, Accepted: 10 August 2022.

[58] T. Higuchi. Approach to an irregular time series on the basis of the fractal theory. *Physica D: Nonlinear Phenomena*, 31:277–283, 1988. Received 18

June 1987, Revised manuscript received 9 January 1988, Communicated by M. Mimura.

[59] Michael J. Katz. Fractals and the analysis of waveforms. *Computer Methods and Programs in Biomedicine*, 18(3):145–156, 1988. Received 29 June 1987; in revised form 23 September 1987.

[60] Marta Borowska. Entropy-based algorithms in the analysis of biomedical signals. *Studies in Logic, Grammar and Rhetoric*, 43(56):157–167, 2015.

[61] PCA for Data Science. Centered and standardized variables. `https://pca4ds.github.io/centered-and-standardized-variable.html`, 2023. Accessed: 2025-05-02.

[62] Xiao-Ben Zheng and Bingo Wing-Kuen Ling. A bci system for imagined speech classification based on optimization theory. *IEEE Transactions on Consumer Electronics*, 70(4):6679, 2024.

[63] Quanquan Gu, Zhenhui Li, and Jiawei Han. Generalized fisher score for feature selection. Technical report, Department of Computer Science, University of Illinois at Urbana-Champaign, Urbana, IL 61801, USA, 2009. Contact: qgu3@illinois.edu, zli28@uiuc.edu, hanj@cs.uiuc.edu.

[64] Hossein Shafizadeh-Moghadam. Fully component selection: An efficient combination of feature selection and principal component analysis to increase model performance. *Expert Systems with Applications*, 2021.

[65] Roberto Todeschini, Davide Ballabio, Viviana Consonni, Faizan Sahigara, and Peter Filzmoser. Locally centred mahalanobis distance: A new distance measure with salient features towards outlier detection. *Analytica Chimica Acta*, 788:52–59, 2013. 0003-2670/$ – see front matter © 2013 Elsevier B.V. All rights reserved.

[66] Aurell Faza Ashilla, Awang Putra R. Sembada, I. Melda Puspita Loka, Sukma Adi Perdana, and Muhammad Ahsan. Kernel pca based on hotelling

multivariate control chart for monitoring breast cancer diagnostic. *IAENG International Journal of Applied Mathematics*, 54(6):1026–1032, June 2024.

[67] Theo A. Knijnenburg, Lodewyk F. A. Wessels, Marcel J. T. Reinders, and Ilya Shmulevich. Fewer permutations, more accurate p-values. *Bioinformatics*, $25(\text{suppl}_1) : i161 - -i168, 2009$.

[68] Misako Sano, Yuko Nishiura, Izumi Morikawa, Aiko Hoshino, Jun-ichi Uemura, Katsuyuki Iwatsuki, Hitoshi Hirata, and Minoru Hoshiyama. Analysis of the alpha activity envelope in electroencephalography in relation to the ratio of excitatory to inhibitory neural activity. *PLOS ONE*, 19(6):e0305082, 2024. Published: June 13, 2024.

[69] Keiichi Mimura. On the periodic alpha fluctuations of waves. *Jap. J. Physiol.*, 21:375–386.

[70] Alexei Ossadtchi, Tatiana Shamaeva, Elizaveta Okorokova, Victoria Moiseeva, and Mikhail A. Lebedev. Neurofeedback learning modifies the incidence rate of alpha spindles, but not their duration and amplitude. *Scientific Reports*, 7:3772, 2017.

[71] David M. Goodman, Jackson Beatty, and Thomas B. Mulholland. Detection of cerebral lateralization of function using eeg alpha-contingent visual stimulation. *Electroencephalography and Clinical Neurophysiology*, 48:418–431, 1980.

[72] C.-K. Peng, Shlomo Havlin, H. Eugene Stanley, and Ary L. Goldberger. Quantification of scaling exponents and crossover phenomena in nonstationary heartbeat time series. *Chaos: An Interdisciplinary Journal of Nonlinear Science*, 5(1):82–87, 1995.

[73] Vadim V. Nikulin, Erik G. Jönsson, and Tom Brismar. Attenuation of long-range temporal correlations in the amplitude dynamics of alpha and beta

neuronal oscillations in patients with schizophrenia. *NeuroImage*, 61(1):162–169, 2012.

[74] Jiapu Pan and Willis J. Tompkins. A real-time qrs detection algorithm. *IEEE Transactions on Biomedical Engineering*, BME-32(3):230–236, March 1985.

[75] Fred Shaffer and J. P. Ginsberg. An overview of heart rate variability metrics and norms. *Frontiers in Public Health*, 5:258, 2017. Published: 28 September 2017.

[76] G. Guruprasath and S. Gnanavel. Effect of continuous and short burst binaural beats on eeg signals. In *Proceedings of the 2nd International Conference on Innovations in Information, Embedded and Communication Systems (ICIIECS)*, pages 1–5. IEEE, 2015. Email: guru121992@hotmail.com, gnanavel.s@ktr.srmuniv.ac.in.

[77] Mona Irrmischer, Simon J. Houtman, Huibert D. Mansvelder, Michael Tremmel, Ulrich Ott, and Klaus Linkenkaer-Hansen. Controlling the temporal structure of brain oscillations by focused attention meditation. *Human Brain Mapping*, 39(7):2647–2658, July 2018.